UNIVERSITÀ DEGLI STUDI DI MILANO
FACOLTÀ DI SCIENZE MATEMATICHE, FISICHE E NATURALI

Corso di laurea in Fisica

TESTING LONG RANGE BEAM-BEAM COMPENSATION FOR THE LHC LUMINOSITY UPGRADE

Relatore Interno :   Prof. Sergio Caracciolo

Relatore Esterno :   Dr. Frank Zimmermann

Tesi di laurea di
Tatiana Libera RIJOFF
Matr. 721003
PACS: 13.60.-r

Contents

List of Figures

List of Tables

Abstract

The performance of the Large Hadron Collider (LHC) at CERN and its minimum crossing angle are limited by long-range beam-beam collisions. A wire compensators can mitigate part of the long-range effects and may allow for smaller crossing angles, or higher beam intensity.

A prototype long-range wire compensator should be installed in the LHC by 2014/15. The originally reserved position for the wire compensator (named BBC) seems not available in this first step, we need so to test other possibilities.

The performed tests consider various longitudinal and transverse locations, different wire shapes, different optics configuration and trying several crossing angles between the beam.

Simulation are done with the weak-strong code BBtrack developed by U. Dorda.

New postprocessing tools were used to analyse tune footprints and particle stability In particular for particle stability was implemented a new method for the Lyapunov coefficient calculation.

Introduction

On 4 July 2012 ATLAS (A Toroidal LHC Apparatus) and CMS (Compact Muon Solenoid), the main experiments in the LHC (Large Hadron Collider) at CERN (Conseil Européen pour la Recherche Nucléaire) announced that they have observed a new particle compatible with the Higgs boson.

These promising results are preliminary and need to be confirmed with further analysis but also by increasing the statistics of events.

For this reason, and also hoping to find other new particles, it is important that LHC operates with the full energy (7 TeV per beam) and that it and that it reaches the highest possible luminosity, well in excess of the design values of L = 10^{34} cm^{-2} s^{-1} [1].

In the frame of the luminosity upgrade it is important to take into account the negative effects due to the electromagnetic interactions between the two beam before and after the collision points, the so called *beam-beam effects* that limit the collider performance.

Wire compensators can mitigate part of the long-range effects and may allow for smaller crossing angles or higher beam intensity.

A prototype long-range wire compensator should be installed in the LHC by 2014/15.

In this thesis I will report my studies on the possible wire compensation solutions, i.e. the analysis of the different longitudinal and transversal locations, on the possible electric current values, and of the different wire shapes.

The simulations were performed with bbtrack, a code developed by U. Dorda that track particles in conditions of weak-strong analysis: the program analyse the interaction between a single particle and the entire counterrotating beam; hence I analysed the different possibilities considering the tune and the dynamical aperture. During the analysis of the dynamical aperture we implemented a new criterion to evaluate the Lyapunov coefficient. We verified that this criterion is stable when we increase the number of turns (we performed tests up to 1 million turns).

---

[1]To set these values into perspective we note that in this year (2012) LHC has operated with beam energies of 4 TeV, and reached a maximum luminosity value of 0.68 10^{34} cm^{-2} s^{-1}

If we use for the compensator the nominal values, i.e. longitudinal position of 105 m from the Interaction points 1 and 5 (Ip1 and Ip5 for short) (where the experiments ATLAS and CMS are located), transversal position equal to 9.5 σ (where σ denotes the rms beam size) and current 177 A, LHC wire compensators should allow for a reduction of the crossing angle by the equivalent of at least 1-2 σ while maintaining the same stable region in phase space, or, alternatively, for a substantial increase in beam current (e.g. by a factor of 2) at constant crossing angle.

This solution will not be available for the 2014/2015 shutdown. Our simulations predict satisfying results also for a wire located in the shadow of the tertiary collimator (TCT, 147 m from Interaction Points 1 and 5), if we use a modified optics based on the ATS scheme and taylored for this scope by S. Fartoukh [10], or if we keep the nominal optics and move the wire position near interaction point 1 by about 300 m from the present TCT position (namely passing from 147 m before the IP1 to 150 m after the IP).

The solutions analyzed in this thesis will guide the installation of a prototype wire compensator in the LHC for operation from 2015 onwards.

I presented part of this work in a poster at the IPAC'12 Conference (International Particle Accelerator Conference). It was referred to by the CERN Director of Accelerators and Technology, Dr. S. Myers, in his opening plenary talk.

1

The Accelerators

1.1 Introduction

A particle accelerator is a device that uses an electromagnetic field $(\vec{E}, \vec{B})$ to accelerate and guide charged particles ([2, 34]); the Lorentz force on a particle with charge e is

$$\vec{F} = e\left(\vec{E} + \vec{v} \times \vec{B}\right) \tag{1.1}$$

with

$$\vec{E} = -\boldsymbol{\nabla}V - \frac{\partial \vec{A}}{\partial t} \tag{1.2}$$

$$\vec{B} = \boldsymbol{\nabla} \times \vec{A} \tag{1.3}$$

where V denotes the electrostatic potential and $\vec{A}$ the magnetic vector potential.

One of the first accelerators was built by Ernest Walton and John Cockcroft, enouraged by Ernest Rutheford, to split the atom. Their success marked the beginning of a new field of subatomic research.

At present the large hadron collider (LHC) at CERB (fig.: 1.1) aims to answer some of the fundamental open questions in physics,

- does the Higgs boson exist? If yes, the masses of the elementary particles can be be explained by the Higgs mechanism via electroweak symmetry breaking, otherwise physicists have to consider Higgs-less model alternatives.

- Is supersymmetry realised in nature? If so, all known particles have supersymmetric partners.

- Do extra dimensions exist, as supposed by string theory?

- What is the nature of the dark matter?
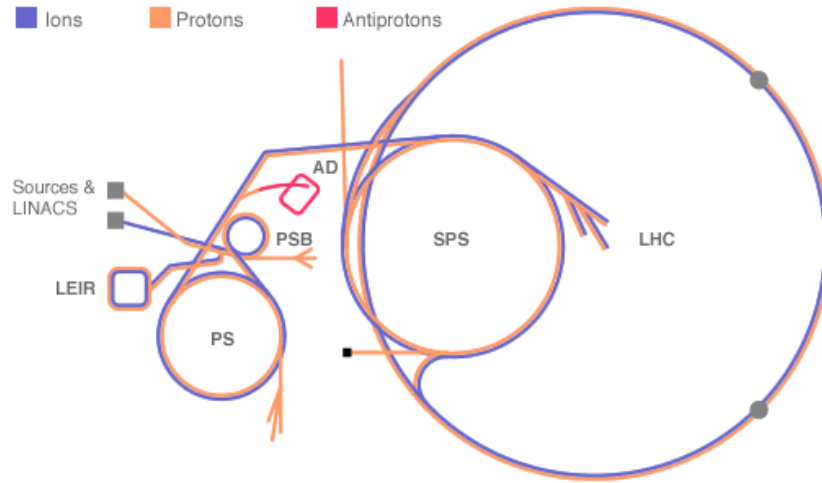
Figure 1.1: The CERN accelerator complex

On July 4th 2012, CERN has announced the probable discovery of the Higgs boson. As emphasized by Rolf Heuer, current Director General of CERN, this is a historic milestone but only the beginning: more data have to be accumulated (implying a lot more work for the LHC) before the discovery can be considered certain. However, these events allow us to be optimistic.

Figure 1.2 shows some slides presented in the official CERN conference on July 4th 2012.

The CMS picture (left image) shows the observed probability (local p-value) that the background-only hypothesis would yield the same or more events as are seen in the CMS data, as a function of the SM Higgs boson mass for the five decay channels considered. The solid black line shows the combined local p-value for all channels.

The ATLAS picture (right image) shows the combined upper limit on the Standard Model Higgs boson production cross section divided by the Standard Model expectation as a function of the Higgs mass is indicated by the solid line. This is a 95% CL limit using the CLs method in in the low mass range. The dotted line shows the median expected limit in the absence of a signal and the green and yellow bands reflect the corresponding 68% and 95% confidence line expected without a Higgs particle.

Although the particle physics community is the original field of science interested in particle accelerators, today accelerators are useful in a lot of other fields. As suggested by Chao (see [4]) we can recognize the following applications:

- in the medical field, for example for cancer therapy and radiology, sterilization, or isotope production,

- in the industial area, where we can cite electron microscope, photo-
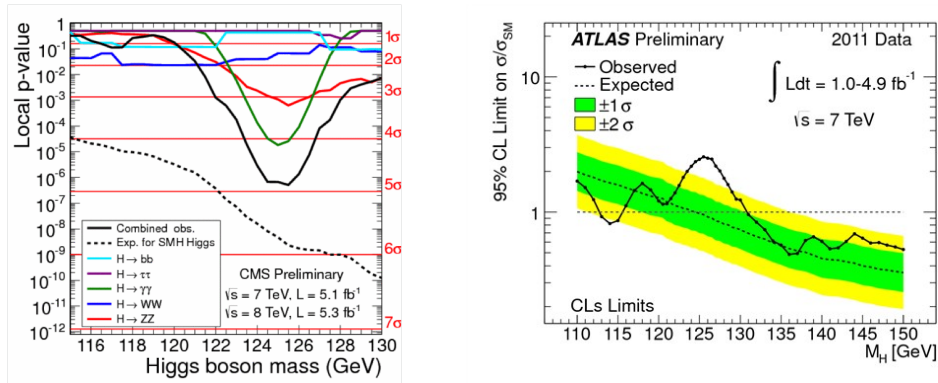
Figure 1.2: On the left: CMS Image from CERN Higgs Seminar, on the Right: ATLAS Image from CERN Higgs Seminar (4 July 2012).

electron-microscope, ion implantation for semiconductors, or for surface metal alloy, lithography, radiation treatment of material, non-destructive detection of material damages/defects, radiography, food sterilization, and nuclear waste treatment.

In addition in the scientific field, accelerators are useful not only for high energy and nuclear physics, but also for

- chemistry,

- material science,

- biology, and

- energy production (inertial fusion).

1.1.1 Accelerator classification

According the target we can classify the accelerators as

- fixed target accelerators

- colliders

On the other hand, considering the method used to accelerate particles, accelerators can be divided into two main categories:

Linear Accelerators (linac) accelerate particles in a straight line; they are used for fixed-target experiments, as injectors for circular accelerators, or as linear colliders.

Circular Accelerators where particles move in a circle until they reach sufficient energy

In circular accelerators, particles pass through the accelerating units many times with an increasing magnetic field, thus acquiring energy at each passage; for this reason, a linac would have to be extremely long to have the equivalent final energy of a circular accelerator.
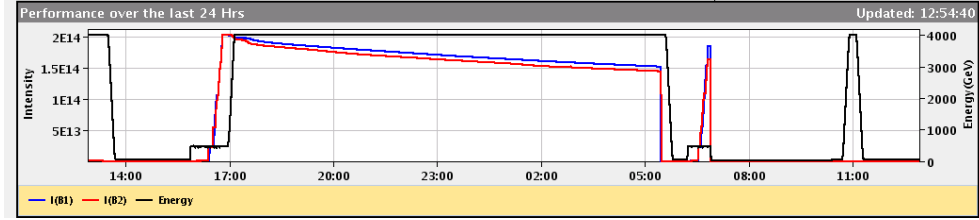
Figure 1.3: The LHC performance on 07/07/2012. The graphics shows the beam intensity (total number of protons) for the two counterrotating beams (line red and blue) and the beam energy (black line)

For a circular collider we can identify

- an injection period, when the beam is put into the accelerator in multiple bunches

- an acceleration period, when the beam is accelerated by using the magnetic fields of dipoles and quadrupoles

- a stable beam phase, in which the beams are mantained in the accelerator (storage ring function) and collide (collider function).

More details are illustrated in the Figure 1.3.

I this thesis we are studying the LHC (Large Hadron Collider), that is a circular collider, in the collision period.

1.2 Circular accelerators

1.2.1 Hamiltonian and Hill equation

Proposition 1 (Hamiltonian for an accelerator)**.** The Hamiltonian for a particle with charge e and mass m_0 in the electromagnetic potential $(V, \vec{A})$ is given by

$$H = c\sqrt{\left(\vec{p} - e\vec{A}(\vec{q}, t)\right)^2 + m_0^2 c^2} + eV(q_k, t) \tag{1.4}$$

where $\vec{p}$ is the momentum conjugated to $\vec{q}$ which is related to the mechanical momentum $m_0 \vec{v}$ by

$$\vec{p} = m_0 \vec{v} + q\vec{A}$$
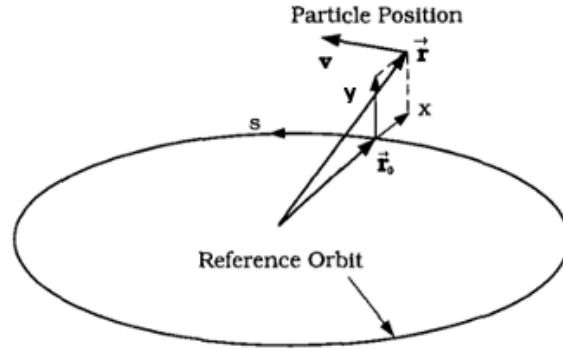
Figure 1.4: orbit in a circular accelerator [22]

For any kind of accelerator we can identify a *design orbit* on which the particles should move and a deviation from this orbit.

Definition 1 (Design Orbit). With design orbit, or reference orbit we indicate the ideal orbit where an ideal particle should move (see fig. 1.4)

Proposition 2. Consider a particle travelling along the design orbit with momentum $\vec{p}$, if we indicate with $\rho(s)$ the radius of curvature (bending radius) of design orbit in the point s, and with B_0 the magnetic field orthogonal to the trajectory one can easily demonstrate that

$$B_0 \rho = \frac{p}{e} \tag{1.5}$$

where $B_0 \rho$ is called the *beam magnetic rigidity*

It is convenient to choose a coordinate system connected to the design orbit, the Frenet-Serret coordinate system.

Definition 2 (Frenet-Serret coordinate system). The Frenet-Serret coordinate system is composed of the triple (x, y, s), where

- s is the motion along the design orbit,

$$\hat{s}(s) = \frac{d\vec{r}_0(s)}{ds} \tag{1.6}$$

($\vec{r}_0$ is the position vector along the orbit)

- x is the displacement from the design orbit in radial direction

$$\hat{x}(s) = -\rho(s)\frac{d\hat{s}(s)}{ds} \tag{1.7}$$

- y is the displacement in the direction perpendicular to s and x

$$\hat{y}(s) = \hat{x}(s) \times \hat{y}(s) \tag{1.8}$$

The traiectory for a given particle can be written as

$$\vec{r}(s) = \vec{r}_0(s) + x\hat{x}(s) + y\hat{y}(s) \tag{1.9}$$

In this system the canonical momentum components are

$$p_s = \left(1 + \frac{x}{\rho}\right) \vec{p} \cdot \hat{s} \tag{1.10}$$

$$p_x = \vec{p} \cdot \hat{x}$$
$$p_y = \vec{p} \cdot \hat{y} \tag{1.11}$$

and the magnetic vector potential components are

$$A_s = \left(1 + \frac{x}{\rho}\right) \vec{A} \cdot \hat{s} \tag{1.12}$$

$$A_x = \vec{A} \cdot \hat{x}$$
$$A_y = \vec{A} \cdot \hat{y} \tag{1.13}$$

Proposition 3 (Hamiltonian in Frenet-Serret coordinate system). Using the curvilinear coordinate system we can write the hamiltonian as

$$H = eV + c\left(m^2c^2 + \left(\frac{p_s - eA_s}{1 + \frac{x}{\rho}}\right)^2 + (p_x - eA_x)^2 + (p_y - eA_y)^2\right)^{1/2} \tag{1.14}$$

In this equation the independent variable is the time t, but since a circular accelerator is periodic in the curvilinear position s, it is convenient to use this as independent variable. From now on we will indicate the derivative respect to the s variable with a prime index and the one respect to the time with an overdot, i.e.

$$x' = \frac{\partial x}{\partial s}$$
$$\dot{x} = \frac{\partial x}{\partial t}$$

With the change of variable $t \to s$ the new Hamiltonian is

Proposition 4 (Hamiltonian in a circular accelerator $(t \to s)$)**.**

$$\tilde{H} = -p_s$$

$$= -eA_s - \left(1 + \frac{x}{\rho}\right)\left(\frac{1}{c^2}(H - eV)^2 - m^2c^2 - (p_x - eA_x)^2 - (p_y - eA_y)^2\right)^{1/2}$$

$$\tag{1.15}$$

Staring from (1.15) and applying some simplifications.

We take $V = 0$ and $\frac{\partial \vec{A}}{\partial t} = 0$ (good approximation in the stable beam period).

We ignore the end fields of our lattice elements and we assume that the magnetic field is only transverse, so that $A_x = A_y = 0$ (good approximation in big accelerators like LHC). Then we obtain

$$B_x = \frac{\partial A_s}{\partial y}$$

$$B_y = -\frac{\partial A_s}{\partial x}$$

We notice that

$$\frac{1}{c^2}\left(H^2 - m_0c^4\right) = m_0c^2\left(\gamma^2 - 1\right) = \vec{p} \cdot \vec{p}$$

and that since the beam is moving at relativistic velocity in the s direction the momentum components in the transverse plane are small compared to the total momentum, i.e. $p_{x,y} \ll p$

We assume that the radial deviation from the reference orbit is infinitesimal compared to the radius of curvature $x << \rho$.

Using the multipole expansion of the magnetic potential

$$A_s = \sum_n A_n (x + iy)^n \tag{1.16}$$

and ignore the terms greater than the quadrupoles.

$$B_y = -B_0 + \frac{\partial B_y}{\partial x}x = -B_0 + B_1 x \tag{1.17}$$

$$B_x = \frac{\partial B_y}{\partial x}y = B_1 y$$

and considering separately the two transverse directions, we obtain

$$H = \frac{p_z^2}{2} + K_z(s)\frac{z^2}{2} \quad z = x \text{ or } y \tag{1.18}$$

$$K_x = \frac{1}{\rho^2} - K_1 \tag{1.19}$$

$$K_y = K_1$$

K_1 = effective focusing function

$$K_1(s) = \frac{B_1(s)}{B\rho} \tag{1.20}$$

Proposition 5 (Hill's equation)**.** The solution of (1.18) is *Hill's equation*

$$z'' + K_z(s)z = 0 \quad (z = x \text{ or } y) \tag{1.21}$$

In a circular accelerator the coefficient K_y in the equation (1.21) is periodic

$$K(s + L) = K(s)$$

The solution of Hill's equation, is a kind of quasi harmonic oscillation, with amplitude and phase dependent on the position s in the ring.

Proposition 6 (Solution of the Hill equation)**.** We can write the solution as [30]

$$z(s) = \sqrt{\epsilon}\sqrt{\beta(s)} \cos\left(\psi(s) + \phi\right) \tag{1.22}$$

where

ϵ is the *single particle emittance*, costant at a given energy

$\beta(s)$ is the *betatron function*, a periodic function given by focusing properties of the lattice (i.e. quadrupoles)

$\psi(s)$ is the phase advance

ϕ is the initial phase

The β and ϵ parameters are related by the equation of the ellipse (often called the Courant and Snyder invariant)

$$\gamma(s)z^2 + 2\alpha(s)yy' + \beta(s)y'^2 = \epsilon \tag{1.23}$$

We can define also a beam emittance as

$$\epsilon_{rms} = \frac{\langle z^2 \rangle}{\beta_z} = \frac{\langle \epsilon \rangle}{2} \tag{1.24}$$

It is useful to define also the *normalized emittance*

$$\epsilon_n = \gamma\beta\epsilon \tag{1.25}$$

where in this case β and γ are the relativistic values: $\beta = v/c$ and $\gamma = (1 - \beta^2)^{-1/2}$

Starting from the equation (1.22) we can define a really important quantity for the accelerator, *the tune*.
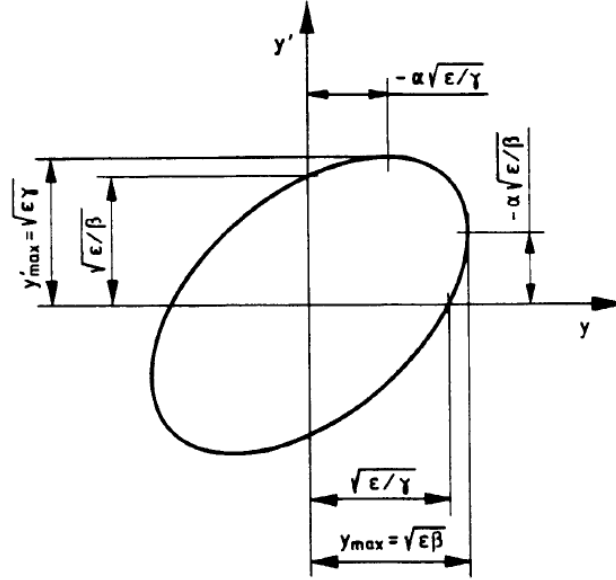
Figure 1.5: The Courant Snyder parameter in the phase space

Definition 3 (Tune)**.** The tune is the number of oscillations per turn in a given transverse direction (x or z), and can be obtained from

$$Q_z = \frac{1}{2\pi} \oint \frac{1}{\beta_z(s)} ds \quad z = x \text{ or } y \tag{1.26}$$

Proof. It is enough to notice that inserting (1.22) in the equation (1.21) we find

$$\psi(s) = \int_0^s \frac{1}{\beta(s)} ds \tag{1.27}$$

again checking the equation (1.22) we understand that when $\psi(s) = 2\pi$ the particle has completed a transverse oscillation and we derive easily our proposition.

$\square$

Proposition 7 (Hamiltonian in action-angle variable)**.** With suitable canonical transformations we can write the system Hamiltonian as

$$H_z = \frac{Q_z}{R} J_z \tag{1.28}$$

where Q_z is the tune in the z direction ($z = x$ or $z = y$), R is the accelerator radius, the action variable J_y is half the single particle emittance (see [24] for more details)

$$2J = \epsilon \tag{1.29}$$

Note that we easily derive

$$\epsilon_{rms} = \langle J \rangle \tag{1.30}$$
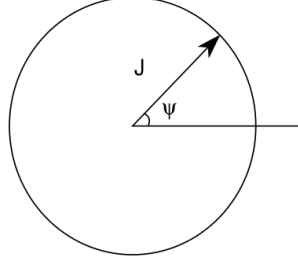
Figure 1.6: Particle trajectory in the phase space (J, ψ)

We notice that the Hamiltonian is independent of s or t, and that, if we plot the phase space trajectory using the coordinates (ψ, J) with $\psi = (Q/R)s$ from

$$z = \sqrt{2J\beta}\cos\psi \tag{1.31}$$

the trajectory of the particle is a circle of radius J.

We can observee the nonlinear components of the motion in the accelerator as distortion of this circle and amplitude dependent change in the tune.

1.2.2   Deviation from ideal orbit

Not all particles have the same orbit and the same momentum; this causes a spread in particle position and in tune Q among the beam particles

Proposition 8 (Inhomogeneus equation of motion)**.** Taking into account the beam spread the equation of motion (1.32) becomes (see [18])

$$z'' + K_z(s)z = \frac{1}{\rho}\frac{\Delta p}{p} \quad (z = x \text{ or } y) \tag{1.32}$$

The general solution is given by

$$z = z_h + z_i$$

where

$$z_h'' + K_z(s)z_h = 0$$
$$z_i'' + K_z(s)z_i = \frac{1}{\rho}\frac{\Delta p}{p}$$

Definition 4 (Dispersion)**.** We define dispersion the spread in position caused by the momentum offset

$$D(s) = \frac{y_i(s)}{\frac{\Delta p}{p}} \tag{1.33}$$

As a nonvanishing dispersion causes an increased beam size, D must be matched to zero at the IP in order to avoid luminosity loss.

If we consider the spread in tune we can define the chromaticity.

Definition 5 (Chromaticity)**.** We define as chromaticity the variation of tune with respect to the variation of momentum, mathematically

$$\Delta Q = Q' \frac{\Delta p}{p_0} \tag{1.34}$$

with the constant Q' called the chromaticity.

We can easily understand the meaning of chromaticity thinking of the formula for the strength of a quadrupole. Remembering the (1.5)

$$K = \frac{1}{B\rho} g = \frac{e}{p} g$$

where

$$g = \frac{\partial B_y}{\partial x} = \frac{\partial B_x}{\partial y}$$

We get

$$\begin{aligned} \Delta K &= \frac{\partial K}{\partial p} \Delta p \\ &= -\frac{eg}{p_0} \frac{\Delta p}{p_0} = \\ &= -K_0 \frac{\Delta p}{p_0} \end{aligned}$$

Proposition 9. We can calculate the chromaticity using the formula

$$Q' = \frac{1}{4\pi} \oint K(s)\beta(s)ds \tag{1.35}$$

1.2.3 Non linearities and resonances

Let

$$H = H_0 + H_1 \tag{1.36}$$

where H_0 is the unperturbed Hamiltonian. Using the coordinate system represented by the triple (x, y, θ) where

$$\theta = \frac{s}{R}$$

we can write

$$H_0 = \frac{1}{2}\left(K_1(\theta)x^2 + K_2(\theta)y^2 + p_x^2 + p_y^2\right)$$

Proposition 10. H_1 depends on the angular coordinate θ in an oscillatory way, where the frequency of oscillation is given by

$$(j-k)\,Q_x + (l-m)\,Q_y + q \tag{1.37}$$

Specifically one can express it, as

$$H_1 = \sum_n \sum_{\substack{j,k,l,m=0 \\ j+k+l+m=n}}^n \sum_{q-\infty}^{\infty} h_{j,k,l,m,q}^{(n)} a_1^j \bar{a}_1^k a_2^l \bar{a}_2^m e^{i((j-k)Q_x+(l-m)Q_y+q)\theta} \tag{1.38}$$

Proof. We can write the general solution as

$$x = a_1 u e^{iQ_x\theta} + \bar{a}_1 \bar{u} e^{-iQ_x\theta} \tag{1.39}$$
$$y = a_2 v e^{iQ_y\theta} + \bar{a}_2 \bar{v} e^{-iQ_y\theta}$$

where $\bar{u}$ designates the complex conjugate of u and

$$a_1 = i\left((\bar{u}' - iQ_x\bar{u})x - \bar{u}p_x\right)e^{-iQ_x\theta} \tag{1.40}$$
$$a_2 = i\left((\bar{v}' - iQ_y\bar{u})z - \bar{v}p_y\right)e^{-iQ_y\theta}$$

From (1.39) we derive

$$p_x = a_1\left(u' + iQ_xu\right)e^{iQ_x\theta} + \bar{a}_1\left(\bar{u}' - iQ_x\bar{u}\right)e^{-iQ_x\theta} \tag{1.41}$$
$$p_y = a_2\left(v' + iQ_yv\right)e^{iQ_y\theta} + \bar{a}_2\left(\bar{v}' - iQ_y\bar{v}\right)e^{-iQ_y\theta}$$

For small perturbation we can write H_1 as

$$H_1 = \sum_n \sum_{\substack{J,K,L,M=0 \\ J+K+L+M=n}}^n b_{J,K,L,M}^{(n)}(\theta)x^J p_x^K y^L p_y^M \tag{1.42}$$

Inserting (1.39), (1.41) and (1.40) in (1.42) we obtain

$$H_1 = \sum_n \sum_{\substack{j,k,l,m=0 \\ j+k+l+m=n}}^n h_{j,k,l,m}^{(n)}(\theta)a_1^j \bar{a}_1^k a_2^l \bar{a}_2^m \exp\left(i\left((j-k)\,Q_x + (l-m)\,Q_z\right)\theta\right) \tag{1.43}$$

where $j + k = J + K$, $l + m = L + M$ and

$$h_{j,k,l,m}^{(n)}(\theta) \approx b_{J,K,L,M}^{(n)} \sqrt[(j+k)]{\frac{\beta_x}{2R}} \sqrt[(l+m)]{\frac{\beta_y}{2R}} \exp\left(i\left((j-k)\,Q_x + (l-m)\,Q_y\right)\theta\right)$$

Taking into account the periodicity of the circular accelerator we can make a Fourier expansion

$$h_{j,k,l,m}^{(n)}(\theta) = \sum_{q-\infty}^{\infty} h_{j,k,l,m,q}^{(n)} e^{iq\theta}$$

where

$$h_{j,k,l,m,q}^{(n)} = \frac{1}{2\pi} \int_0^{2\pi} h_{j,k,l,m}^{(n)}(\theta) e^{-iq\theta} d\theta$$

Therefore we can write

$$H_1 = \sum_n \sum_{\substack{j,k,l,m=0 \\ j+k+l+m=n}}^{n} \sum_{q-\infty}^{\infty} h_{j,k,l,m,q}^{(n)} a_1^j \bar{a}_1^k a_2^l \bar{a}_2^m e^{i((j-k)Q_x+(l-m)Q_y+q)\theta}$$

As supposed.   □
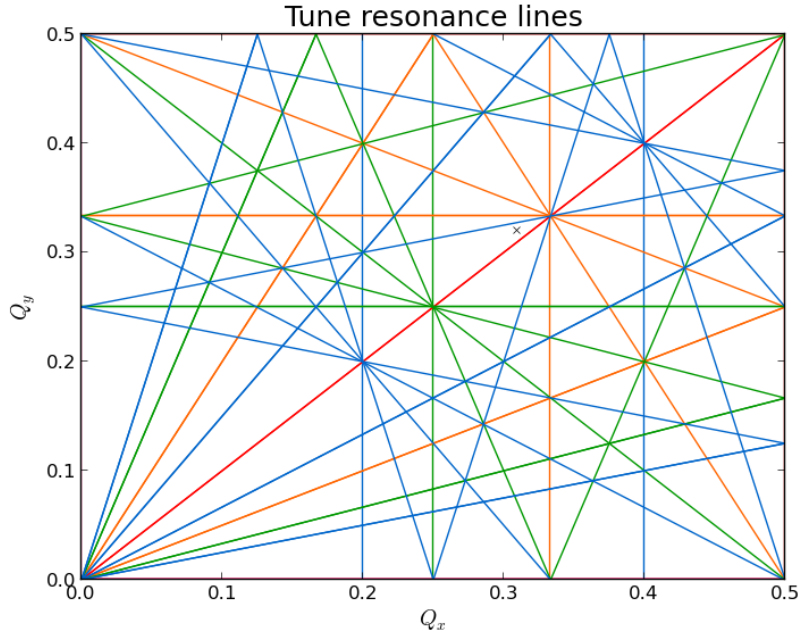
Figure 1.7: resonance lines of order 1 to 6 in the tune region $[0, 0.5] \times [0, 0.5]$ and the fractional value of the LHC nominal tune (black 'X')

For small perturbations the significant contributions take place only at

low frequency. With this assumption we can obtain

$$H_1 = \sum_{\nu} \sum_{q+s=\nu} h_{qqss0}^{(2\nu)} (a_1 \bar{a}_1)^q (a_2 \bar{a}_2)^s + \tag{1.44}$$
$$+ \kappa \, a_1^j \, \bar{a}_1^k \, a_2^l \, \bar{a}_2^m \, e^{i(n_x Q_x + n_y Q_y - p)\theta} +$$
$$+ \bar{\kappa} \, \bar{a}_1^j \, a_1^k \, \bar{a}_2^l \, a_2^m \, e^{-i(n_x Q_x + n_y Q_y - p)\theta}$$

Where

$$j - k = \pm n_x \tag{1.45}$$
$$l - m = \pm n_y$$
$$q = \mp p$$

$n_x, n_y, p \in \mathbb{Z}$ The coefficients $h_{qqss0}^{(2\nu)}$ can stabilize the resonances on the other hand $\kappa = h_{jklm-p}$ are excitation coefficients and create instabilities.

When the transverse tune satisfy the resonance condition

$$n_x Q_x + n_y Q_y = p \tag{1.46}$$

the effect of a perturbation becomes important, the amplitude of the motion may grow rapidly and the particle can be lost.

This is why in the circular accelerators we try to have a tune far away from any integer and fractional values. In addition if we define as *order of resonance*

$$N = |n_x| + |n_z| \tag{1.47}$$

we see that the destabilizing effects are more important for smaller resonance order, so that it is better to stay away from resonance lines of lower order. The picture 1.7 gives an idea of the resonance line where lines with red colors correspond to a smaller resonance order (so are more critic) than the ones with blue colors. In our tests we worked with two LHC optics for both the fractional part of tune was $[0.31, 0.32]$, in the figure 1.7 a black 'x' mark this point.

1.2.4   Intuitive description of Resonances

Suppose that a particle has the tune $Q_z = A + 1/n$ where $A \in \mathbb{Z}$ from the tune definition we can easily derive that after n turns the particle will be at the same point.

Let we think that in a given point s_1 there is a machine imperfection that gives a transversal kick to our particle in a given direction. It is evident that after N turns the particle has received N/n kicks in the same direction potentially not compensated, this should cause the particle loss.

This give us an intuitive feeling for the reason why resonances order of lower order (smaller n) are more dangerous respect to the ones of higher order.

1.3 Colliders

In a beam beam collision we are interested to

- the center of mass energy available

- the number of events (particle-particle scattering)

1.3.1 Energy

With regard to the available energy we note that the collision between two beams provides more energy than sending a single beam on a stationary target (see [16])[1].

Let us consider two particles with mass m_1 and m_2 and energy E_1 and E_2 , the the center of mass energy available in the collision is

$$E_{cm}^2 = \left(\mathbf{p}_1^2 + \mathbf{p}_2^2\right)^2 = (E_1 + E_2)^2 - (\vec{p_1} + \vec{p_2})^2$$

where $\mathbf{p}_i$ is the quadrimomentum

$$\mathbf{p}_i^2 = E^2 - \vec{p}^2 = m^2$$

For a p-p collider $\vec{p_1} = -\vec{p_2}$ so

$$E_{cm}^2 = (E_1 + E_2)^2$$

for a fixed target accelerator $\vec{p_2} = 0$, and we have

$$E_{cm}^2 = \left(m_1^2 + m_2^2 + 2m_2 E_{1,lab}\right)$$

If we consider a beam energy of 7 TeV (this is the nominal LHC energy, for proton proton collision we have

$$E_{CM\,coll} = 14 \text{ TeV}$$
$$E_{CM\,fix} = 0.1 \text{ TeV}$$

1.3.2 Luminosity

The luminosity measures the ability of a collider to produce interactions. Mathematically we can define it as follows.

Definition 6 (Luminosity). The luminosity is the number of wanted events N_{events} per unit of time t of cross section σ_{events}

$$L = \frac{dN_{events}}{dt} \frac{1}{\sigma_{events}} \qquad (1.48)$$

---

[1]for simplicity we adopt natural units with c=1

The luminosity depends on the energy at the center of mass of the collision and it is a relativistic invariant [33].

Proposition 11. Let us consider a multibunch beam [2] with n_b bunches, and let us indicate with f the revolution frequency of the beam. We can write the luminosity L as

$$L = n_b f L_{SC}$$

where L_{SC} is the single crossing luminosity.

Also the single crossing luminosity is a relativistic invariant. If we indicate with

- N_i the number of particles in the bunch of beam i ($i = 1, 2$)

- $\vec{v}_i$ the bunch velocity

- ρ_i the particles distribution in the bunch

we can write

$$L_{SC} = R(\vec{v}_1, \vec{v}_2) \int_{-\infty}^{\infty} \int_{-\infty}^{\infty} \int_{-\infty}^{\infty} \int_{-\infty}^{\infty} N_1 N_2 \rho_1(x, z, s, t) \rho_2(x, z, s, t) dx dz ds dt$$

where

$$R(\vec{v}_1, \vec{v}_2) = \frac{1}{c} \sqrt{c^2 \|\vec{v}_1 - \vec{v}_2\|^2 - \|\vec{v}_1 \times \vec{v}_2\|^2}$$

Suppose to have two Gaussian beams

$$\rho_i(x, y, s, t) = \frac{1}{(2\pi)^{3/2} \sigma_{x i} \sigma_{y i} \sigma_{s i}} \exp\left(-\frac{x^2}{2\sigma_{x i}^2} - \frac{y^2}{2\sigma_{y i}^2} - \frac{(s - v_i t)^2}{2\sigma_{s i}^2} \right) \quad (1.49)$$

where the σ are the standard deviation of the distribution, in the transverse direction we have

$$\sigma_z = \sqrt{\epsilon_z \beta_z} \quad z = x \text{ or } y \tag{1.50}$$

ϵ is the emittance and β the betatron function as derived in (1.22)

We can obtain

$$L = \frac{N_1 N_2 f n_b}{2\pi \sqrt{\sigma_{x 1}^2 + \sigma_{x 2}^2} \sqrt{\sigma_{y 1}^2 + \sigma_{y 2}^2}}$$

In particular if we have two equals beam, i.e. $\sigma_{z 1} = \sigma_{z 2} = \sigma_z$, z= x, y and $N_1 = N_2 = N$ we can write

$$L = \frac{N^2 f n_b}{4\pi \sigma_x \sigma_y} \tag{1.51}$$
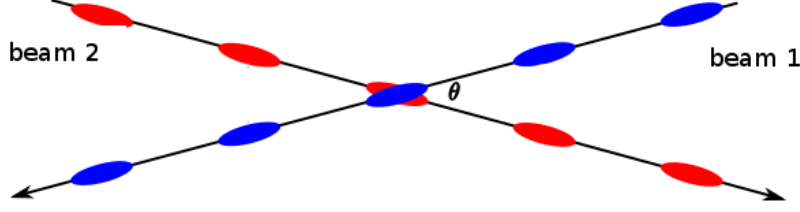
Figure 1.8: Schematic view of beam beam collision, for two beams with a crossing angle of θ

1.3.3 Crossing angle

In a collider in general two counterrotating bunches cross each other with a crossing angle θ, as shown in Figure 3.2. This is not only motivated by technical reasons but also allows one to contain destructive effects on the beam, the so-called long range beam beam effects that are the subject of the next chapter.

On the other hand the crossing angle reduces the luminosity.

Proposition 12. Let us consider two beams that cross in the plane z ($z = x$ or y) with an angle of θ. The luminosity becomes

$$L = \frac{N^2 f n_b}{4\pi\sigma_x\sigma_z}\tilde{F}_G(\theta, \sigma_y, \sigma_s) \quad z = x \text{ or } y \qquad (1.52)$$

where $\tilde{F}_G(\theta, \sigma_y, \sigma_s)$ is the luminosity reduction factor and can be written as

$$\tilde{F}_G(\theta, \sigma_z, \sigma_s) = \frac{\sigma_z\left(\sec\left(\theta\right) + 1\right)}{\sqrt{2}\sqrt{\cos\left(\theta\right)\left(\sigma_z^2 - \sigma_s^2\right) + \sigma_z^2 + \sigma_s^2}}$$

In particular for small crossing angle $\theta \ll 1$

$$\tilde{F}_G(\theta, \sigma_z, \sigma_s) \approx \frac{1}{\sqrt{1 + \theta_{PA}^2}}$$

where θ_{PA} is the *Piwinski Angle*

$$\theta_{PA} = \frac{\theta\sigma_s}{2\sigma_z} \qquad (1.53)$$

Proposition 13. Let us indicate with Δ_{in} the *inner normalized separation*

$$\Delta_{in} = \theta\sqrt{\frac{\beta_z^*}{\epsilon_z}} \qquad (1.54)$$

where β^* is the value of the betatron function at the interaction point. We can write

$$\theta_{PA} = \frac{\Delta_{in}\sigma_s}{2\beta_z^*} \qquad (1.55)$$

---

[2]this is the case for LHC, SPS, and so on

2

Beam Beam Interaction and Wire Compensation

2.1 Beam beam interaction
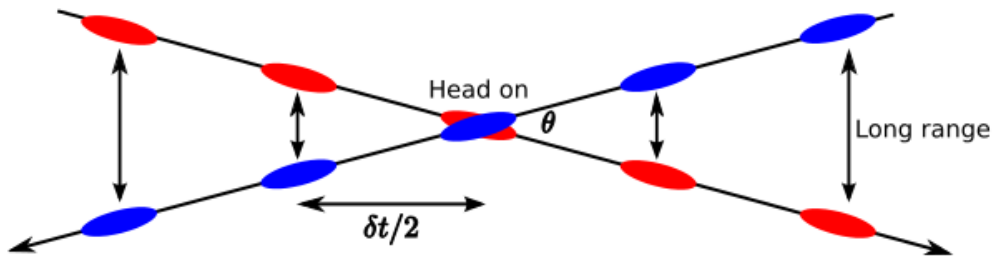
Figure 2.1: Schematic view of Head On and Long Range effects, for two beams with a crossing angle of θ and a bunch spacing of $\delta/2$ (courtesy of U. Dorda [6])

In a collider we have two charged beams that cross each other. This produces two effects:

HO the head-on beam beam interaction, which occurs when the counterrotating bunches cross each other with their center transversely aligned (without offset and without crossing angle).

LRBBI long-range beam beam interaction, which occurs at a transverse offset large compared with the beam size.

The distortion of one beam caused by the electromagnetic forces exerted by the other beam, is an effect unwanted but unavoidable. We can partially compensate the long-range beam beam ffect that is the most problematic.

To understand the beam beam effect it is easiest to start from the HO. In the analysis we can consider the interaction of a single particle of one

beam with the electromagnetic field generated by the other beam. This is the so called *weak-strong* point of view.

2.1.1   Head On

Proposition 14. The transverse force exerted on a particle with velocity $\vec{v}_1$ from a counter-rotating bunch that moves with velocity $\vec{v}_2$ is

$$F_\perp = (1 + \beta_1\beta_2)\, eE_\perp \tag{2.1}$$

Where β_i is the relativistic function: $\beta_i = \frac{v_i}{c}$

Proof. Obviously $F_\perp$ is a Lorentz Force

$$F = e\left(\vec{E} + \vec{v_1} \times \vec{B}\right)$$

We need to find $\vec{E}$ and $\vec{B}$. We notice that in the rest frame the magnetic field is zero. Applying the transformation we have

$$E_s = E'_s \qquad\qquad\qquad B_s = 0$$
$$E_\perp = \gamma_2 E'_\perp \qquad\qquad\qquad B_\perp = -\frac{\gamma_2}{c^2}\vec{v}_2 \times \vec{E}'$$

where the primed quantity refers to the rest frame, we obtain

$$F_\perp = (1 + \beta_1\beta_2)\, e\gamma_2 E'_\perp = (1 + \beta_1\beta_2)\, eE_\perp \tag{2.2}$$

$\square$

Proposition 15 (Gaussian Beam beam)**.** Let us consider a Gaussian beam distribution

$$\rho(x, y, s) = \frac{Ne}{(2\pi)^{3/2}\sigma_x\sigma_y\sigma_s} \exp\left(-\frac{x^2}{2\sigma_x^2} - \frac{y^2}{2\sigma_y^2} - \frac{s^2}{2\sigma_s^2}\right)$$

since $\sigma_s \gg \sigma_z$ (z = x, y) we can consider a bidimensional gaussian distribution in the plane $x - y$ ([19])

$$\rho(x, y) = \frac{ne}{(2\pi)^{3/2}\sigma_x\sigma_z} \exp\left(-\frac{x^2}{2\sigma_x^2} - \frac{y^2}{2\sigma_y^2}\right)$$

where n is the line density. The potential V that satisfies the equation

$$\nabla^2 V = \frac{\rho}{\varepsilon_0}$$

with this distribution function is (see [20, 1, 14, 19])

$$V(x, y, \sigma_x, \sigma_y) = \frac{ne}{4\pi\varepsilon_0} \int_0^\infty \frac{\exp\left(-\frac{x^2}{2\sigma_x^2+q} - \frac{z^2}{2\sigma_y^2+q}\right)}{\sqrt{2\sigma_x^2 + q}\sqrt{2\sigma_y^2 + q}} \tag{2.3}$$

If we indicate with $erf(z)$ the complex error function

$$w(z) = e^{-z^2} \left(1 + \frac{2i}{\sqrt{\pi}} \int_0^z e^{\zeta^2} d\zeta \right) \tag{2.4}$$

we can write

$$
\begin{aligned}
E_x - iE_y &= -\frac{\partial V}{\partial x} + i\frac{\partial V}{\partial y} \\
&= -\frac{ine}{2\varepsilon_0 \sqrt{2\pi \left(\sigma_x^2 - \sigma_y^2 \right)}} \cdot \\
&\quad \cdot \left(w(a + ib) - exp\left(-(a + ib)^2 + \left(ac + i\frac{b}{c} \right) \right) w\left(ac + i\frac{b}{c} \right) \right)
\end{aligned}
$$

where

$$a = \frac{x}{\sqrt{2 \left(\sigma_x^2 - \sigma_y^2 \right)}}$$

$$b = \frac{y}{\sqrt{2 \left(\sigma_x^2 - \sigma_y^2 \right)}}$$

$$c = \frac{\sigma_y}{\sigma_x}$$

hence [1]

$$
\begin{aligned}
E_x = &\frac{ine}{2\varepsilon_0 \sqrt{2\pi \left(\sigma_x^2 - \sigma_y^2 \right)}} \cdot \\
&\cdot \Im \left(w\left(\frac{x + iy}{\sqrt{2 \left(\sigma_x^2 - \sigma_y^2 \right)}} \right) - \exp\left(-\frac{x^2}{2\sigma_x^2} + \frac{y^2}{2\sigma_y^2} \right) w\left(\frac{x\frac{\sigma_z}{\sigma_x} + iy\frac{\sigma_x}{\sigma_z}}{\sqrt{2 \left(\sigma_x^2 - \sigma_y^2 \right)}} \right) \right) \cdot
\end{aligned}
$$

$$
\begin{aligned}
E_y = &\frac{ine}{2\varepsilon_0 \sqrt{2\pi \left(\sigma_x^2 - \sigma_y^2 \right)}} \\
&\cdot \Re \left(w\left(\frac{x + iy}{\sqrt{2 \left(\sigma_x^2 - \sigma_y^2 \right)}} \right) - \exp\left(-\frac{x^2}{2\sigma_x^2} + \frac{y^2}{2\sigma_y^2} \right) w\left(\frac{x\frac{\sigma_y}{\sigma_x} + iy\frac{\sigma_x}{\sigma_y}}{\sqrt{2 \left(\sigma_x^2 - \sigma_y^2 \right)}} \right) \right)
\end{aligned}
$$

And for the force, thinking that the particle and the bunch have the same velocity ($\beta_1 = \beta_2 = \beta$)

$$F_x - iF_y = -e \left(1 + \beta^2 \right) \left(E_x - iE_y \right)$$

In particular for a round beam we have
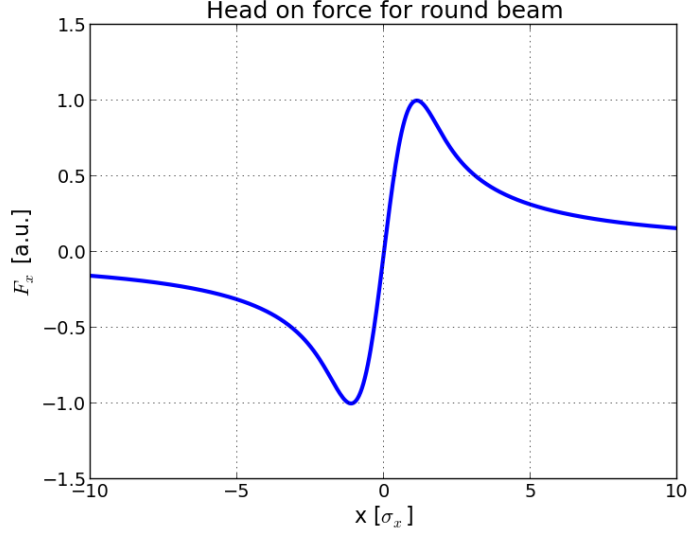
Figure 2.2: Head on force for a round Gaussian beam in arbitrary units

Proposition 16 (Head On force for a Gaussian round beam)**.**

$$F_x = \frac{-ne^2\left(1+\beta^2\right)}{2\pi\varepsilon_0}\frac{x}{r^2}\left(1 - \exp\left(\frac{r^2}{2\sigma^2}\right)\right) \qquad (2.5)$$

$$F_y = \frac{-ne^2\left(1+\beta^2\right)}{2\pi\varepsilon_0}\frac{y}{r^2}\left(1 - \exp\left(\frac{r^2}{2\sigma^2}\right)\right)$$

where $r = \sqrt{x^2 + y^2}$

The dependence is shown in Figure 2.2

Proposition 17 (Beam beam kick)**.** Using the newton law from the force we obtain the deflection of the particle for head-on beam beam effect

$$\Delta x' = \frac{-eNr_0}{\gamma}\frac{x}{r^2}\left(1 - \exp\left(\frac{r^2}{2\sigma^2}\right)\right) \qquad (2.6)$$

$$\Delta y' = \frac{-eNr_0}{\gamma}\frac{y}{r^2}\left(1 - \exp\left(\frac{r^2}{2\sigma^2}\right)\right)$$

where r_0 is the classical particle radius

$$r_0 = \frac{e^2}{4\pi\varepsilon_0 mc^2}$$

Proof. To simplify consider radial coordinates and the radial force. We can write the force as

$$F_r(r) = -\frac{ne^2\left(1+\beta^2\right)}{2\pi\epsilon_0 r}\left(1 - \exp\left(-\frac{r^2}{2\sigma^2}\right)\right)$$

To obtain the total force we have to multiply by the longitudinal distribution density. Supposing that we have a Gaussian shape with a width of σ_s and that the bunch is moving in the negative s direction with speed v, we have

$$F_r(r,s,t) = -\frac{Ne^2\left(1+\beta^2\right)}{(2\pi)^{3/2}\epsilon_0\sigma_s}\frac{1}{r}\left(1-\exp\left(-\frac{r^2}{2\sigma^2}\right)\right)\exp\left(-\frac{(s+vt)^2}{2\sigma_s^2}\right)$$

Using the Newton law

$$mc\beta\gamma\Delta r' = \int_{-\infty}^{+\infty}F_r(r,s,t)dt$$

we obtain

$$\Delta r' = \frac{-eNr_0}{\gamma}\frac{1}{r}\left(1-\exp\left(\frac{r^2}{2\sigma^2}\right)\right)$$

$\square$

From the deflection we can easily derive the linear tune shift

Proposition 18 (Linear tune shift). The linear tune shift is given, for an elliptic beam by

$$\xi_z = \frac{Nr_0\beta_z^*}{2\pi\gamma\sigma_y\left(\sigma_x+\sigma_z\right)}$$

where $z = x$ or y. For a round beam

$$\xi_z = \frac{Nr_0\beta_z^*}{4\pi\gamma\sigma_z^2}$$

Proof. For simplicity we consider here only the round case. The tune shift for the elliptic case is obtained in a similar way.

We notice that the tune shift in the transverse direction z (with $z = x$ or y) due to the beam beam head-on effect is given by

$$\Delta Q_z = \frac{1}{4\pi}\int\beta_z(s)K_z(s)ds$$

where, supported by what we have derived in the section 2.1.1 we can write

$$K_z = \frac{1+\beta^2}{B\rho v}\frac{\partial E_z}{\partial z}$$

$$= \frac{1+\beta^2}{mc^2\beta^2\gamma}\frac{\partial E_z}{\partial z}$$

Remembering what we found in (2.2) we can write

$$\Delta Q_z \propto \frac{\partial F_z}{\partial z} \tag{2.7}$$
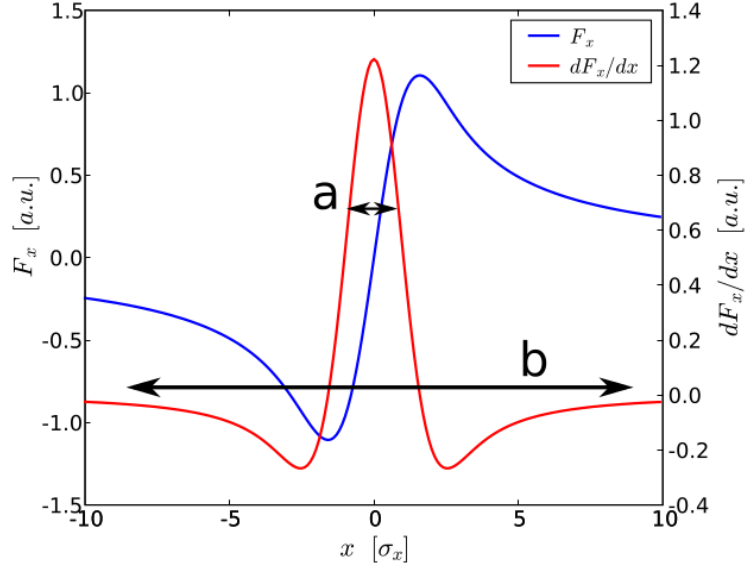
Figure 2.3: Head on force and its derivative for a round Gaussian beam (courtesy of U. Dorda [6])

Figure 2.3 shows the behaviour of the force derivative. As we see better in the Chapter 3 the head-on beam-beam collision causes a tune spread dependent on the particle position.

For $r \ll \sigma$ and $\beta \to 1$ we can consider the linear kick

$$\Delta r' \approx \frac{eNr_0}{\gamma\sigma^2}r$$

Let define f the focal length of the linear kick

$$\frac{1}{f} = \frac{\Delta r'}{r} \approx \frac{eNr_0}{\gamma\sigma^2}$$

the linear tune shift is simply obtained as

$$\xi = \frac{1}{4\pi}\frac{\beta^*}{f} \approx \frac{eNr_0\beta^*}{4\pi\gamma\sigma^2}$$

where β^* indicate the betatron function at the interaction point.   □

The head-on collisions happen at the Interaction point (IP). In our simulation we considered only the IP1 (s=0 m) and IP5 (13329.29 m) in the LHC, where the ATLAS and CMS experiments are located.
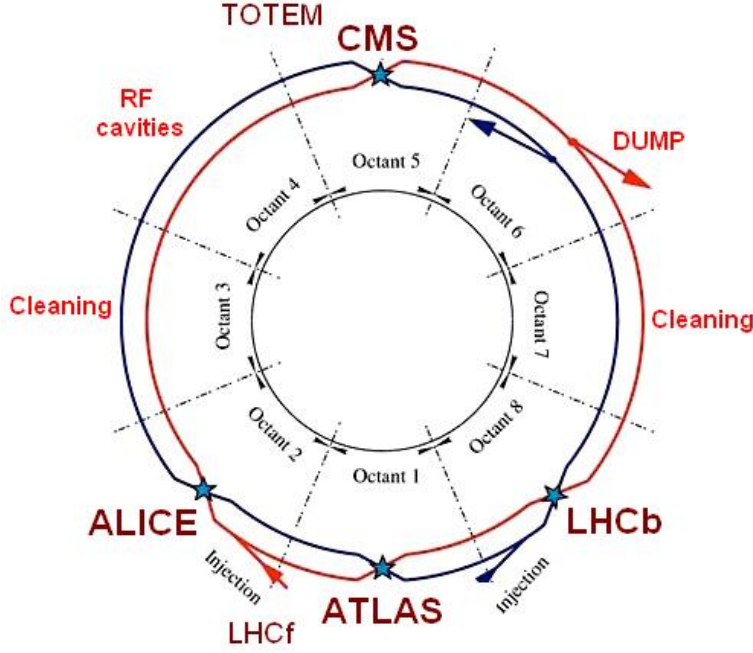
Figure 2.4: Interaction Points in LHC

2.1.2 Long Range

We speak of long-range collision when we have a transverse offset large compared with the beam size.

We can obtain the formulas for long-range starting from the ones found for the head-on and applying the transformation $z \rightarrow z + d$ where z is the coordinate of the separation (x or y) and d is the separation length.

Suppose for example to have a horizontal crossing angle, the equations (2.6) become

$$\Delta x' = \frac{-eNr_0}{\gamma} \frac{x+d}{r^2} \left(1 - \exp\left(\frac{r^2}{2\sigma^2} \right) \right) \tag{2.8}$$

$$\Delta y' = \frac{-eNr_0}{\gamma} \frac{y}{r^2} \left(1 - \exp\left(\frac{r^2}{2\sigma^2} \right) \right)$$

where

$$r = \sqrt{(x+d)^2 + y^2}$$

And for the tune shift we have [6]

$$\Delta Q_x = \frac{2Nr_0}{4\pi\gamma\epsilon_x r^2} \left(1 - \exp\left(\frac{r^2}{2\sigma^2} \right) \left(1 + r^2 \right) \right) \tag{2.9}$$

$$\Delta Q_y = \frac{2Nr_0}{4\pi\gamma\epsilon_y r^2} \left(1 - \exp\left(\frac{r^2}{2\sigma^2} \right) \right)$$

We notice that the long-range effects break the symmetry between the two planes. Choosing alternate crossing planes (HV), as actually is done in LHC helps in reducing the long-range effect [25, 13].

We notice [15, 14]) that

$$\Delta Q_{HO} \propto \frac{N}{\epsilon_n}$$

$$\Delta Q_{lr} \propto -\frac{N}{d^2} = \frac{N\epsilon_n}{\theta^2 \beta^* \gamma}$$

where ϵ_n is the normalised beam emittance defined in (1.25)

Therefore for the head-on point of view it is advantageous to increase the transverse emittance, and we can also reduce β^* to increase luminosity without any effect on the tune shift.

The situation changes for the long-range where the effect depends on β^*, and it is advantageous to decrease the transverse emittance. We also see that the dependence on the separation is quadratical. A small reduction in the crossing angle causes a big effect on the tune shift.

Could be interesting to follow the approach of [26] to understand better the dependence of long-range interaction on the crossing angle.

We can try to lump together the long-ranges, supposing that they occur at a betatron phase advance close to $\pi/2$ with respect to the IP. This allows us to express the kick as a change in the coordinate Δz instead of the slope $\Delta z'$.

Proposition 19. Let us indicate with n_{par} the number of long-range encounter (parasitic collision), and with θ_c the crossing angle between the beam. For a horizontal crossing angle we can write

$$\Delta x = -n_{par}\frac{2r_0 N}{\gamma}\left(\frac{x' + \theta_c}{\theta_t^2}\left(1 - \exp\left(-\frac{\theta_t^2}{2\sigma_{x'}^2}\right)\right) - \frac{1}{\theta_c}\left(1 - \exp\left(-\frac{\theta_c^2}{2\sigma_{x'}^2}\right)\right)\right)$$

$$\Delta y = -n_{par}\frac{2r_0 N}{\gamma}\frac{y'}{\theta_t^2}\left(1 - \exp\left(-\frac{\theta_t^2}{2\sigma_{y'}^2}\right)\right)$$

where

$$\theta_y = \sqrt{\left(x' + \theta_c\right)^2 + y'^2}$$

and $\sigma_{x',y'}$ is the rms beam divergence at the IP.

2.1.3   Resonances

If we add the beam-beam effects the Hamiltonian (1.28) with small manipulation becomes [38, 27, 22])

$$H(J_x, J_y, \psi_x, \psi_y, \theta) = Q_{0\,x}J_x + Q_{0\,y}J_y + V(J_x, J_y, \psi_x, \psi_y)\sum_p \frac{e^{ip\theta}}{2\pi} \quad (2.10)$$

where Q_0 is the unperturbed tune and V is the beam beam potential.

$$V = \frac{1}{2\pi} \sum K_{m,n}(J_x, J_y) e^{-j(m\psi_x + n\psi_y - l\theta)}$$

with

$$K_{m,n} = \frac{N r_0}{(2\pi)^2 \gamma} \iint \frac{-\exp\left(-\frac{\beta_x J_x \cos^2 \phi_x}{2\sigma_x^2 + t} - \frac{\beta_y J_y \cos^2 \phi_y}{2\sigma_y^2 + t}\right)}{\sqrt{2\sigma_x^2 + t}\sqrt{2\sigma_y^2 + t}} e^{j(m\phi_x + n\phi_y)} d\phi_x d\phi_y dt$$

For the head-on we can write

$$V(J, \psi) = \frac{8\pi\xi\sigma^2}{\beta}\left(-E_i\left(-\frac{r^2}{2\sigma_y^2}\right) + \ln\left(\frac{r^2}{2\sigma_y^2}\right)\right)$$

with $r = \sqrt{x^2 z^2}$. where E_i is the exponential integral

$$E_i(u) = \int_{-\infty}^{u} \frac{e^{u'}}{u'} du'$$

If we consider the long-range beam beam potential in one direction can be written as

$$V(J, \psi) = -\frac{r_0 N n_{par}}{\gamma}\left(-E_i\left(-\frac{(y' + \theta_c)^2}{2\sigma_{y'}^2}\right)\right.$$
$$\left. + \ln\left(\frac{(y' + \theta_c)^2}{2\sigma_{y'}^2}\right) - \frac{2y'}{\theta_c}\left(1 - \exp\left(-\frac{\theta_c^2}{2\sigma_{y'}^2}\right)\right)\right)$$

When the tune is near a resonance line we can approximate the Hamiltonian as

$$H(J_x, J_y, \psi_x, \psi_z, \theta) = Q_{0\,x} J_x + Q_{0\,y} J_y + g(J_x, J_y) + h \cos\left(m\psi_x + n\psi_y - l\theta\right)$$

The beam beam head-on interaction produces non linear resonances at

$$mQ_x + nQ_y = l$$

with m and n *even*. The long-range beam beam interactions also produce resonances with m and n *odd*.

2.2 Wire Compensation

2.2.1 Principles of the wire compensation

To compensate the long-range effect we need a non-linear lens that can be assimilated to a separated beam. If the separation is large enough the long-range forces scale with $1/r$, this can be simulated by a wire parallel to the beam like the one shown in Figure 2.5.
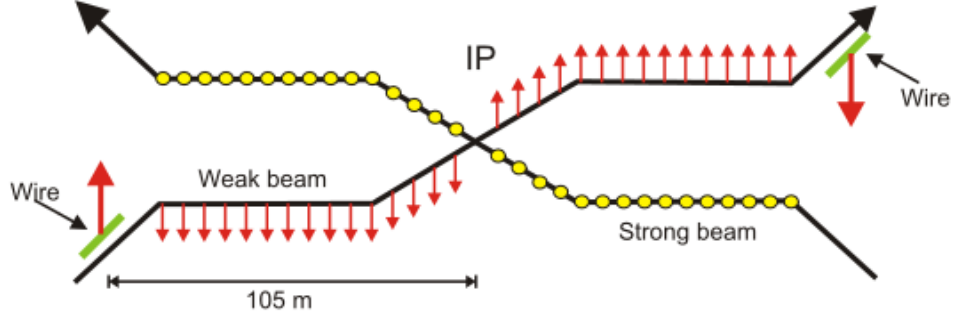
Figure 2.5: Schematic view of the wire correction (courtesy of U. Dorda [6])

Suppose to have a thin wire long l_w with a DC current I_w located in the horizontal plane the change in IP coordinates is

$$\Delta x = \frac{\mu_0 I_w l_w}{2\pi (B\rho)} \left(\frac{x' + \theta_{c,w} \pm \phi_x \frac{x}{\beta_x^*}}{\theta_{t,w}^2} - \frac{1}{\theta_{cw}} \right)$$

$$\Delta x' = -(\pm) \phi_x \frac{\Delta x}{\beta_x^*}$$

$$\Delta y = \frac{\mu_0 I_w l_w}{2\pi (B\rho)} \left(\frac{y' + \pm \phi_y \frac{y}{\beta_y^*}}{\theta_{t,w}^2} - \frac{1}{\theta_{cw}} \right)$$

$$\Delta y' = -(\pm) \phi_y \frac{\Delta y}{\beta_y^*}$$

where $\theta_{c,w}$ is the angle at the IP representing the transverse distance between the beam and the wire,

$$\theta_{t,w} = \sqrt{\left(x' + \theta_{c,w} \pm \phi_x \frac{x}{\beta_x^*} \right)^2 + + \left(y' + \pm \phi_y \frac{y}{\beta_y^*} \right)^2}$$

an the $\pm$ sign depends on the wire position with respect to the IP side.

With some manpulation we can obtain for a wire positioned in (x_w, z_w)

$$\Delta x' = \frac{\mu_0 I_w l_w}{2\pi (B\rho)} \left(\frac{x - x_w}{r^2} + \frac{x_w}{d^2} \right)$$

$$\Delta y' = \frac{\mu_0 I_w l_w}{2\pi (B\rho)} \left(\frac{y - y_w}{r^2} + \frac{y_w}{d^2} \right)$$

where

$$d = \sqrt{x_w^2 + y_w^2}$$

We can use this formula to compare the long-range kick with the wire kick, as shown in the Figure 2.6. For large distance the two effects are identical.
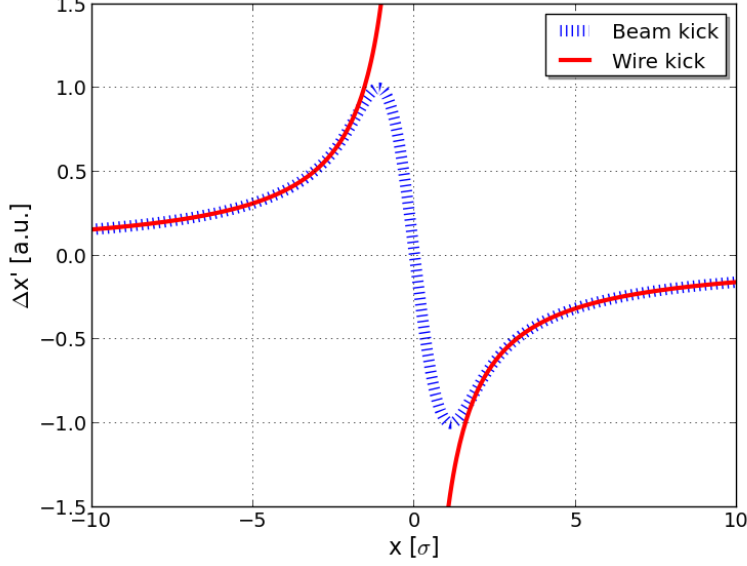
Figure 2.6: Schematic view of the beam beam kick and possible wire compensation

To calculate the tune shift we start as usual from

$$\Delta Q_z = \pm \frac{1}{4\pi} \int \beta_z(s) \Delta K_z(s) ds$$

with

$$\Delta K_z(s) = \frac{1}{B\rho} \frac{\partial B_{w\,z}}{\partial z}$$

where $B_{w\,z}$ is the magnetic field generated by the wire. For a DC wire with current I_w located in the vertical plane $(0, y_w)$ We have

$$B_{w\,x}(0, y) = \frac{\mu_0 I_w}{2\pi \, (y_w - y)}$$

hence

$$\left. \frac{\partial B_{w\,x}}{\partial y} \right|_{(0,0)} = \frac{\mu_0}{2\pi y_w^2} = \left. \frac{\partial B_{w\,y}}{\partial x} \right|_{(0,0)}$$

Assuming that the betatron function is constant along the wire's length, l_w, and neglecting the fringe field effect of the wire, we obtain

$$\Delta Q_z = \pm \frac{\mu_0 I_w l_w \beta_z}{8\pi^2 B\rho z_w^2} \tag{2.11}$$

If we consider a wire located in a generic point (x_w, y_w) with some cal-

culation we can write the tune shift as

$$\Delta Q_x = -\frac{\mu_0 I_w l_w}{2\pi(B\rho)} \frac{\beta_x}{4\pi} \left(-\frac{dx_w^2}{(dx_w^2 + dy_w^2)^2} \right) \tag{2.12}$$

$$\Delta Q_y = -\frac{\mu_0 I_w l_w}{2\pi(B\rho)} \frac{\beta_y}{4\pi} \left(-\frac{dx_w^2}{(dx_w^2 + dy_w^2)^2} \right)$$

2.2.2   Wire longitudinal position

Equation (2.12) shows that the tune shift caused by the wire compensator depends on the betatron function. As we want compensate in the same way the tune shift in both the x and z plane, a requirement for the s position is

$$\beta_x(s) \approx \beta_y(s) \tag{2.13}$$

Suppose that this is not possible, [1] and that we have two wire locations to use, we obtain the best results where

$$\frac{\beta_x(s_1)}{\beta_y(s_1)} \approx \frac{\beta_y(s_2)}{\beta_x(s_2)} \tag{2.14}$$

We also need to choose a location where the betatron phase advance between the LR collision points and the wire is as small as possible [6].

position	IP	IP dist [m]	β_x [m]	β_y [m]	$\Delta\mu_x$ [2 π]	$\Delta\mu_y$ [2 π]
BBC	IP1	104.9	1738.1	1734.8	0.25	0.25
	IP5	104.9	1739.2	1734.9	0.25	0.25
TCT opt β	IP1	149.7	559.4	1566.9	-0.26	0.26
	IP5	-147.3	1575.7	606.8	-0.26	-0.26

Table 2.1: Optics parameters at the BBC location and at the TCT opt β with the nominal optics ($\beta^* = 0.55$ m).

If we use the nominal LHC optics [2] a good solution proposed by Koutchouk [11] was to put the wire at 105 m after IP1 and IP5. This location is called the BBC (Beam Beam Compensator). For technical reason ([32]) this location is not immediately available. To install a prototype for test pourposes we have found another location, a location at 150 m after IP1 and at 148 m before IP5. We called this location TCT opt β because we find it starting from a TCT (Tertiary Collimator) location (147 m before each IP) and moving one of the two wires to the other side of the Ip to obtain a better result.

Table 2.1 shows the optics values for these two possible solutions. Betatron function and phase advance from the nearest IP. Our tests involved a lot of other different solution, more details are shown in Chapter 4

---

[1] this is what is happening at the moment in LHC
[2] See 3.1 for more details

2.2.3 Wire Transverse position and current
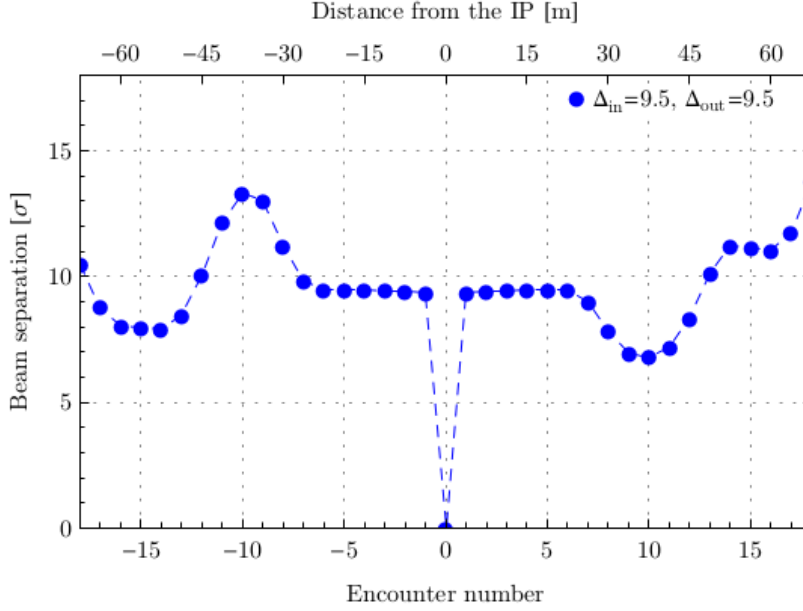
Figure 2.7: Beam separation for nominal LHC (courtesy of Guido Sterbini [33])

The transverse position of the wire should be equal to the average distance at the long-range collisions. For nominal LHC we can considere 16 Long range collision at each IP side with an average distance of 9.5 σ (see figure 2.7).

The optimum current is obtained by equating the effects of the sum of $n_p ar$ long-range kick and the effect of the wire kick. We can write

$$I_{opt} = \frac{n_{par}ceN_b}{l_w} \tag{2.15}$$

where N_b is the number of particles per opposite bunch. For the nominal LHC $N_b = 1.15\,10^{11}$, Using this value we find that the optimum wire current for a 1 m long wire is $I_{opt} = 176.8$ A [28].

The wire must be positioned in the shadow of a collimator this forces us to move the basic transverse position from 9.5σ to 11σ. From (2.12) that

$$\Delta Q_z \propto \frac{I_w}{z_w^2}$$

and to obtain the same tune shift therefore we need to scale the current quadratically and we obtain $I_{scal} = 237.0$ A.

3

Simulation Tools and Concepts

3.1 MADX and LHC Optics

To calculate the optics parameters for the LHC we used the MAD-X (Methodical Accelerator Design) program [17, **?**].

More in details we define in the input files the properties of the machine, the crossing angle and the offset between the two beams at the IPs, the energy (7 TeV), the type of particles (protons) and the number of particles for each beam $(1.15 \ 10^{11})$, we add markers in the points we are interested to, hence for these points we use MAD-X to obtain the parameters (the Courant Snider parameters, β, α and γ and so on) and the rotation map between two points.

All these values are furnished as input to the bbtrack program using a personal script that automatically produces the conversion between the two formats.

We tested two different optics:

- The nominal LHC Optics (with $\beta* = 0.55$ m)

- A modified optics (with $\beta 6* = 0.60$ m, courtesy of S. Fartoukh)

Optics	β_x^* [m]	β_y^* [m]	Q_x	Q_y	σ_x $[10^{-5}$ m]	σ_y $[10^{-5}$ m]
Nominal LHC Optics	0.55	0.55	64.31	59.32	1.6627	1.6627
Modified LHC Optics	0.60	0.60	62.31	60.32	1.7366	1.7366

Table 3.1: Main Optics parameters, computed with MAD-X .

The modified optics was based on the ATS scheme [10] and taylored by S. Fartoukh so as to give optimized compensator performance with a wire
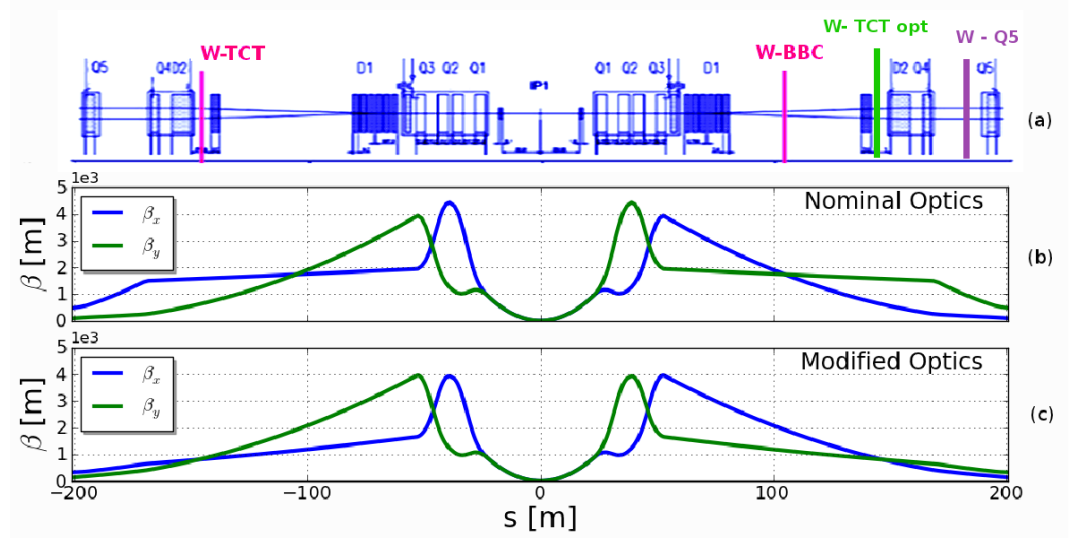
Figure 3.1: Wire locations (top), and β functions for the nominal (center) and for the modified optics (bottom).

placed at the TCT (2012). The main optics values for the nominal optics and modified are summarized in the Table 3.1.

For both the optics we have

- Energy: 7 TeV

- Relativistic Lorentz factor $\gamma = 7460$

- Proton current (i.e. number of proton considered in the "strong beam") $= 1.15\,10^{11}$

As visible in Figure 3.1 and in the Table 3.2, the values of betatron functions are equal at the BBC location with the nominal optics, and almost equal for the modified optics and the TCT positions.

We will show in the Chapter 4 that the BBC locations give us still better results. This is because the values of the β functions are greater in BBC location with nominal optics than at TCT location with the modified optics.

In our tests we also tried some other locations searching for a good compromise between technical requirements and compensations. These positions are indicated in Figure 3.1.

position	Optics	IP	IP dist [m]	β_x [m]	β_y [m]
BBC	Nom	IP1	104.9	1738.1	1734.8
		IP5	104.9	1739.2	1734.9
Q5	Nom	IP1	199.0	105.9	503.0
		IP5	199.0	105.9	503.0
TCT	Nom	IP1	-146.9	1577.2	614.9
		IP5	-147.3	1575.7	606.8
TCT opt β	Nom	IP1	149.7	559.4	1566.9
		IP5	-147.3	1575.7	606.8
TCT opt β 2	Nom	IP1	-146.9	1577.2	614.9
		IP5	149.5	563.2	1567.6
BBC	Mod	IP1	104.9	1914.9	1142.1
		IP5	104.9	1915.9	1142.4
TCT	Mod	IP1	-146.9	801.0	802.5
		IP5	-147.3	798.0	794.1

Table 3.2: Optics parameters for all tested locations, Nominal LHC Optics ("Nom") and the modified optics ("Mod") ([29]).

3.2   Tune Footprint Analysis

As we have seen it is important that the particles tune doesn't touch resonance lines with low order, it means that the tune doesn't satisfy the condition

$$n_x Q_x + n_y Q_y = p$$

where

$$N = |n_x| + |n_y|$$

is the resonance order.

In our tests we plot resonance until the order 9 but we can see that the dangerous effects are visibles until the resonance order 5 [35].

Since the tune shift effects are more visible for particles with big amplitude we modify a Gaussian distribution to have more particles with a radius between 4 and 6.5 σ.

We track each particles using the bbtrack code for 50.000 turns and calculate the tune using the fast fourier transform (FFT) method, we plot the results with the resonance lines checking whenthe tuen footprint touches one resonance line (see fig.: 3.3).
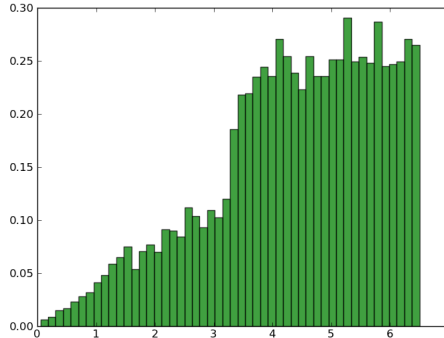
Figure 3.2: Particle distribution used for the Tune tests
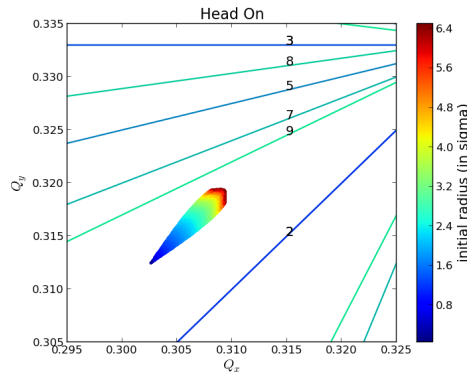
Figure 3.3: The Figure shows the tune footprint for the Head On test with the resonance lines until the order 9

3.3 Stability Analysis

Examining the size and location of the tune footprint allows to understand the causes of the instabilities but it does not provide a quantitative values.

We could think to examine the particle loss, i.e. the particles exceeding a certain amplitude, but with simulation we can simulate a maximum of 1 milion of turns. If we think that the LHC is long 27 km and that the protons move with a velocity near to the speed of light (300.000 km/s), we can model at the best of our possibilities the fist 9 seconds of the experiment, evidently this criterion turns out not to be sufficiently sensitive.

We decide to choose the Lyapunov exponent as stability criterion. This tends to overestimate the impact of the resonances but it still shows the best agreement with experimental data.

From a theoretical point of view we can define the Lyapunov exponent in the following way [31].

Definition 7 (Lyapunov exponent)**.** Let us indicate with $d(N)$ the transverse distance between two particles at the turn N taken in the longitudinal position s, we define the Lyapunov exponent as

$$\lambda = \lim_{N\to\infty} \lim_{d(0)\to 0} \frac{1}{N} \log \frac{d(N)}{d(0)} \tag{3.1}$$

The Lyapunov exponent describes the rate of divergence of the nearby trajectories in the phase space. If we have a regular motion the distance between two nearby trajectories grows linearly when averaged over long periods of rime

$$d(N) \propto N$$

On the other hand, if we are in the chaotic situation we have an exponential growth of the distance

$$d(N) \propto e^{\lambda N}$$

where λ is the Lyapunov exponent.
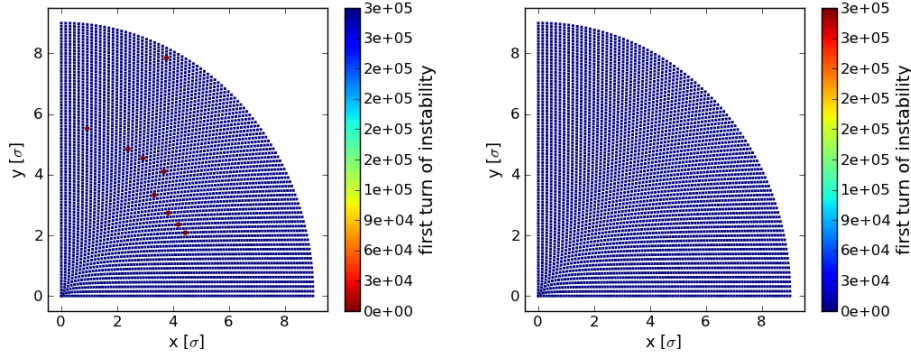
Figure 3.4: Test of stability for Head On in IP1 and IP5. Figure reports the particles initial distribution normalized, colored following the criterion of the first turn of instability, the dark blue indicates a sTable particle. In the left plot the bbtrack criterion is used here, some sTable particles are indicated as unstable. In the right plot the new criterion is used here, as expected we don't have any unstable particles.

For this kind of test it is more useful to track an uniform distribution of particles between 0 and a given maximum radius (in the most part of our tests 8 σ). We tracked the particles for at least 300.000 turns, as shown in the fig.: 3.4 we plot the initial distribution and colored the particles following the first turn of instability.

In the bbtrack code the Lyapunov exponent is calculated in the following way.

Two particles with an initial offset of 10^{-8} m are tracked. At each turn the program calculates the normalized 4D distance between the two particles $d_n(i)$ where the subscript n stand for "normalized" and i indicate the turn

$$
\begin{aligned}
d_n(i)^2 =& (x_{n\,1}(i) - x_{n\,2}(i))^2 + (x'_{n\,1}(i) - x'_{n\,2}(i))^2+ \\
&+(y_{n\,1}(i) - y_{n\,2}(i))^2 + (y'_{n\,1}(i) - y'_{n\,2}(i))^2
\end{aligned}
\tag{3.2}
$$

the normalized coordinates are calculated with the formulas

$$
z_n = \frac{z}{\sigma_y} \tag{3.3}
$$

$$
z'_n = z'\sqrt{\frac{\beta_z}{\epsilon_z}} + z\frac{\alpha_z}{\sigma_z} \tag{3.4}
$$

(z = x or y).

A particle is set as unstable if the difference between the normalized distance at the given turn and the initial normalized distance is greater than K times the normalized distance at the half the turn

$$
\frac{d_n(i) - d_n(0)}{2d_n(i/2)} > K \tag{3.5}
$$

The suggested value for the key parameter was 3.
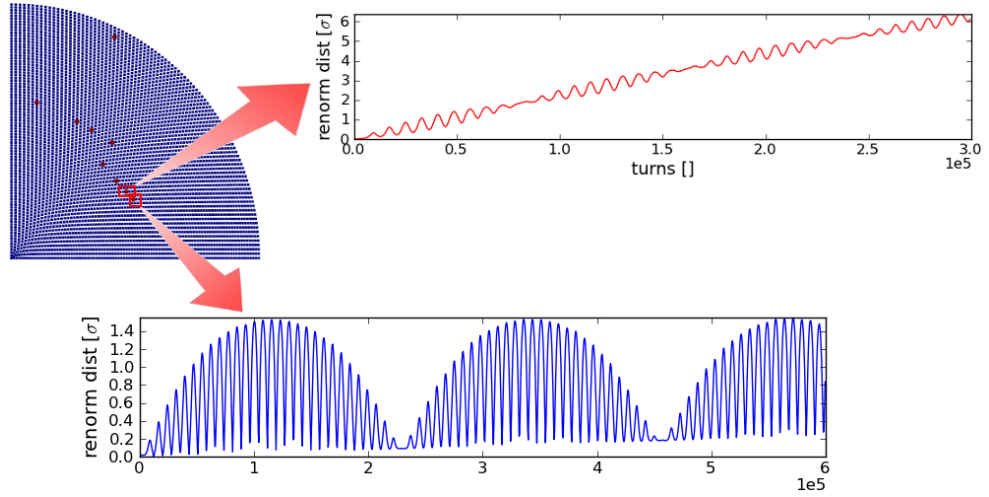
Figure 3.5: On the top left it is indicated the stability plot for the Head On test using the bbtrack criterion to calculate the Lyapunov coefficient. We notice that some particles are indicated as unstables when, if we check the normalized distance plot (top right and bottom), we don't see an exponential behaviour.

This method sometimes give us false unstables as shown in the fig.: 3.5.

We found a good agreement with the plot information if we use the following criterion:

$$\lambda[j](\text{new}) = \frac{\left\langle d_r[\frac{j}{2} : j]\right\rangle - \left\langle d_r[0 : \frac{j}{2}]\right\rangle}{\langle d_r[j/4 : 3j/4]\rangle} \, , \tag{3.6}$$

with $\langle d_r[m1 : m2]\rangle$ denoting the average value of d between turns $m1$ and $m2$.
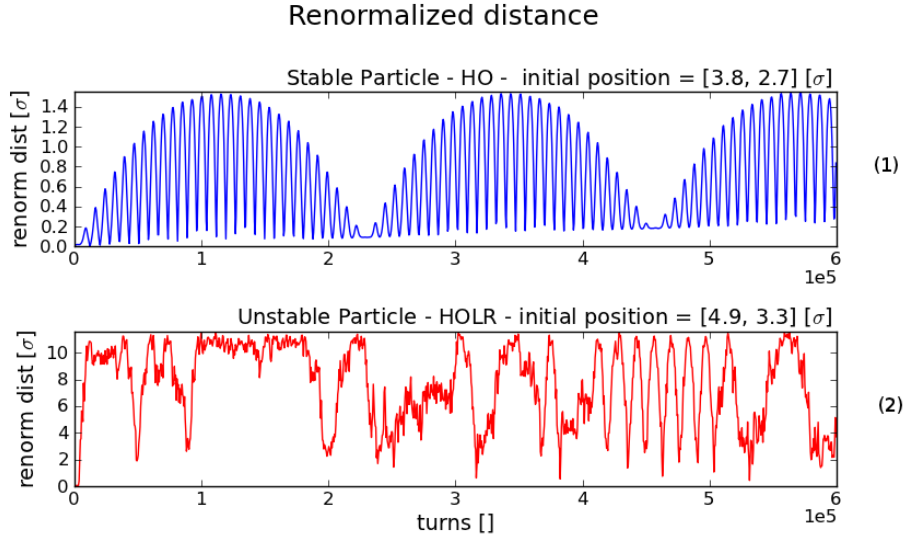
Figure 3.6: Normalized distance for a sTable particle (line 1) and an unstable one (line 2) in function of the turn i. The bbtrack program sets also the first particle as unstable, the new criterion correctly recognizes the first case as sTable and the second one as unstable.

With the new Lyapunov criterion the top case in Fig. 3.6 is correctly identified as sTable, the bottom case as unstable.

We verified that the results are sTable when we increase the number of turns as shown in fig.: 3.7.
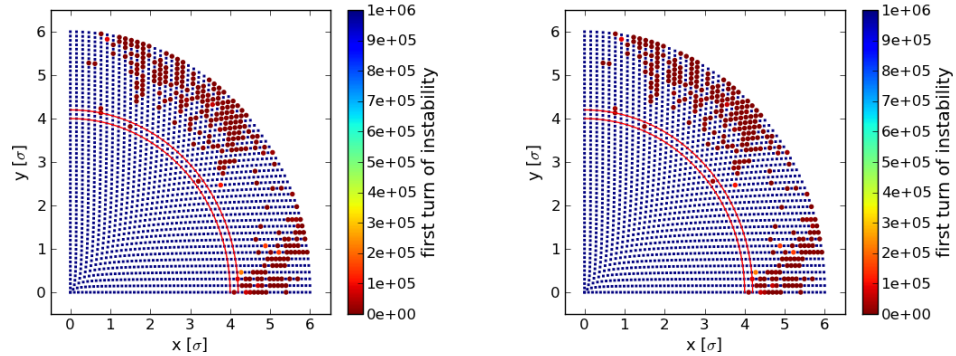
Figure 3.7: On the left: Stability analysis for 600.000 turns , on the Right: Stability analysis for 1.000.000 turns.

3.4   BBTrack code and add on

We can simulate the beam-beam effects in two way:

Weak-strong simulations where we test the behaviour of a single particle that interacts with the entire counterrotating bunch (incoherent effects). This implicitly assumes that the opposing bunch (strong) is not to be modified by the interaction with the particle (weak).

Strong-strong simulations where is studied the effect of the two beams moving relative to each other (σ and π modes).

We use the bbtrack code developed by U. Dorda to make our simulations [5].

Almost no accelerator (Tevatron, RHIC, SPS, HERA) has been limited by the strong-strong beam-beam interaction as the associated coherent motion is either Landau damped or can be suppressed by a transverse feedback system. Only in dedicated experiments coherent modes could deliberately be excited.

Therefore we use a weak-strong simulation program: BBTrack, a Fortran 90 program developed by U. Dorda [5].

In BBTrack every action which is performed once every turn is referred to as a kick. This includes real kicks to the beam, e.g. a kick due to a wire, but also analyst steps, e.g: writing the current position to a file.

To generate manually the code for each of our tests seems not efficient, we developed for this some python scripts that produces, starting from the MAD-X outputs and some other input informations (for example the wire position), the correct BBtrack input files (input parameter and particles distributions). With python and in particular using the potential of pylab

library we develop a series of tools for postprocessing analysis, as already mentioned lyapunov and tune calculation, plot generation, the calculation of the minimum radius where we found a particle instability and of the dynamical aperture radius [1].

The use of a database MySQL where the python scripts insert automatically the postprocessing informations allows, in many cases, a faster analysis and comparison of our results.

---

[1]We define as dynamical aperture radius the last radius where the number of sTable particles is greater than the number of unstable ones

4

Main Simulation Results

4.1 Introduction

We analyse the following scenarios with different wire positions:

HO (Head On) 2 head-on collisions at IPs1 and 5

HOLR (Head On Long Range) 2 HO collisions plus 16 LR collisions at each side of the IP1 and IP5

BBC (Beam Beam Compensator] HOLR plus a wire at 105 m after IP1 and IP5

TCT (Tertiary Collimator Target) HOLR plus a wire at 147 m before IP1 and IP5

TCT opt β HOLR plus a wire at 150 m after IP1 and 147 m before IP5

TCT opt β 2 HOLR plus a wire at 147 m before IP1 and 150 m after IP5

Q5 (Quadrupole 5) HOLR plus a wire at 199 m after IP1 and IP5

We simulate the case of a wire with a distance equal to the average long-range distance (9.5 σ for the nominal crossing angle) as well as with a bigger distance, namely 16% larger (11 σ for the nominal crossing angle).

When we simulate a change of crossing angle between the beam we obviously need to also move the wire. For example for a crossing angle of 6.3 σ we have a first distance of 6.3 σ and a second distance of 7.3 σ.

For distance 2 we tested the nominal current (177 A) and a value quadratically scaled with the distance (237 A).

4.2 Head-on and head-on long-range

If we ignore the long-range effects and suppose that our particles suffer only of the head-on effect in IP1 and IP5 we see that all the particles remain

47
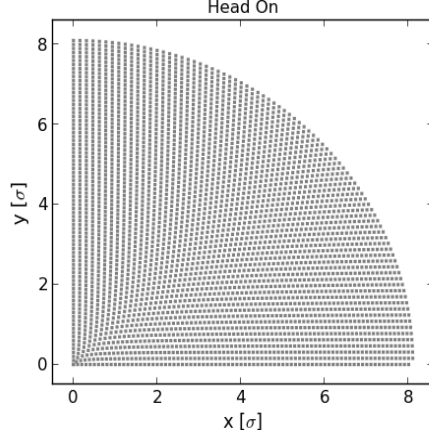
Figure 4.1: Test of stability for head-on in IP1 and IP5. Initial particles distribution normalized. The particles are all stable after 300.000 turns
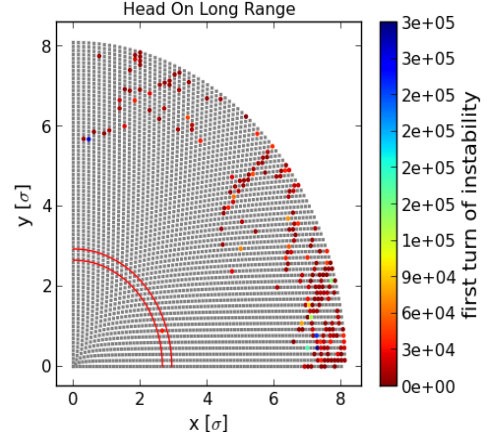
Figure 4.2: Test of stability for head-on in IP1 and IP5 + 16 long-range at each head-on side. Initial particles distribution normalized. The turn when particle become unstable is identified by the colors.
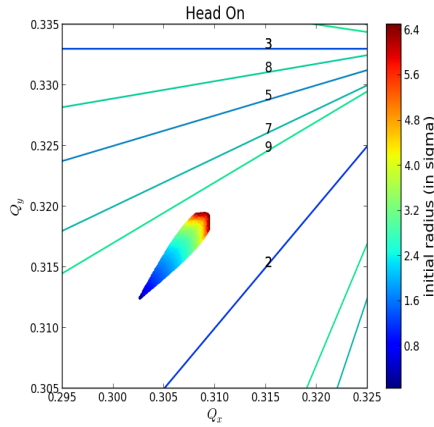
Figure 4.3: Tune footprint for head-on in IP1 and IP5. Particles do not touch any resonance line
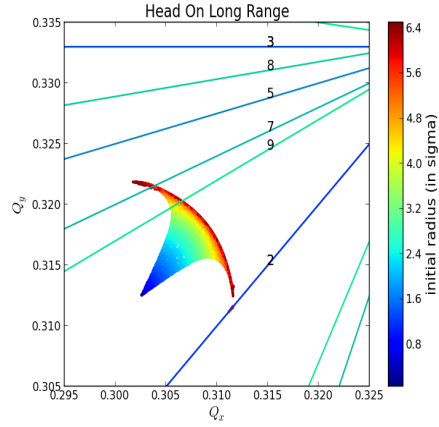
Figure 4.4: Tune footprint for Head On in IP1 and IP5 + 16 Long Range at each Head on side.

stable (see Figure 4.1) , and the tune does not touch any resonance line (see Figure 4.3).

To reach or at least to approximate this same behaviour when we have the long-range effect and the wire compensation is our goal.

When we add the long-range effects some of the particle become unstable. As emphasized in 2.1.2 the effect is more important for particles with bigger

amplitude.

As we can see in Figure 4.2 the 5% of particles become unstable and the radius of minimum instability is 2.8 σ.

If we observe the tune we see that we pass from a closed to an open umbrella. Some of the particles that start at bigger amplitude touch resonance lines of order 2, 7 or 9 (see 4.4).
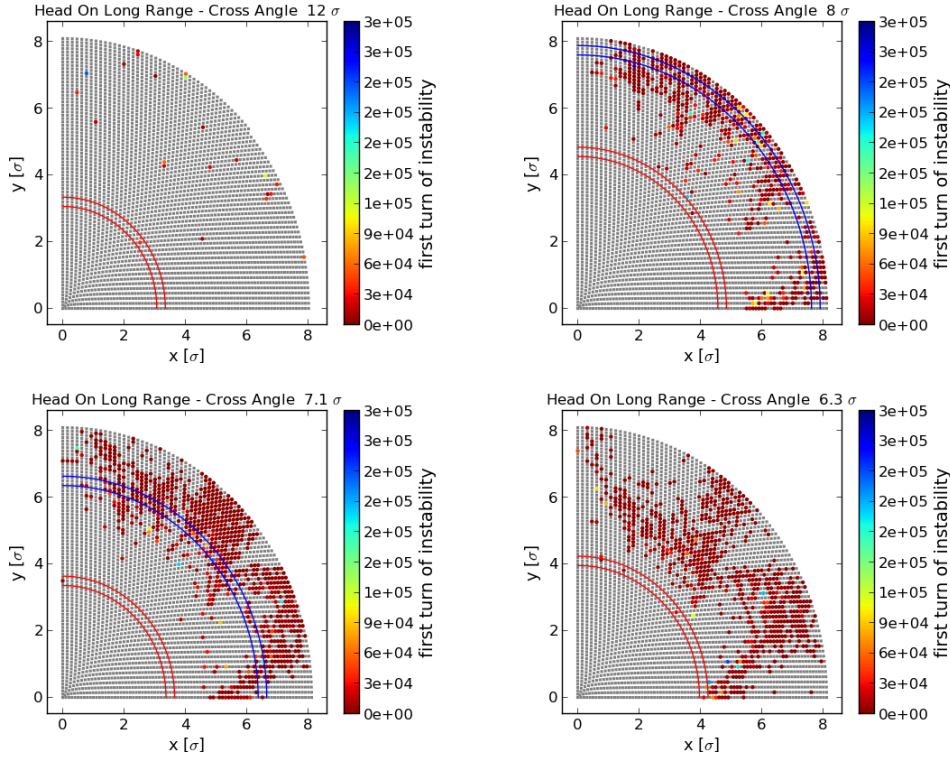
Figure 4.5: Test of stability for Long Range with nominal Optics and Different Crossing Angle: 12 σ (top left) , 8 σ (top right) 7.1 σ (bottom left), 6.3 σ (bottom right)

The effect depends directly on the crossing angle, as we can see in Figure 4.5 where we report the results for a crossing angle of 12 σ, 8 σ, 7.1 σ and 6.3 σ. For smaller crossing angle we considered smaller distibution to compare the results with the one obtained when we insert the wire compensator. In this latter case in fact we have to remove particles that pass too close to the wire.

In Table 4.1 we indicate the percentage of unstable particles and the minimum radius of instability to have a feeling of the behaviour. We remark, on the other hand, that it is more important to get an idea of the distribution of unstable particles given as the figure.

Crossing Angle	Unstables Particles	Minimum Radius
$[\sigma]$	$[\%]$	$[\sigma]$
12	0.6	3.2
9.5	5.7	2.8
8	15.6	4.7
7.1	22.3	3.5
6.3	20.5	4.1

Table 4.1: Summary of the stability test for long-range, using the nominal LHC optics and performing the tests for differents crossing angles.
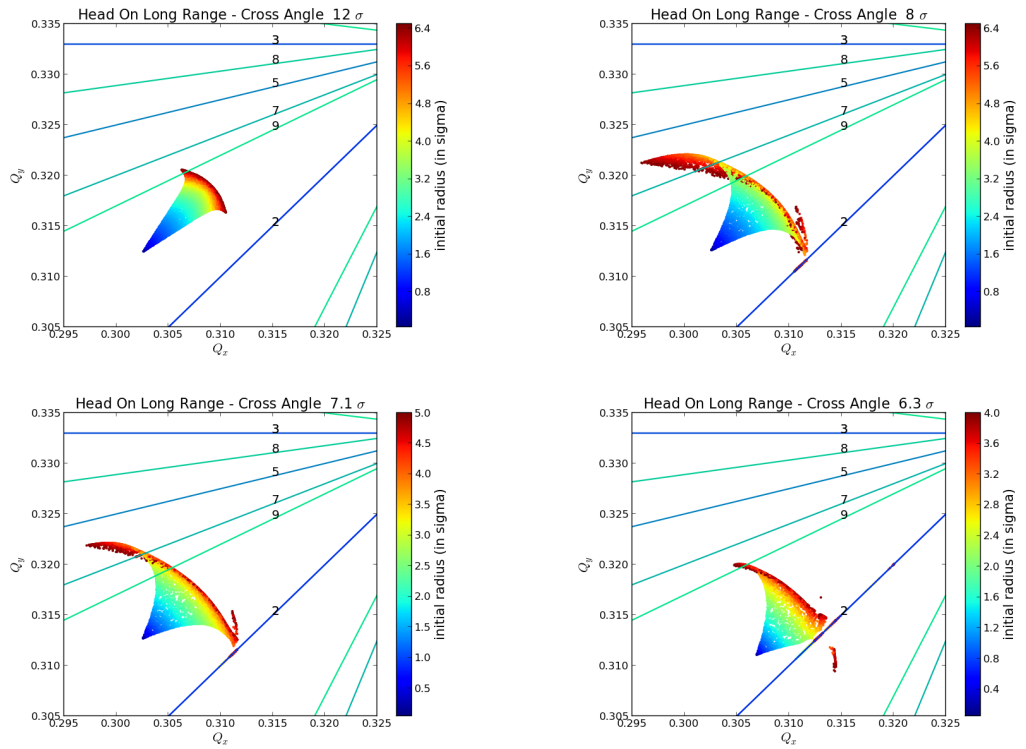
Figure 4.6: Tune footprint for Long Range with nominal Optics and Different Angle: 12 σ (top left) , 8 σ (top right) 7.1 σ (bottom left), 6.3 σ (bottom right)

As visible from the Figure 4.6 also if we consider a crossing angle bigger than the nominal one (9.5 σ) some of the particles touch resonance lines.

Table 4.2 and Figures 4.8 and 4.7 show us that the results for the modified optics [1] are similar to those obtained using the nominal one. Figure 4.7 and 4.8, report the results for the tests made with the following crossing angles

---

[1]see Table 3.2 for the optics parameters
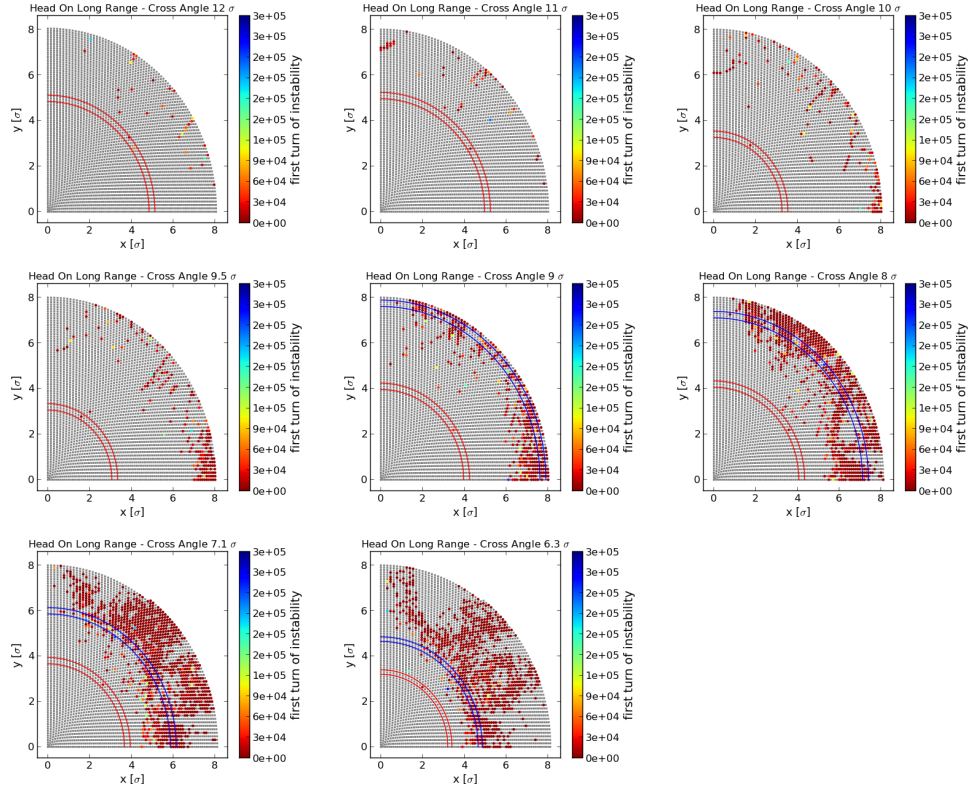
Figure 4.7: Test of stability for Long Range with modified Optics and Different Crossing Angle: 12 σ , 11 σ , 10 σ , 9.5 σ (first row) 9 σ , 8 σ , 7.1 σ , 6.3 σ (second row)

Crossing Angle [σ]	Unstables Particles [%]	Minimum Radius [σ]
12	0.9	5.0
11	1.2	5.1
10	3.8	3.4
9.5	5.3	3.2
9	11.7	4.1
8	22.1	4.2
7.1	28.0	3.8
6.3	24.1	3.3

Table 4.2: Summary of the stability test for long-range, using modified LHC optics and performing the tests for differents crossing angles.

12 σ , 11 σ , 10 σ , 9.5 σ 9 σ , 8 σ , 7.1 σ and 6.3 σ .
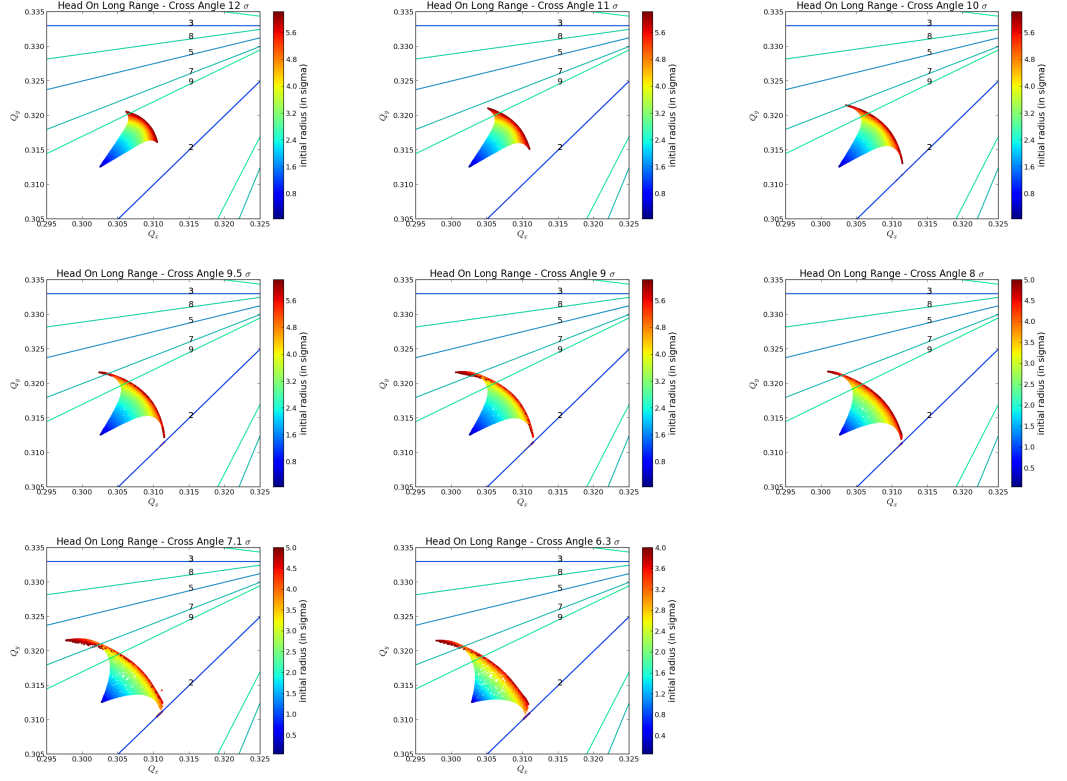
Figure 4.8: Tune footprint for Long Range with modified Optics and Different Crossing Angles: 12 σ , 11 σ , 10 σ , 9.5 σ (first row) 9 σ , 8 σ , 7.1 σ , 6.3 σ (second row)

4.3   BBC wire position Nominal Optics

4.3.1   Tests with the Nominal Crossing Angle

IP	IP dist	β_x	β_y	σ_x	σ_y
	[m]	[m]	[m]	$[10^{-3} \text{ m}]$	$[10^{-3} \text{ m}]$
IP1	105	1738.1	1734.8	0.94	0.94
IP5	105	1739.2	1734.9	0.94	0.94

Table 4.3: Summary of the optics parameter at the BBC location.

As shown in Table 4.3 when we consider LHC with the nominal optics we have in BBC location after IP1 $\beta_x = 1738.1$ m , $\beta_y = 1734.8$ m and for IP5 $\beta_x = 1739.2$ m , $\beta_y = 1734.9$ m. These big and almost equal values for betatron function allow us to obtain a very good compensation if we put the wire at a distance equal to the average long-range distance, 9.5 σ. Seeing that in

this point the rms beam size, σ, at the wire position is $\sigma = 0.000934$ m the transverse wire position in IP1 (vertical crossing) is [0,-0.00888] m and in IP5 [-0.00888,0] m.
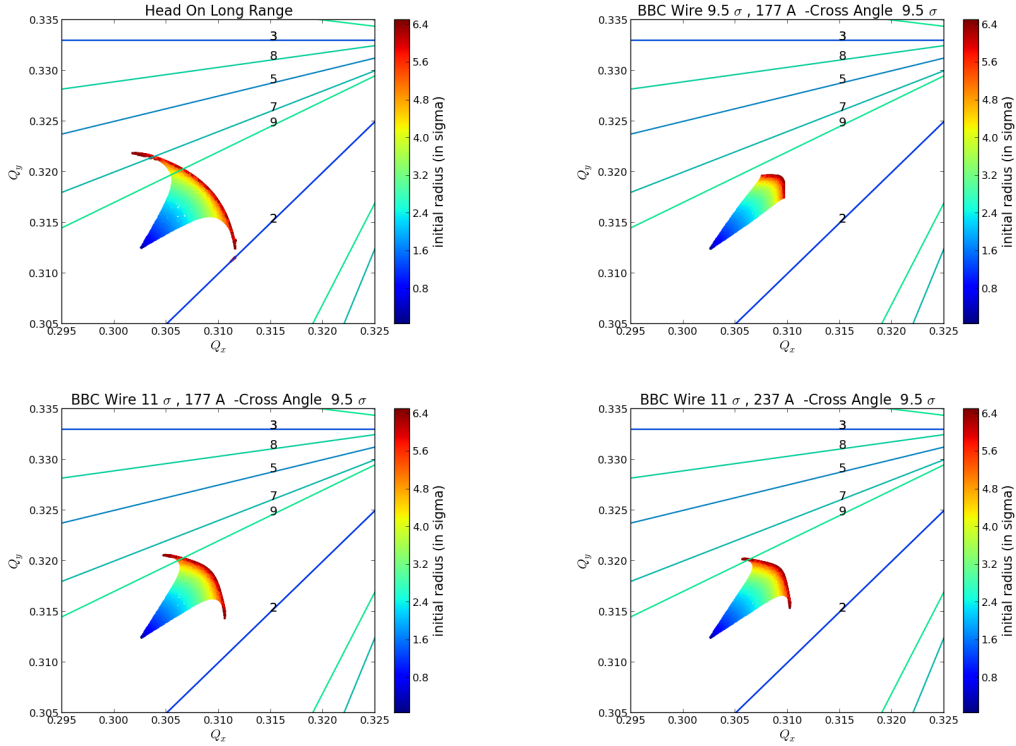
Figure 4.9: Tune footprint for BBC with nominal Optics, nominal crossing angle (9.5 σ) and different transverse position and current: 9.5 σ 177 A (top right), 11 σ 177 A (bottom left) , 11 σ 237 A (bottom right) . The first plot (top left) shows the Head On long-range to allow a faster comparison.

Transverse position $[\sigma]$	Current A	Unstables Particles [%]	Minimum Radius $[\sigma]$
HoLr		5.7	2.8
9.5	177	2.2	4.8
11	177	0.8	5.4
11	237	0.5	4.7

Table 4.4: Summary of the stability test for BBC, using the nominal LHC optics and performing the tests for differents transverse positions and current values, with nominal crossing angle.

Comparing Figure 4.9 with Figure 4.3 we notice that the tune footprint
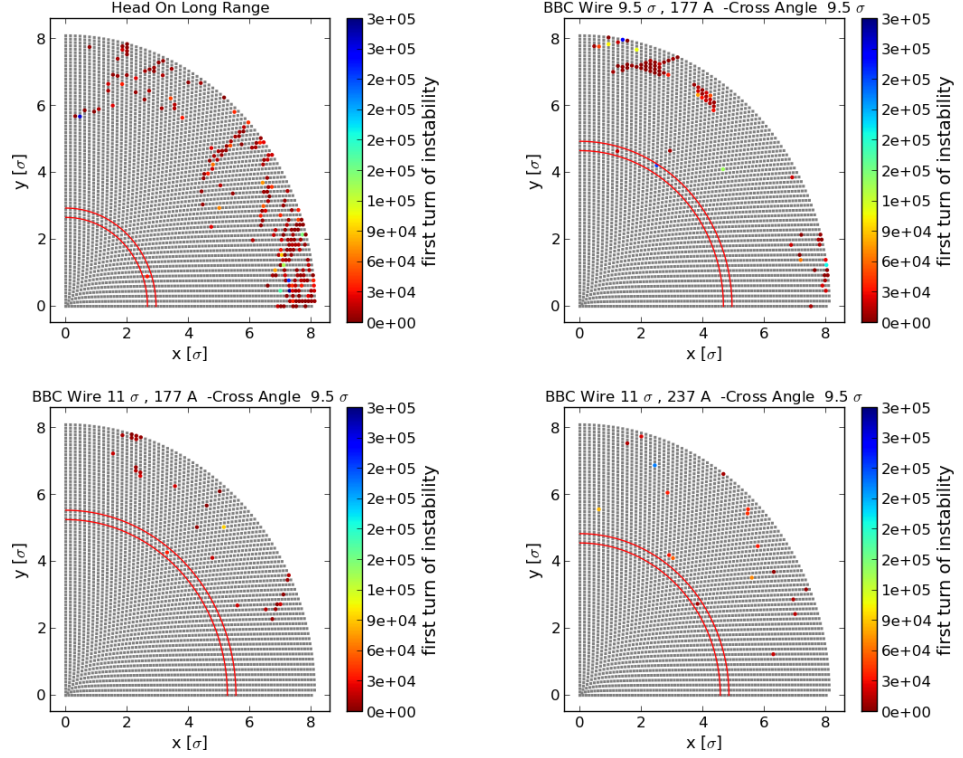
Figure 4.10: Test of stability for BBC with nominal Optics, nominal crossing angle (9.5 σ) and different transverse position and current: 9.5 σ 177 A (top right), 11 σ 177 A (bottom left) , 11 σ 237 A (bottom right) . The first plot (top left) shows the Head On long-range to allow a faster comparison.

for the wire compensator at 9.5 σ with a current of 177 A (top right in Figure 4.9) is almost identical to the tune footprint for head-on.

For technical requirements we need to move the wire at 11 σ (in IP1, for example, this means to a transverse distance of [0 ,-0.01028] m). Doing this we tried both the nominal current (177 A) and a scaled one (237 A). The corresponding tune footprints are good enough: only a small number of particles touch a resonance line of order 9 (not so dangerous). The result for the stability is even better than the one for the nominal case (see Table 4.4).

4.3.2   Test of different crossing angles
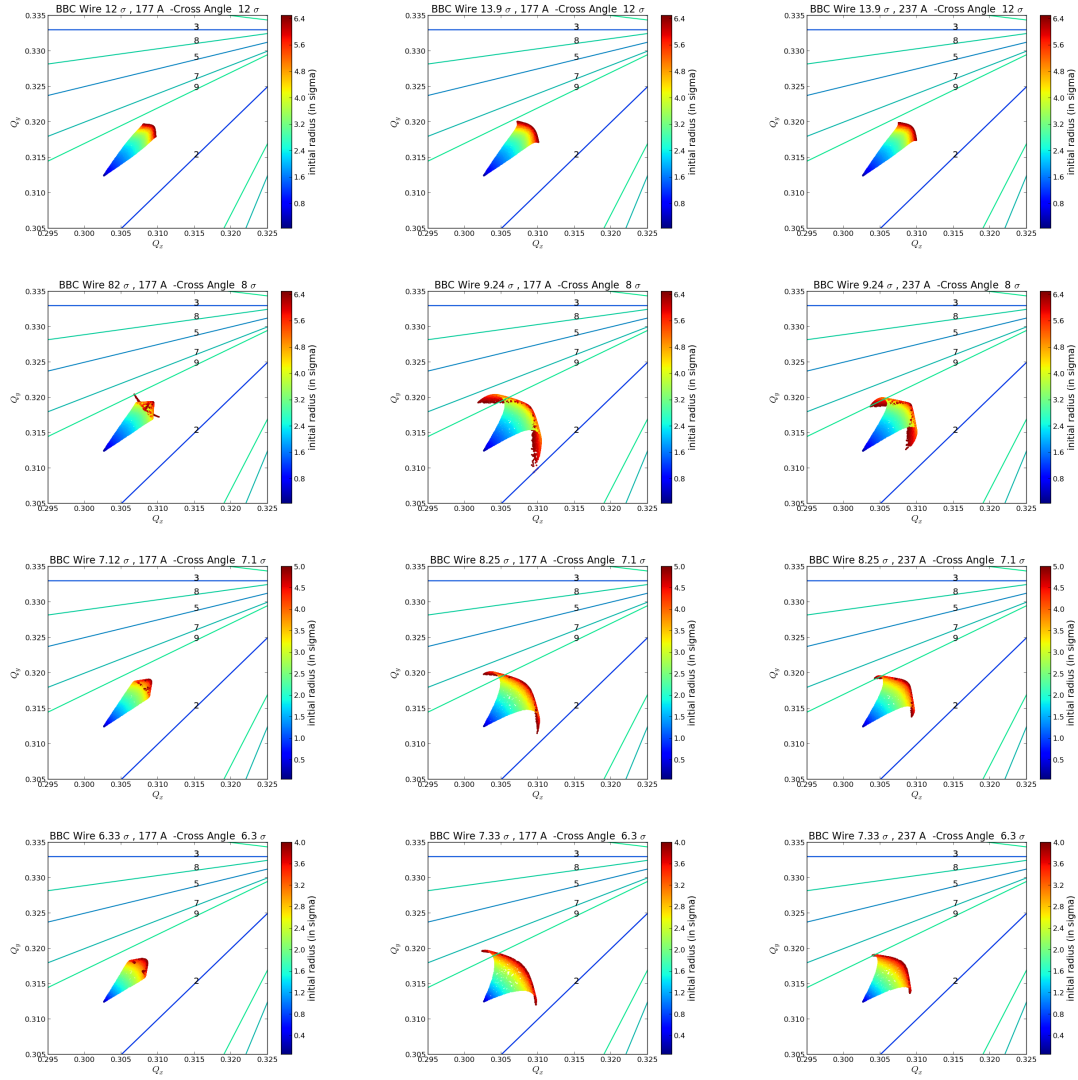
Figure 4.11: Tune footprint for BBC with nominal Optics and crossing angle of: 12 σ (row 1), 8 σ (row 2), 7.1 σ (row 3), 6.3 σ (row 4). The first column shows tests for a wire at the average long-range distance, with current 177 A, the second column the wire at scaled distance with current 177 A and the third column the wire at scaled distance and current (237 A)

When we reduce the crossing angle the effects of beam beam become more dangerous and the compensation cannot give us an optimal result. However we can see also in this case the benefit of the wire compensator as shown in Figure 4.12 and 4.11.
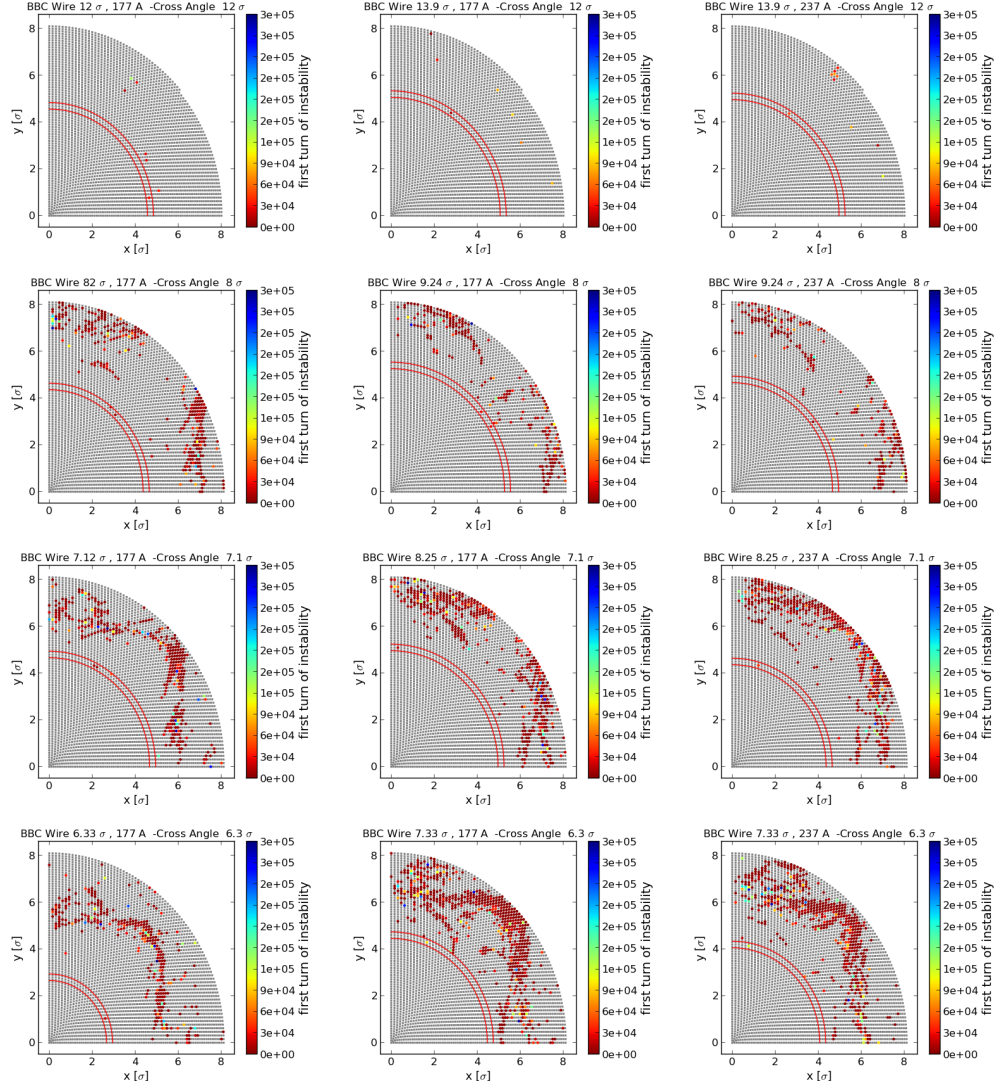
Figure 4.12: Test of stability for BBC with nominal Optics and crossing angle of: 12 σ (row 1), 8 σ (row 2), 7.1 σ (row 3), 6.3 σ (row 4). The first column shows tests for a wire at the average long-range distance, with current 177 A, the second column the wire at scaled distance with current 177 A and the third column the wire at scaled distance and current (237 A) .

Looking the Tables 4.5, 4.4, 4.6, 4.7 and 4.8 we can notice that the wire compensator can decrease the percentage of unstable particles by a factor 2 to 6 (for the nominal crossing angle) with respect to the head-on long-range case.

Transverse position [σ]	Current A	Unstables Particles [%]	Minimum Radius [σ]
HoLr		0.6	3.2
12	177	0.2	4.7
14	177	0.2	5.2
14	237	0.3	5.1

Table 4.5: Summary of the stability test for BBC, using the nominal LHC optics and performing the tests for differents transverse positions and current values, crossing angle 12 σ.

Transverse position [σ]	Current A	Unstables Particles [%]	Minimum Radius [σ]
HoLr		15.6	4.7
8	177	8.6	4.5
9.2	177	6.3	5.4
9.2	237	6.0	4.8

Table 4.6: Summary of the stability test for BBC, using the nominal LHC optics and performing the tests for differents transverse positions and current values, crossing angle 8 σ.

Transverse position [σ]	Current A	Unstables Particles [%]	Minimum Radius [σ]
HoLr		22.3	3.5
7.1	177	9.8	4.8
8.25	177	12.3	5.1
8.25	237	12.6	4.5

Table 4.7: Summary of the stability test for BBC, using the nominal LHC optics and performing the tests for differents transverse positions and current values, crossing angle 7.1 σ.

Transverse position [σ]	Current A	Unstables Particles [%]	Minimum Radius [σ]
HoLr		20.5	4.1
6.3	177	8.7	2.8
7.3	177	17.4	4.6
7.3	237	15.2	4.2

Table 4.8: Summary of the stability test for BBC, using the nominal LHC optics and performing the tests for differents transverse positions and current values, crossing angle 7.1 σ.

Figure 4.13 demonstrate that adding the wire allows us to reduce the
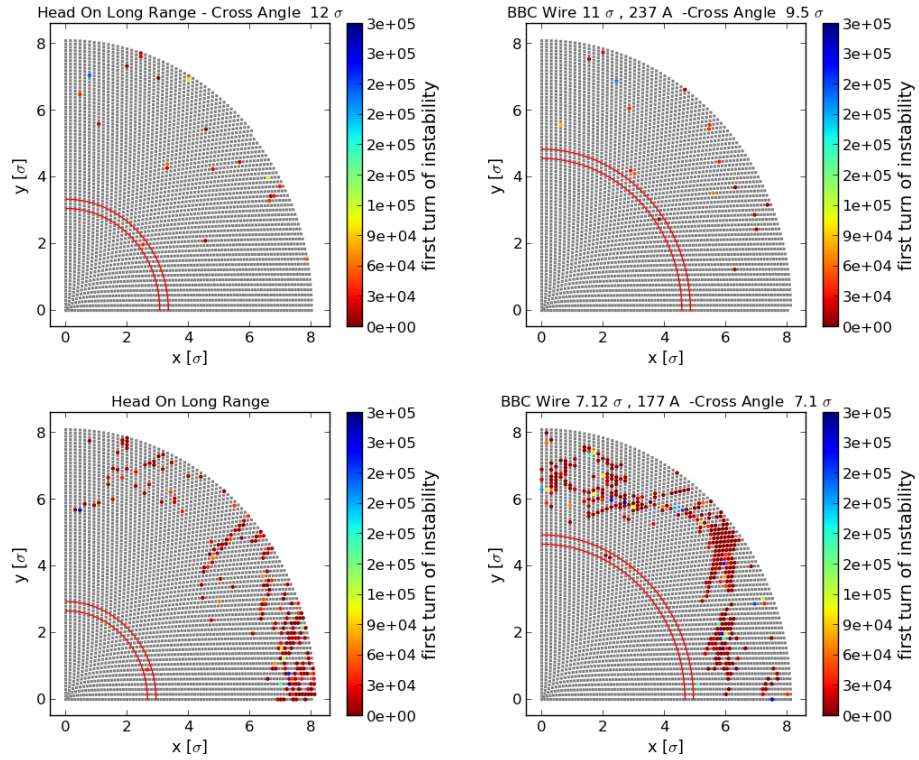
Figure 4.13: Test Stability BBC location, Nominal Optics: particles distribution at 9.5 σ with a wire compensator at 11 σ 237 A is almost equal to the particle distribution at 12 σ without compensator (first row) particles distribution at 7.1 σ with a wire compensator at 7.1 σ 177 A is almost equal to the particle distribution at 9.5 σ without compensator (second row).

angle from 12 to 9.5 σ or from 9.5 to 7.1 σ without significant changes in the stability region.

4.4 TCT wire position Nominal Optics

4.4.1 Tests with the Nominal Crossing Angle

IP	IP dist [m]	β_x [m]	β_y [m]	σ_x $[10^{-3}$ m]	σ_y $[10^{-3}$ m]
IP1	-147	1577.2	614.9	0.89	0.56
IP5	-147	1575.7	606.8	0.89	0.56

Table 4.9: Summary of the optics parameter at the TCT location.

For technical reasons the wire cannot be installed at the BBC location during the technical stop of 2014/2015. The proposed alternatives were the TCT location (147 m before the IPs 1 and 5) or the Q5 location (199 m after the IPs 1 and 5).

As we can see in Table 4.9 at the TCT location the betatron function is

- lower than in the BBC points

- asymmetric (β_x is 2.6 times the β_y value!)

- with the same aymmetry in both IPs

From the asymmetry of the β function and remembering that

$$\sigma_z = \sqrt{\beta_z \epsilon_z} \ \ z = x \text{ or } y \tag{4.1}$$

we derive that σ has asymmetric values in the two directions and that the transverse wire position is different in the two IPs: for the nominal crossing angle in IP1 the wire is located at [0.0 ,-0.0053] m and in IP5 at [-0.0084, 0.0] m.

It is evident from the figure 4.14 that the tune results for TCT location are worse than the ones of BBC case, we emphasize in particular that for 9.5 σ 177 A and 11 σ 237 A the tune twists.

Transverse position [σ]	Current A	Unstables Particles [%]	Minimum Radius [σ]
HoLr		5.7	2.8
9.5	177	4.2	5.2
11	177	1.8	4.8
11	237	2.5	3.9

Table 4.10: Summary of the stability test for the TCT, using the nominal LHC optics and performing the tests for differents transverse locations and current values, with nominal crossing angle.
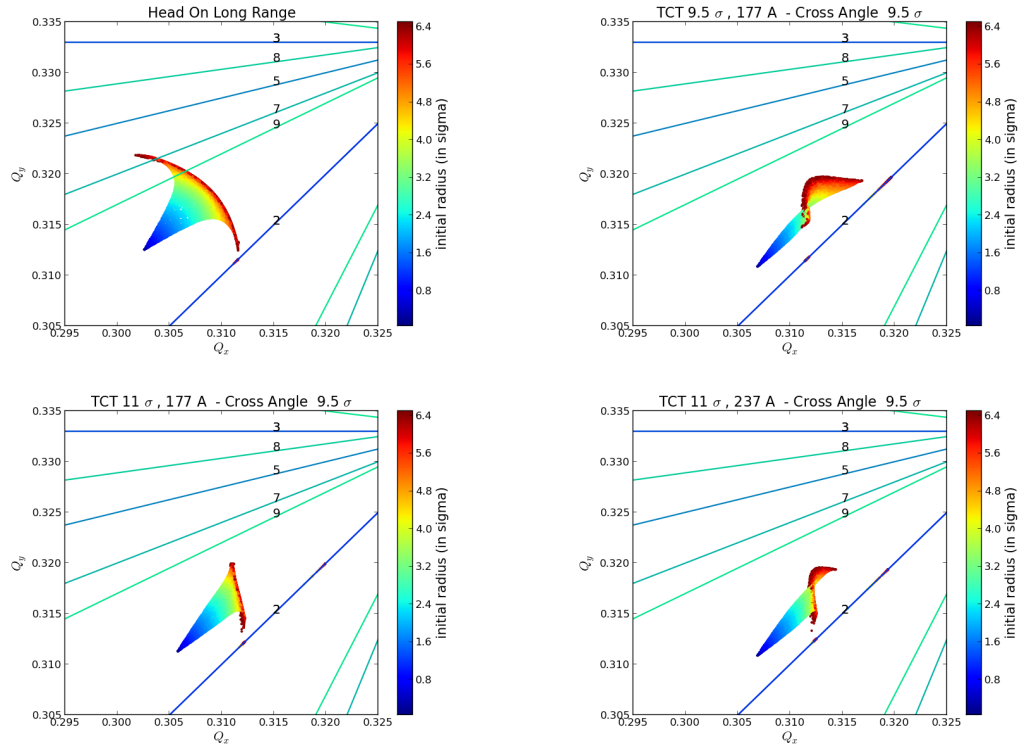
Figure 4.14: Tune footprint for TCT with nominal Optics, nominal crossing angle (9.5 σ) and different transverse position and current: 9.5 σ 177 A (top right), 11 σ 177 A (bottom left) , 11 σ 237 A (bottom right).

If with a wire at BBC location we can reach the 0.5 % of unstable particles, for the TCT location our best result is 1.8 %: the maximum gain in terms of stable particles degrades from a factor 6 to a factor 3!
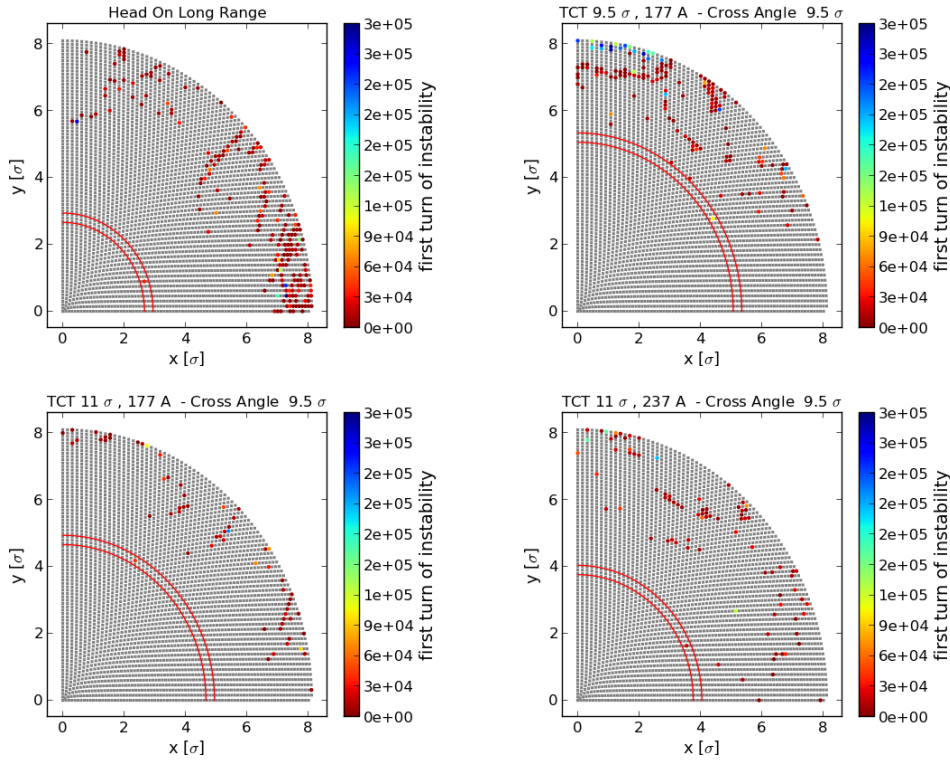
Figure 4.15: Test of stability for TCT with nominal Optics, nominal crossing angle (9.5 σ) and different transverse position and current: 9.5 σ 177 A (top right), 11 σ 177 A (bottom left) , 11 σ 237 A (bottom right).

4.4.2 Test of different crossing angles

Figure 4.16 shows that when we reduce the crossing angle to 7.1 σ or 6.3 σ the central tune comes dangerously close to the resonance line of order 2. If the wire distance is the average long-range distance (7.1 σ, for the crossing angle 7.1 σ and 6.3 σ, for the crossing angle 6.3 σ) with current 177 A or is the scaled distance (8.25 σ, for the crossing angle 7.1 σ and 7.3 σ, for the crossing angle 6.3 σ) the central tune touches the resonance lines and the destructive effects for the tune are evident.

This is visible also checking the stability: if we observe the tables 4.11 and 4.14 we see that we go from a maximum gain of 0.6 % to the worst case where we do not have any gain respect the head-on long-range case.
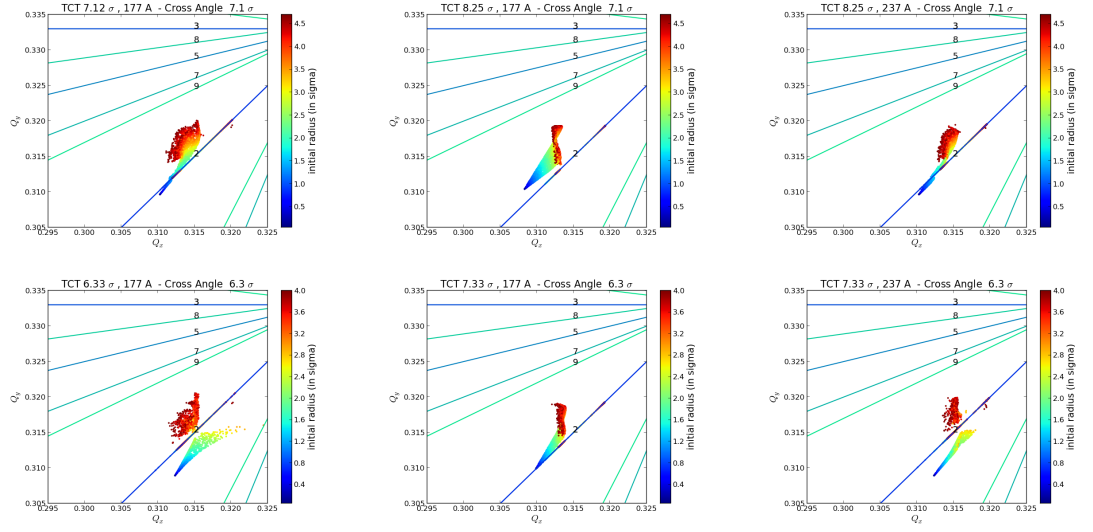
Figure 4.16: Tune footprint for TCT with nominal Optics and crossing angle of: 7.1 σ (row 1), 6.3 σ (row 2). The first column shows tests for a wire at the average long-range distance, with current 177 A, the second column the wire at scaled distance with current 177 A and the third column the wire at scaled distance and current (237 A) .
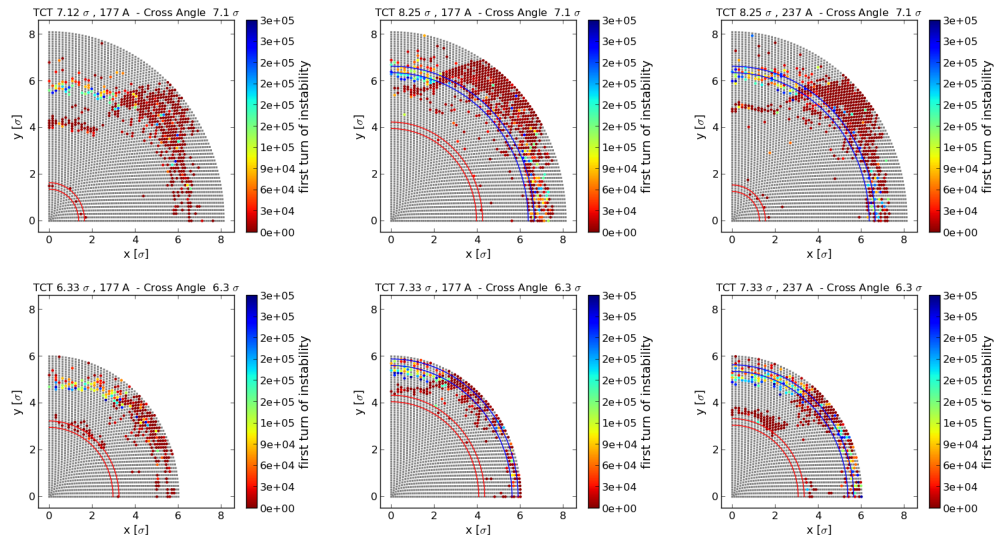
Figure 4.17: Test of stability for TCT with nominal Optics and crossing angle of: 7.1 σ (row 1), 6.3 σ (row 2).

Transverse position [σ]	Current A	Unstables Particles [%]	Minimum Radius [σ]
HoLr		22.3	3.5
7.1	177	15.4	1.5
8.25	177	20.3	4.1
8.25	237	17.9	1.4

Table 4.11: Summary of the stability test for TCT, using the nominal LHC optics and performing the tests for differents transverse positions and current values, crossing angle 7.1 σ.

Transverse position [σ]	Current A	Unstables Particles [%]	Minimum Radius [σ]
HoLr		20.5	4.1
6.3	177	15.0	3.1
7.3	177	14.2	4.2
7.3	237	19.0	3.2

Table 4.12: Summary of the stability test for TCT, using the nominal LHC optics and performing the tests for differents transverse positions and current values, crossing angle 7.1 σ.

4.4.3 Central tune moved back

As emphasized in the previous section the fact that the central tune is near, or in the worst cases touches the resonance line causes very bad results. We tried so, to simulate the case when the central tune is moved back to the original value. In IP1 this means

$$\Delta Q_x = -\frac{r_0 \, I_w \, l_w \, \beta_x}{2 \, \pi \, \gamma \, e \, c \, d^2}$$
$$\Delta Q_y = \frac{r_0 \, I_w \, l_w \, \beta_y}{2 \, \pi \, \gamma \, e \, c \, d^2} \tag{4.2}$$

where r_0 is the classical proton radius ($1.5 \; 10^{-18}$ m), c is the velocity of light ($2.99 \; 10^8$ ms^{-1}) , e is the proton charge ($1.602 \; 10^{-19}$ C), γ is the relativistic γ (for nominal LHC 7460.52), I_w is the wire current, l_w is the wire length (in our tests 1 m) β_u is the β at the wire position (u = x, y) d is the wire y-distance.

The values for IP 5 are obtained by reversing the signs and by setting d = wire x-distance instead of wire y-distance.

Comparing the Figure 4.16 and 4.18, it is evident that we obtain an improvement but if we compare these results with the one in Figure 4.12 it is clear that this case does not reach the same quality of compensation as with the correspondent BBC location options.

The analisys of stability leads us to the same conclusions.
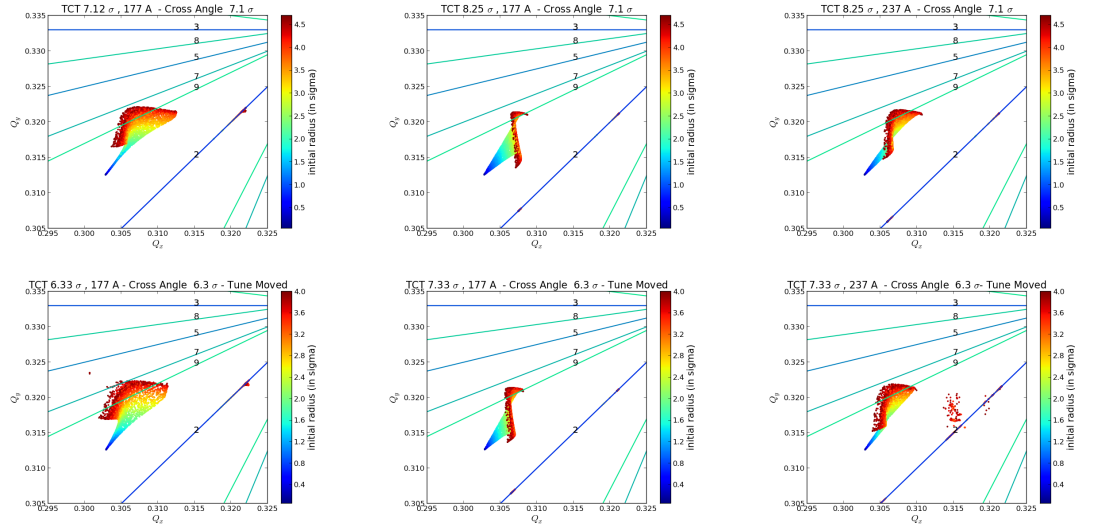
Figure 4.18: Tune footprint for TCT with nominal Optics and crossing angle of: 7.1 σ (row 1), 6.3 σ (row 2). Central tune moved back to the original value.
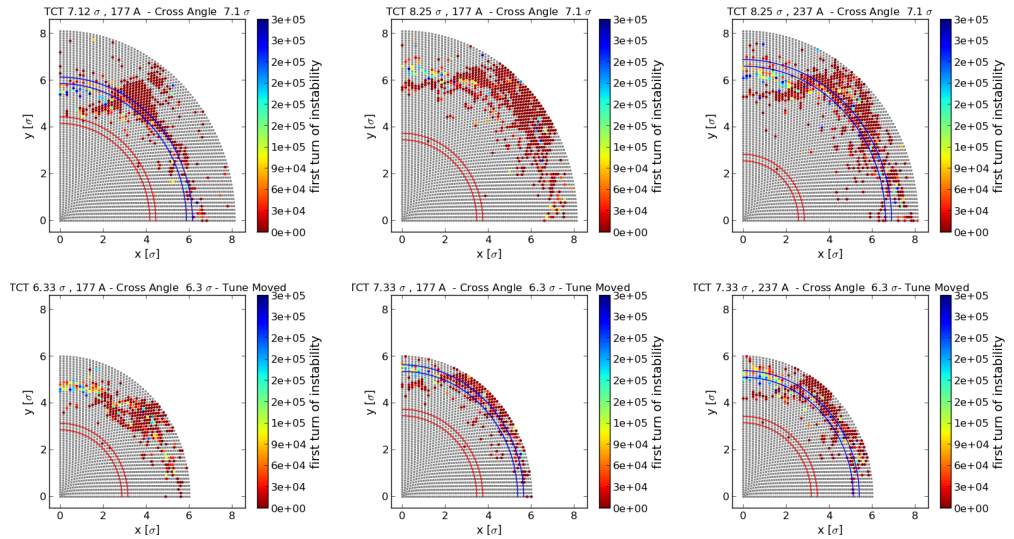
Figure 4.19: Test of stability for TCT with nominal Optics and crossing angle of: 7.1 σ (row 1), 6.3 σ (row 2). Central tune moved back to the original value.

Transverse position	Current	Unstables Particles	Minimum Radius
$[\sigma]$	A	$[\%]$	$[\sigma]$
HoLr		22.3	3.5
7.1	177	12.6	4.3
8.25	177	17.7	3.6
8.25	237	18.2	2.7

Table 4.13: Summary of the stability test for TCT, using the nominal LHC optics and performing the tests for differents transverse positions and current values, crossing angle 7.1 σ. Central tune moved back to the original value.

Transverse position	Current	Unstables Particles	Minimum Radius
$[\sigma]$	A	$[\%]$	$[\sigma]$
HoLr		20.5	4.1
6.3	177	16.6	3.0
7.3	177	13.6	3.6
7.3	237	16.7	3.3

Table 4.14: Summary of the stability test for TCT, using the nominal LHC optics and performing the tests for differents transverse positions and current values, crossing angle 7.1 σ.Central tune moved back to the original value.

4.5   TCT opt β wire position Nominal Optics

4.5.1   Tests with the Nominal Crossing Angle

If we use the nominal LHC optics TCT locations with $\beta_x \approx 1580$ m and $\beta_y \approx$ 610 m in both the IPs does not seem a good choice for the wire compensator, but we can try to move one of two wire to obtain

$$\frac{\beta_x(s_1)}{\beta_y(s_1)} \approx \frac{\beta_y(s_5)}{\beta_x(s_5)}$$

Where we have indicated with s_1 the longitudinal wire position near to the IP1 and with s_5 the longitudinal wire position near to the IP1 and with We find two possible solutions:

TCT opt β move the wire in IP1 150 m after the IP

TCT opt β 2 move the wire in IP5 150 m after the IP

Where 'opt' stand for optimized.

For both the IPs after 150 m we have $\beta_x \approx 560$ m and $\beta_y \approx 1570$ m. The TCT opt β location has the bigger β value in the crossing direction, this situation leads to better results.

IP	IP dist [m]	β_x [m]	β_y [m]	σ_x [10^{-3} m]	σ_y [10^{-3} m]
IP1	150	559.4	1566.9	0.53	0.89
IP5	-147	1575.7	606.8	0.56	0.89

Table 4.15: Summary of the optics parameter at the TCT opt β location.

Table 4.15 shows the optics parameters for the TCT opt β, the physical location for the wire is again symmetric, more in details we have in IP1 the wire located in [0.0 ,-0.0084] m and in IP5 in [-0.0084, 0.0] m.

Transverse position [σ]	Current A	Unstables Particles [%]	Minimum Radius [σ]
HoLr		5.7	2.8
9.5	177	2.4	3.7
11	177	3.4	5.6
11	237	2.6	3.7

Table 4.16: Summary of the stability test for TCT opt β , using the nominal LHC optics and performing the tests for differents transverse positions and current values, with nominal crossing angle.

The footprint results are similar to the one obtained for a wire at the BBC longitudinal location and with a transverse position of 11 σ, also if we
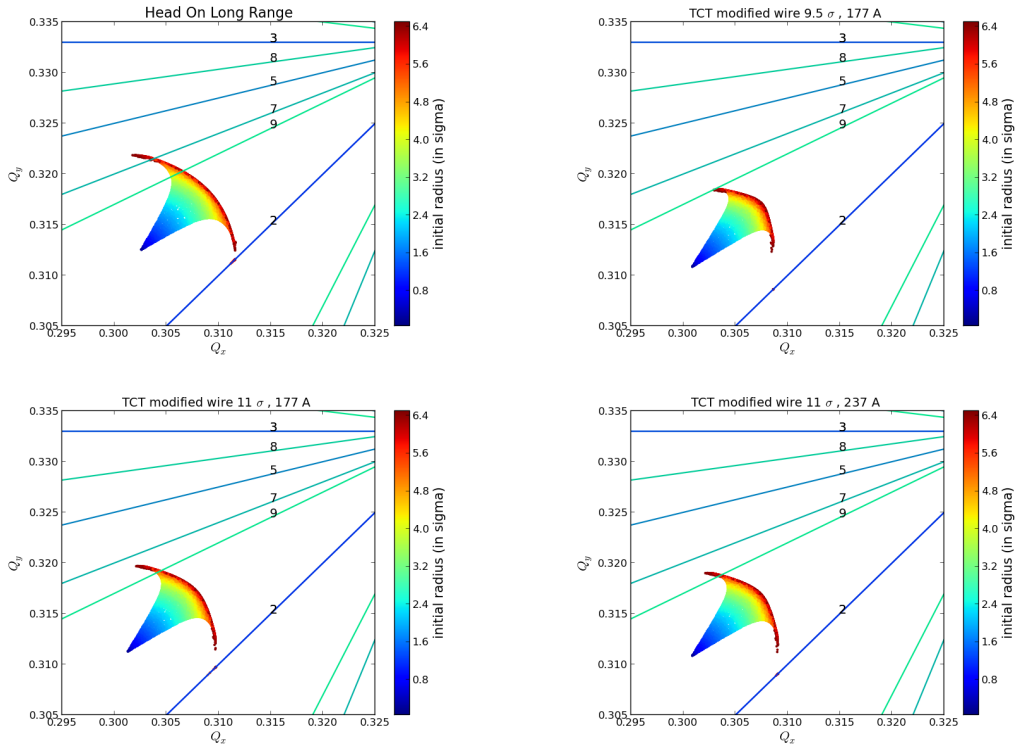
Figure 4.20: Tune footprint for TCT opt β with nominal Optics, nominal crossing angle (9.5 σ) and different transverse position and current.

haven't reached the best (that we have seen for the wire at BBC at 9.5 σ) we can consider this solution good enough: the tune footprint touches only a resonance line of order 9.

If we analyse the stability we notice that in the better case the percentage of unstables particles is the half of the one for head-on long-range simulation. Changing the current or the wire position we can otherwise improve the minimum radius at which we see the first instability obtaining a radius double respect to the head-on long-range case.
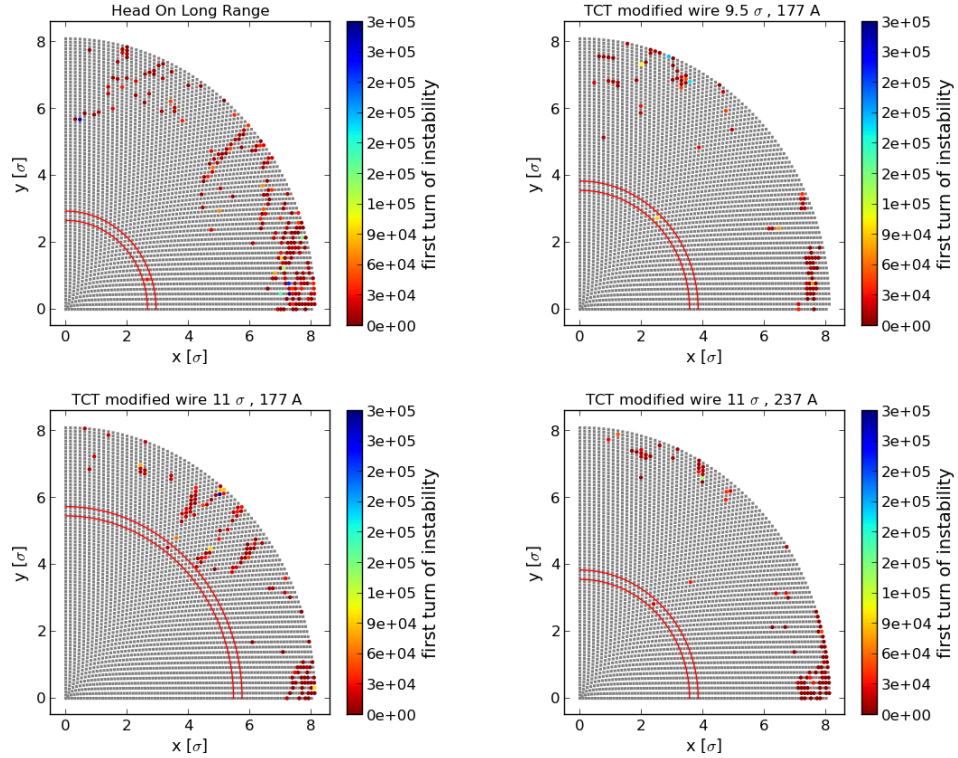
Figure 4.21: Test of stability for TCT opt β with nominal Optics, nominal crossing angle (9.5 σ) and different transverse position and current.

4.5.2   Test of different crossing angles

Changing the crossing angle we can see that even in the worst case a wire compensator in the TCT opt β location gives us a gain both for the tune footprint point of view and for stability point of view.

In the stability analysis we notice that the number of unstable particles is reduced at least to the half of the ones without the wire.

Transverse position [σ]	Current A	Unstables Particles [%]	Minimum Radius [σ]
HoLr		0.6	3.2
12	177	0.2	4.6
14	177	0.3	4.4
14	237	0.5	4.0

Table 4.17: Summary of the stability test for TCT opt β, using the nominal LHC optics and performing the tests for differents transverse positions and current values, crossing angle 12 σ.
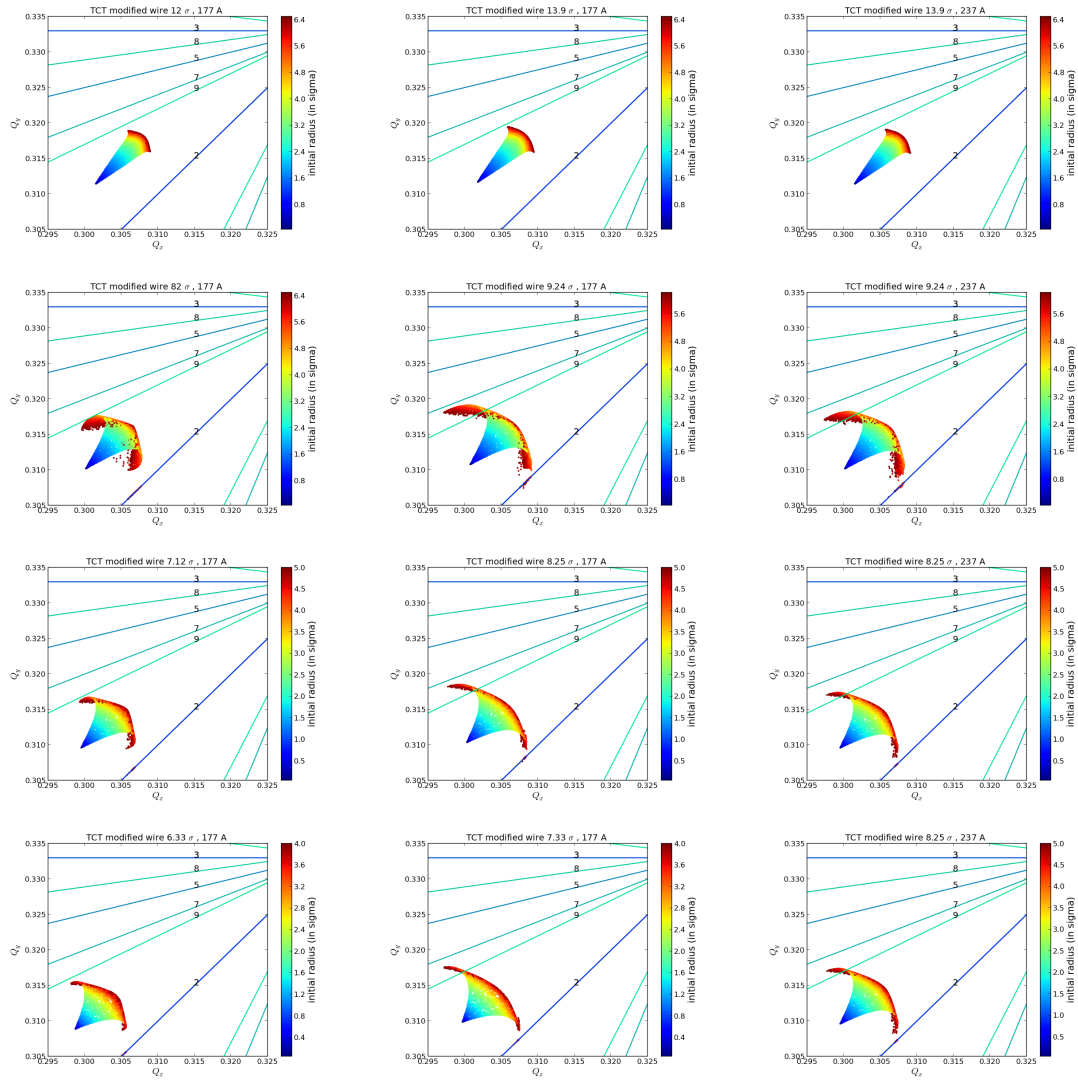
Figure 4.22: Tune footprint for TCT opt β with nominal Optics and crossing angle of: 12 σ (row 1), 8 σ (row 2), 7.1 σ (row 3), 6.3 σ (row 4).

In addition as emphasized in the Figure 4.24 we can obtain with a crossing angle of 9.5 σ and a wire at TCT opt β location, a distribution almost equal to the one for 12 σ without wire compensator, or for a crossing angle of 7.1 σ a distribution similar to the one at 8 σ without the wire compensator.
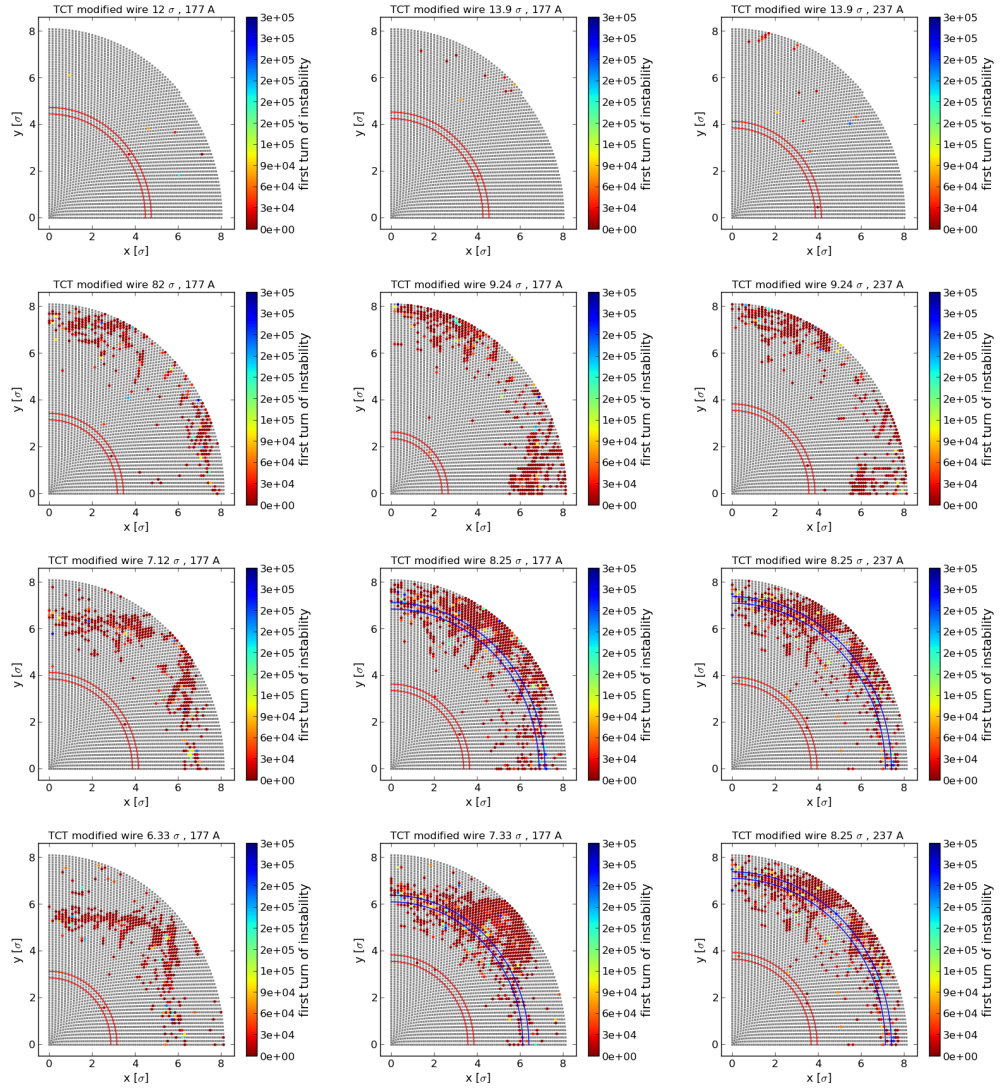
Figure 4.23: Test of stability for TCT opt β with nominal Optics and crossing angle of: 12 σ (row 1), 8 σ (row 2), 7.1 σ (row 3), 6.3 σ (row 4).

Transverse position [σ]	Current A	Unstables Particles [%]	Minimum Radius [σ]
HoLr		15.6	4.7
8	177	8.8	3.3
9.2	177	13.3	2.5
9.2	237	10.8	3.7

Table 4.18: Summary of the stability test for TCT opt β, using the nominal LHC optics and performing the tests for differents transverse positions and current values, crossing angle 8 σ.

Transverse position [σ]	Current A	Unstables Particles [%]	Minimum Radius [σ]
HoLr		22.3	3.5
7.1	177	11.1	4.0
8.25	177	20.3	3.5
8.25	237	16.8	3.8

Table 4.19: Summary of the stability test for TCT opt β, using the nominal LHC optics and performing the tests for differents transverse positions and current values, crossing angle 7.1 σ.

Transverse position [σ]	Current A	Unstables Particles [%]	Minimum Radius [σ]
HoLr		20.5	4.1
6.3	177	11.2	3.0
7.3	177	21.1	3.7
7.3	237	20.3	4.0

Table 4.20: Summary of the stability test for TCT opt β, using the nominal LHC optics and performing the tests for differents transverse positions and current values, crossing angle 6.3 σ.
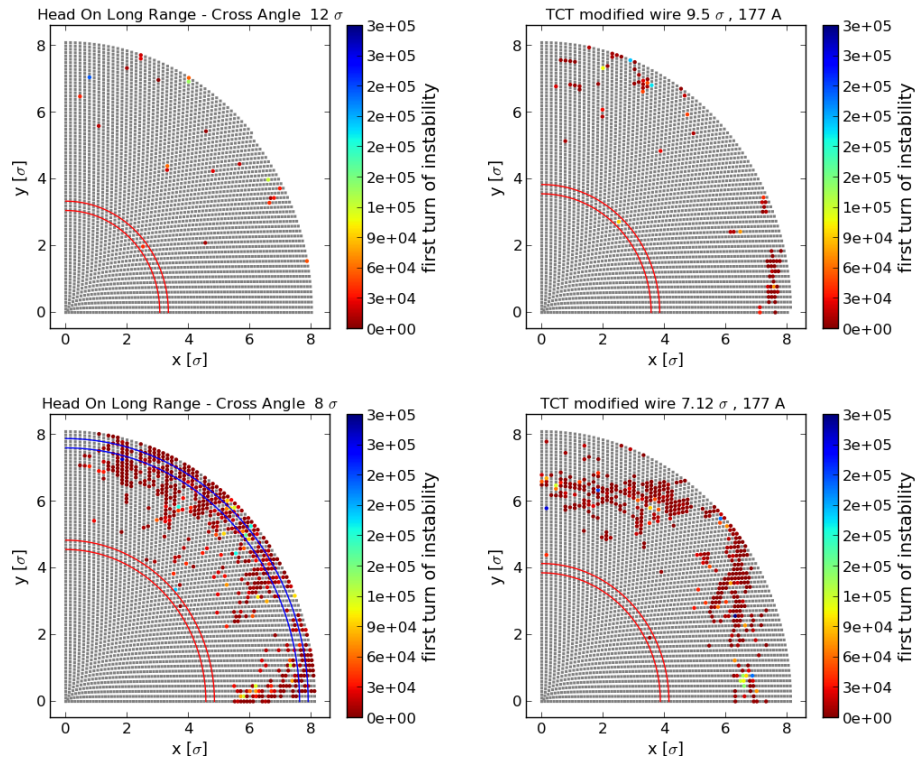
**Figure 4.24:** Test Stability BBC location, Nominal Optics: particles distribution at 9.5 σ with a wire compensator at 9.5 σ 177 A is almost equals with a particles distribution at 12 σ without compensator (first row) particles distribution at 7.1 σ with a wire compensator at 7.1 σ 177 A is almost equals with a particles distribution at 8 σ without compensator (second row).

4.6 TCT wire position Modified Optics

4.6.1 Tests with the Nominal Crossing Angle

IP	IP dist [m]	β_x [m]	β_y [m]	σ_x [10^{-3} m]	σ_y [10^{-3} m]
IP1	-147	801.0	802.5	0.63	0.63
IP5	-147	798.0	794.1	0.63	0.63

Table 4.21: Summary of the optics parameter at the TCT location for Modified Optics.

To improve the TCT solution and thinking that a different optics is in analysis for LHC S. Fartoukh produce for us a new optics where the betatron function has equal values in the two directions (x and y) and in the two IPs (1 and 5). The optics values for this optics are shown in Table 4.21
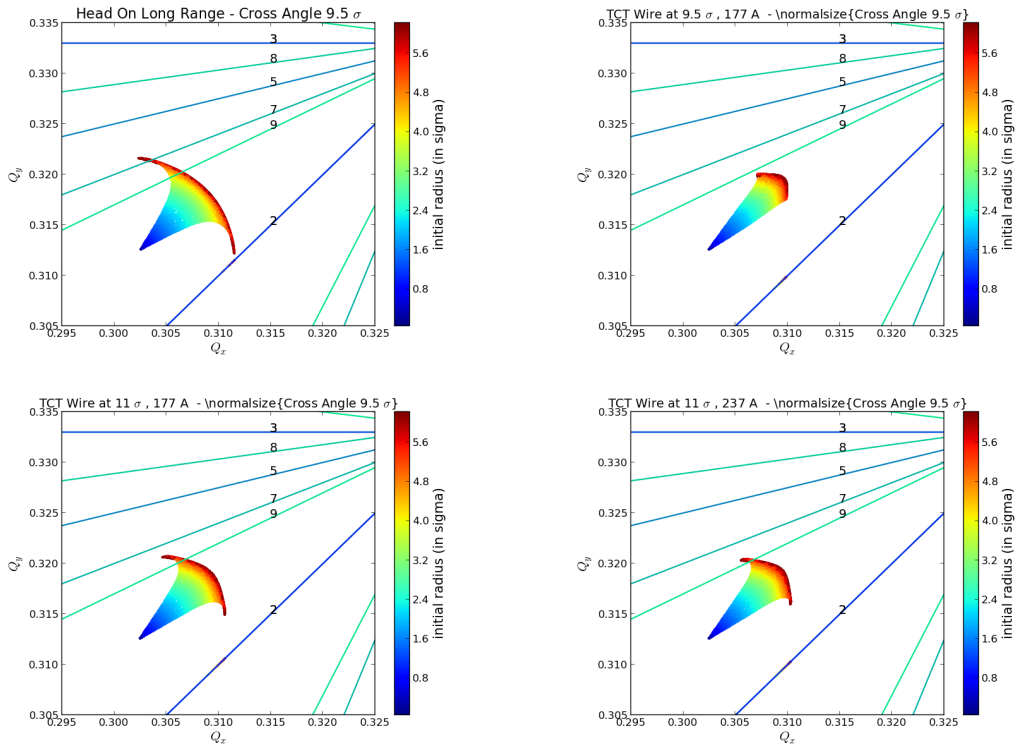

Figure 4.25: Tune footprint for TCT with modified Optics, nominal crossing angle (9.5 σ) and different transverse position and current.

With a wire located at 9.5 σ with a current of 177 A we have a footprint almost equal to the one for the Head on (and for the one with the same
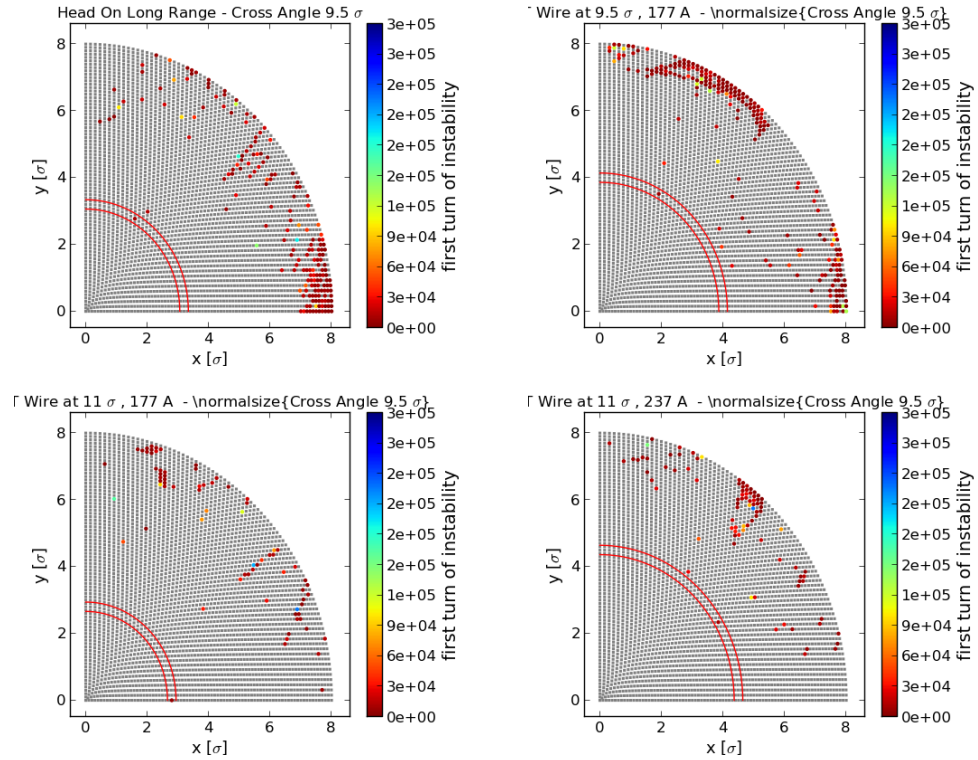
Figure 4.26: Test of stability for TCT with modified Optics, nominal crossing angle (9.5 σ) and different transverse position and current.

Transverse position	Current	Unstables Particles	Minimum Radius
[σ]	A	[%]	[σ]
HoLr		5.3	3.2
9.5	177	6.2	4.0
11	177	2.1	2.8
11	237	2.6	4.5

Table 4.22: Summary of the stability test for TCT, using modified LHC optics and performing the tests for differents transverse positions and current values, with nominal crossing angle.

transverse position and current but at BBC location and with nominal LHC optics).

If we examine instead the stability we see that the improvement is smaller than the expected and for 9.5 σ with a current of 177 A, we have a situation even worse of the one of head-on long-range with a big percentage of unstable particles at a radius of 8 σ. However if we consider the wire at 11 σ there appear to be some benefit.

4.6.2   Test of different crossing angles
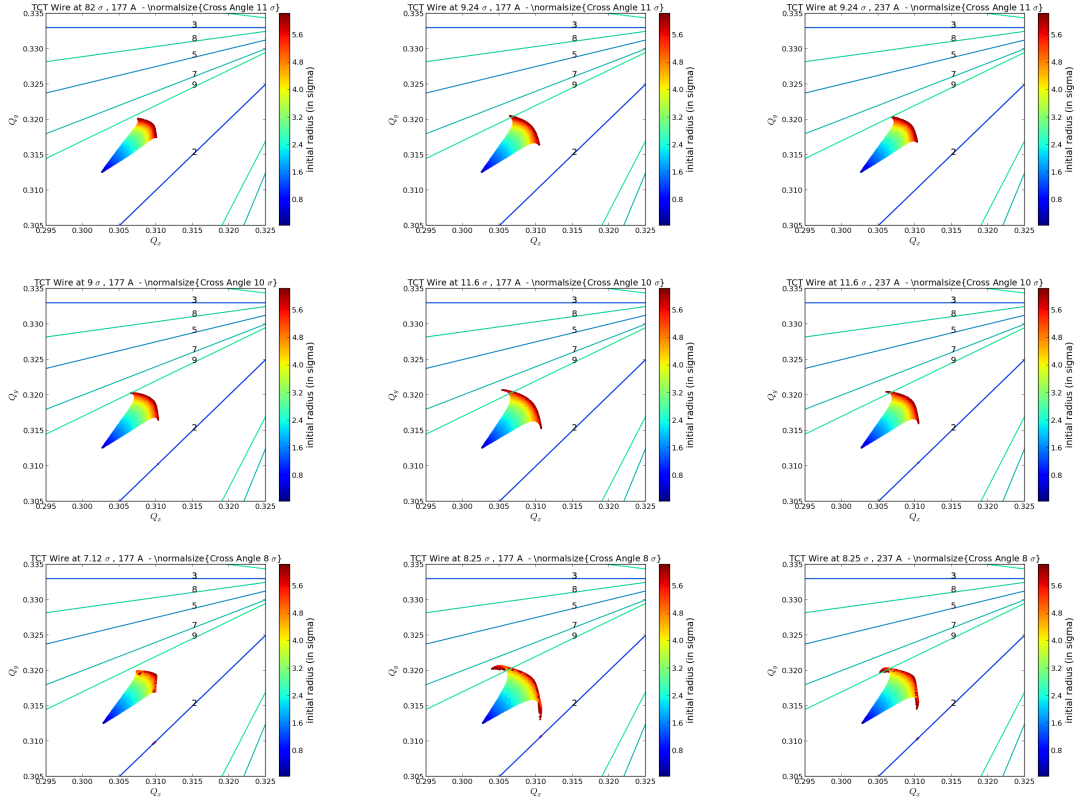
Figure 4.27: Tune footprint for TCT with modified Optics and crossing angle of: 11 σ (row 1), 10 σ (row 2), 9 σ (row 3).

Changing the crossing angle we can see that the gain is better for big crossing angle (until 9 σ we reduce the number of unstable particles to half the value that we have without the wire), for angle smaller than 8 σ we have a smaller gain.

We see in figure 4.13 that the particles distribution at 9.5 σ with a wire compensator located at 11 σ with a current of 177 A is almost equals with a particles distribution at 11 σ without the compensator, particles distribution at 8 σ with a wire compensator at 9.24 σ with a current of 237 A is almost equals with a particles distribution at 9 σ without compensator.
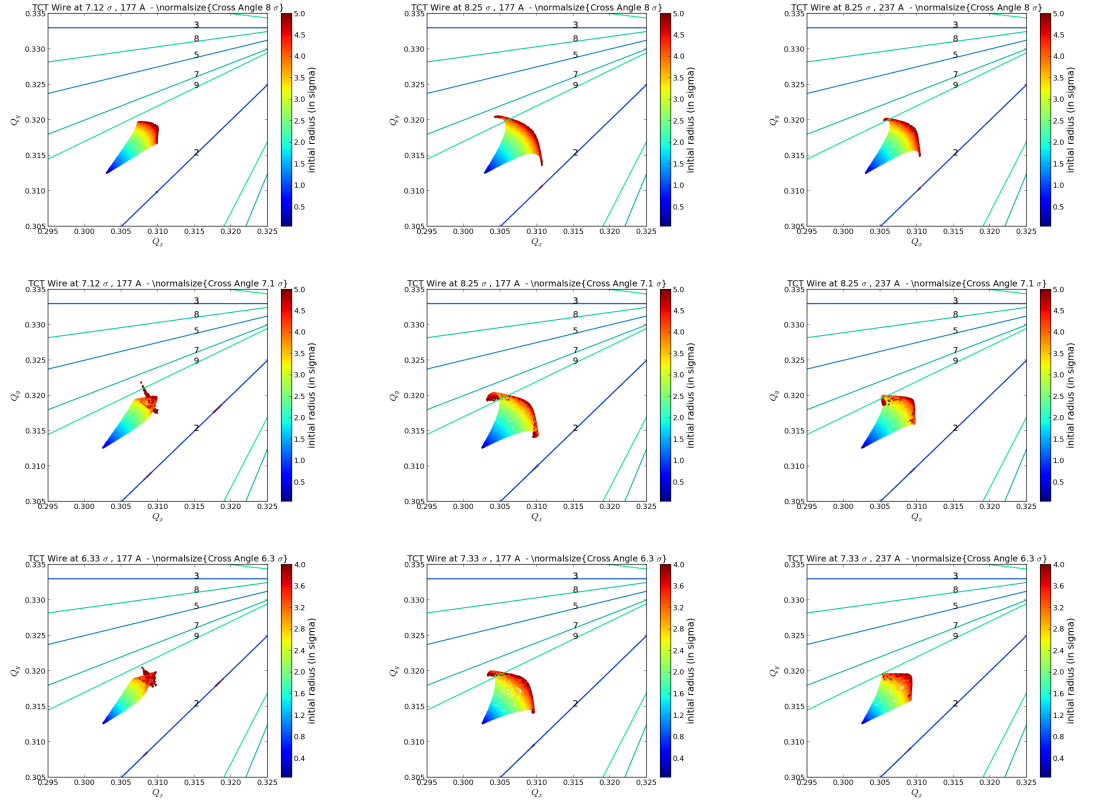
Figure 4.28: Tune footprint for TCT with modified Optics and crossing angle of: 8 σ (row 1), 7.1 σ (row 2), 6.3 σ (row 3).

Transverse position	Current	Unstables Particles	Minimum Radius
[σ]	A	[%]	[σ]
HoLr		1.2	5.1
11	177	0.3	4.5
12.7	177	0.5	4.7
12.7	237	0.8	4.3

Table 4.23: Summary of the stability test for TCT, using modified LHC optics and performing the tests for differents transverse positions and current values, with crossing angle 11 σ .
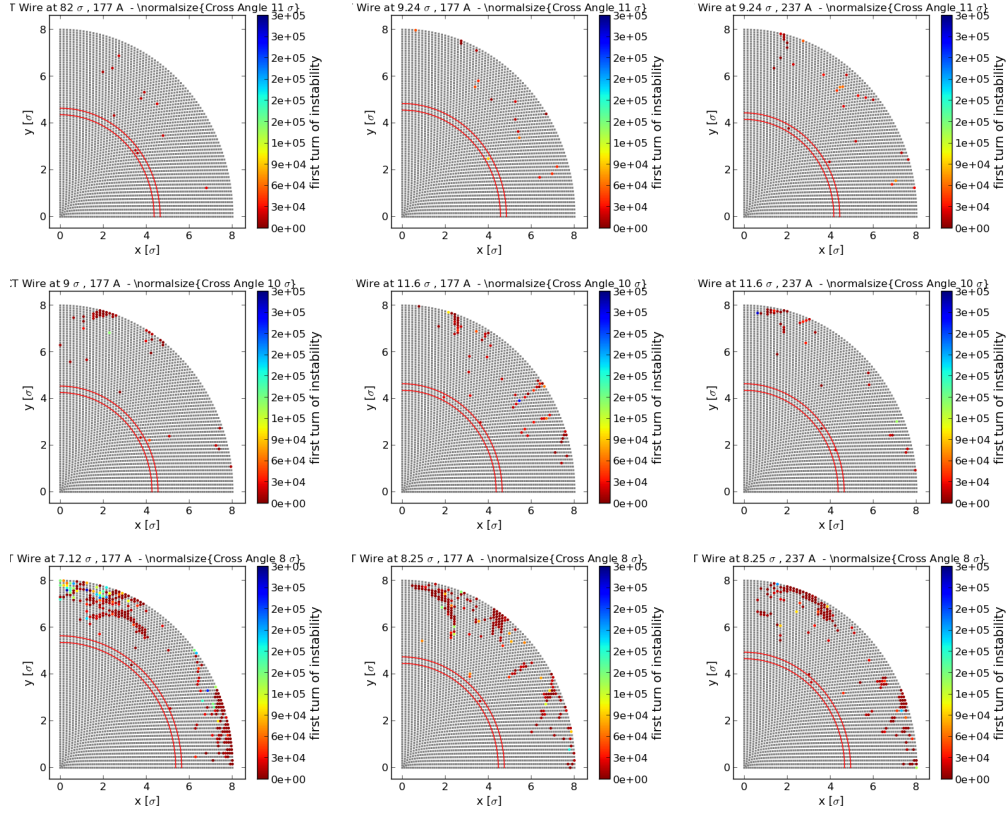
Figure 4.29: Test of stability for TCT with modified Optics and crossing angle of: 11 σ (row 1), 10 σ (row 2), 9 σ (row 3).

Transverse position [σ]	Current A	Unstables Particles [%]	Minimum Radius [σ]
HoLr		3.8	3.4
10	177	1.3	4.4
11.6	177	1.8	4.5
11.6	237	1.0	4.5

Table 4.24: Summary of the stability test for TCT, using modified LHC optics and performing the tests for differents transverse positions and current values, with crossing angle 10 σ .
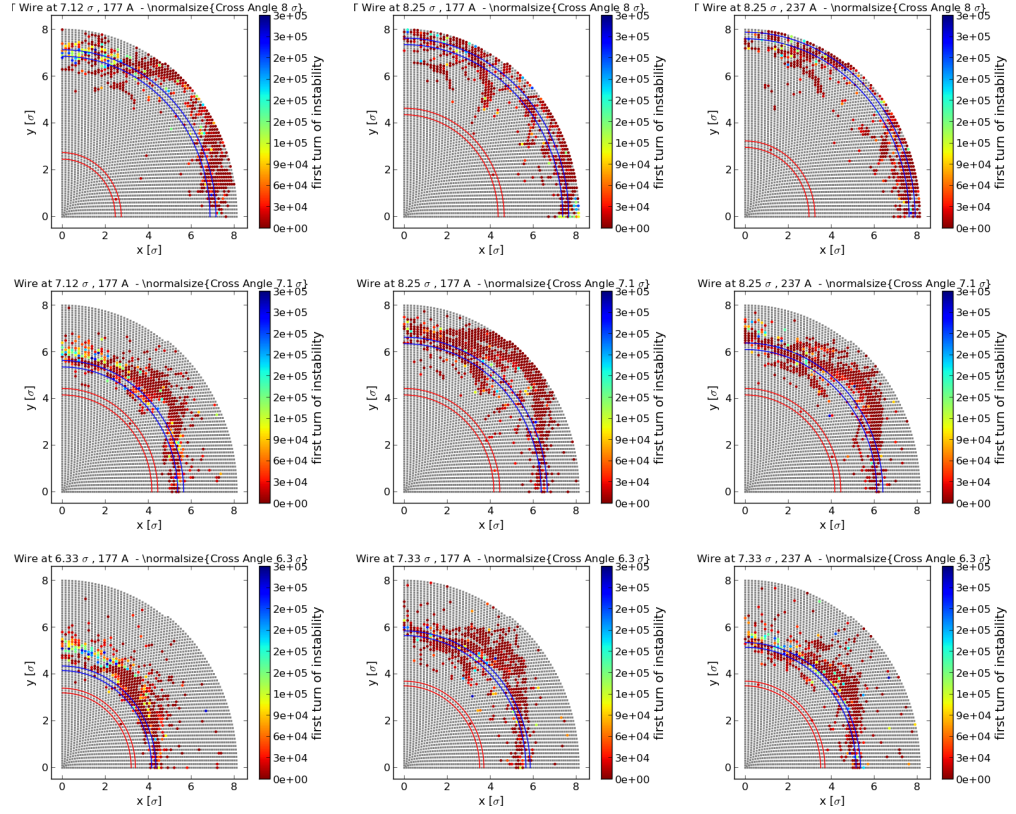
Figure 4.30: Test of stability for TCT with modified Optics and crossing angle of: 8 σ (row 1), 7.1 σ (row 2), 6.3 σ (row 3).

Transverse position [σ]	Current A	Unstables Particles [%]	Minimum Radius [σ]
HoLr		11.7	4.1
9	177	7.5	5.5
10.3	177	5.2	4.6
10.3	237	4.4	4.8

Table 4.25: Summary of the stability test for TCT, using modified LHC optics and performing the tests for differents transverse positions and current values, with crossing angle 9 σ .

Transverse position [σ]	Current A	Unstables Particles [%]	Minimum Radius [σ]
HoLr		22	4.2
8	177	17.4	2.6
9.2	177	16.1	4.5
9.2	237	14.2	3.1

Table 4.26: Summary of the stability test for TCT, using modified LHC optics and performing the tests for differents transverse positions and current values, with crossing angle 8 σ .

Transverse position [σ]	Current A	Unstables Particles [%]	Minimum Radius [σ]
HoLr		28.0	3.8
7.1	177	16.0	4.3
8.25	177	21.0	4.3
8.25	237	18.4	4.3

Table 4.27: Summary of the stability test for TCT, using modified LHC optics and performing the tests for differents transverse positions and current values, with crossing angle 7.1 σ .

Transverse position [σ]	Current A	Unstables Particles [%]	Minimum Radius [σ]
HoLr		24.1	3.3
6.3	177	14.2	3.3
8.25	177	17.0	3.6
8.25	237	14.2	3.6

Table 4.28: Summary of the stability test for TCT, using modified LHC optics and performing the tests for differents transverse positions and current values, with crossing angle 6.3 σ .
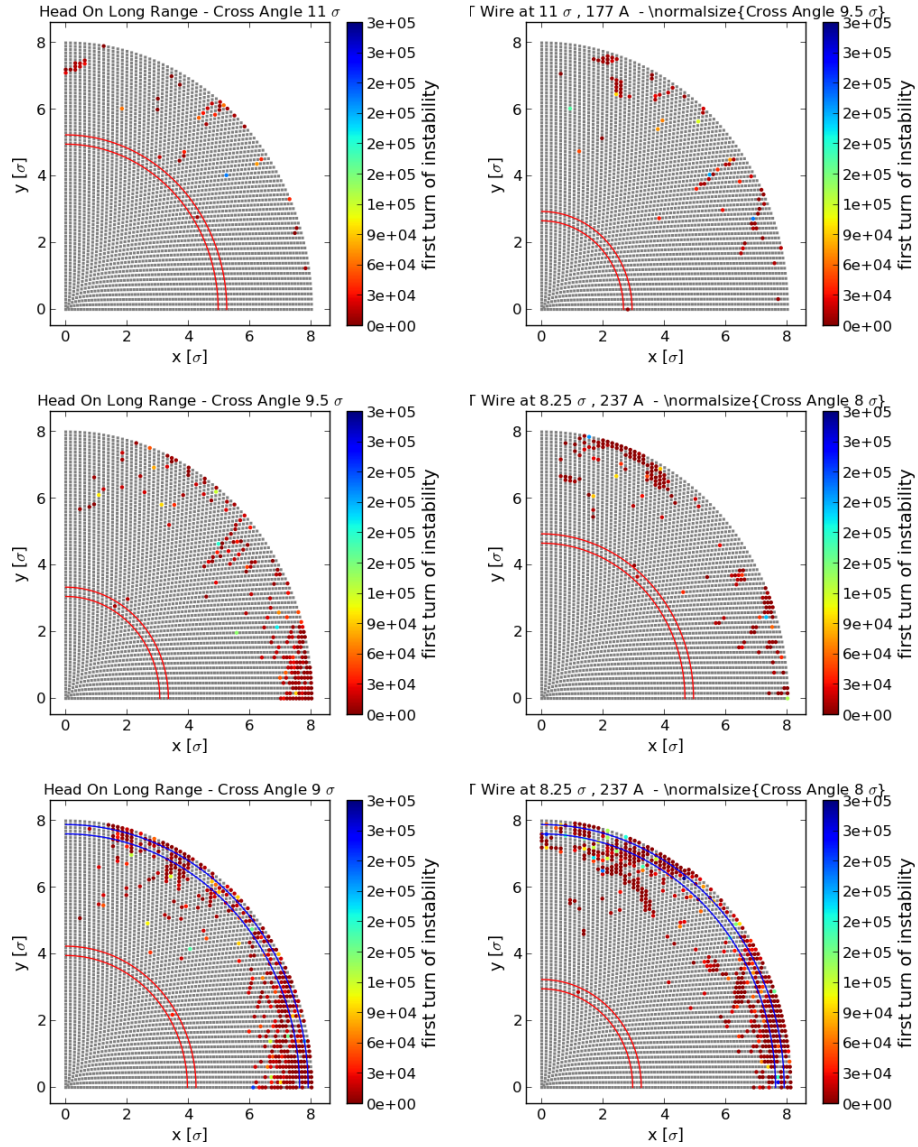
Figure 4.31: Test Stability TCT location, modified Optics: particles distribution at 9.5 σ with a wire compensator at 11 σ 177 A is almost equals with a particles distribution at 11 σ without compensator (first row), particles distribution at 9 σ with a wire compensator at 10.3 σ 237 A is almost equals with a particles distribution at 9.5 σ without compensator (second row), particles distribution at 8 σ with a wire compensator at 9.24 σ 237 A is almost equals with a particles distribution at 9 σ without compensator (third row).

5

Additional Simulation Results

5.1 Q5 wire position Nominal Optics

IP	IP dist [m]	β_x [m]	β_y [m]	σ_x $[10^{-3}$ m]	σ_y $[10^{-3}$ m]
IP1	199	105.9	503.0	0.23	0.50
IP5	199	105.9	503.0	0.23	0.50

Table 5.1: Summary of the optics parameter at the Q5 location for nominal Optics.

The two proposed alternative for the wire compensator were the TCT location (150 m before the IPs) and the Q5 location (199 m after the IPs).

As shown in the Table 5.1 in the Q5 location we have again an asymmetry of βs with the same kind of asymmetry in IP1 and IP5 (in this case β_x lower than β_y). In addition in the Q5 location the β are really smaller with respect to the value in BBC location (for nominal optics $\beta \approx 1700$ m) or in the TCT one (for nominal optics $\beta_x \approx 1600$ m and $\beta_x \approx 600$ m), not surprisingly, this location does not give us good results.

For the stability point of view in some cases the results are even worse than the case without wire.

As we did for some of the TCT tests we tried to improve the results by moving back the central tune using the formula (4.2), but, in this case, without encouraging results.
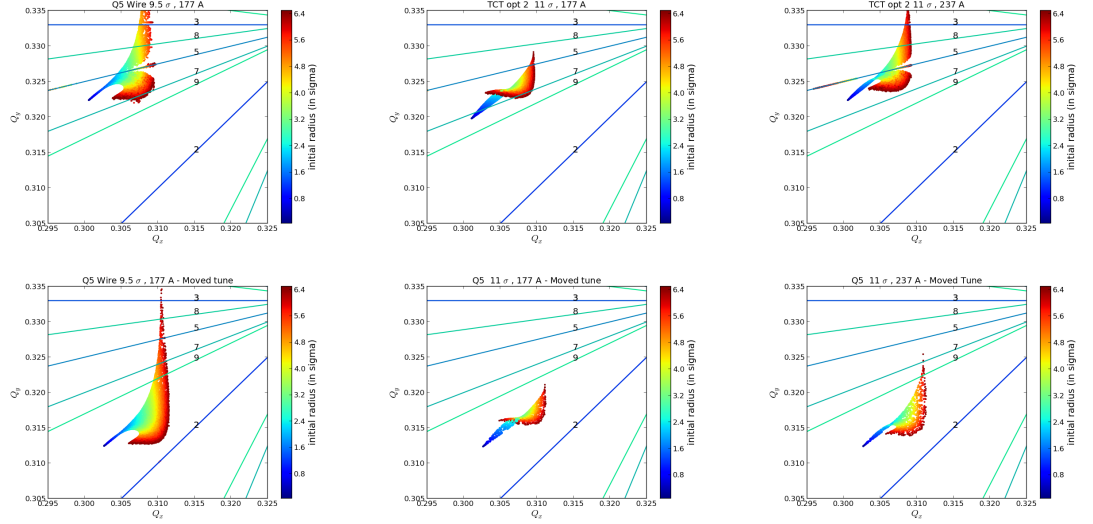
Figure 5.1: Tune footprint for Q5 position with nominal Optics. Line 2 reports the value if we move back the central tune.
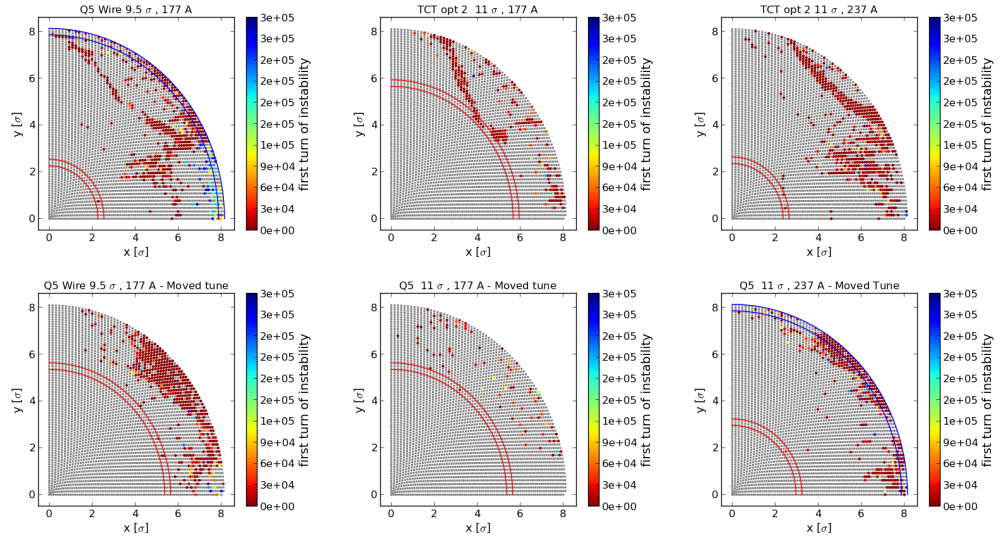

Figure 5.2: Test of stability for Q5 position with nominal Optics. Line 2 reports the value if we move back the central stab.

Transverse position [σ]	Current A	Unstables Particles [%]	Minimum Radius [σ]
HoLr		5.7	2.8
9.5	177	14.6	2.4
11	177	6.5	5.8
11	237	14.0	2.5

Table 5.2: Summary of the stability test for Q5 , using nominal LHC optics and making the tests for different transverse positions and current values, with nominal crossing angle.

Transverse position [σ]	Current A	Unstables Particles [%]	Minimum Radius [σ]
HoLr		5.7	2.8
9.5	177	13.6	5.5
11	177	2.2	5.5
11	237	9.7	3.1

Table 5.3: Summary of the stability test for Q5 , using nominal LHC optics and making the tests for different transverse positions and current values, with nominal crossing angle. Central Tune Moved Back

5.2   TCT opt β 2 wire position Nominal Optics

IP	IP dist [m]	β_x [m]	β_y [m]	σ_x [10^{-3} m]	σ_y [10^{-3} m]
IP1	-147	1575.2	614.9	0.89	0.56
IP5	150	563.2	1567.6	0.53	0.88

Table 5.4: Summary of the optics parameter at the TCT opt β 2 location for nominal Optics.

We can change the TCT configuration moving the wire in IP5 instead of the one in IP1. We have obtained a mirrored situation, but in this case the β is smaller in the crossing angle direction. As expected this test is not a good solution.
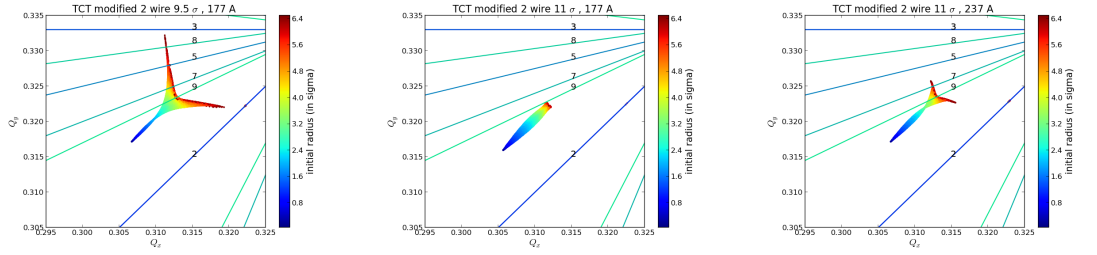

**Figure 5.3:** Tune footprint for TCT opt β 2 position with nominal Optics.
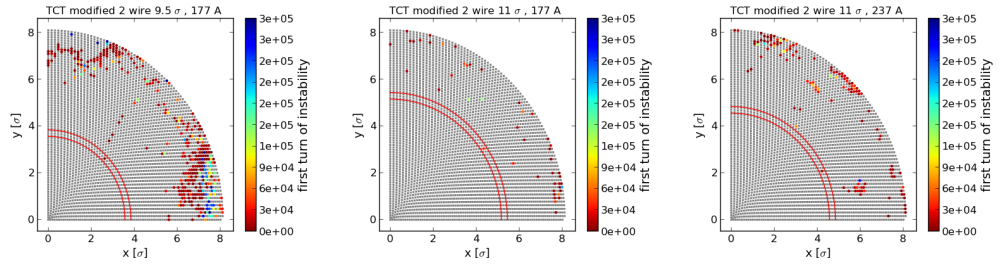
Figure 5.4: Test of stability for TCT opt β 2 position with nominal Optics.

Transverse position	Current	Unstables Particles	Minimum Radius
$[\sigma]$	A	[%]	$[\sigma]$
HoLr		5.7	2.8
9.5	177	9.6	3.7
11	177	1.3	5.3
11	237	3.5	4.7

Table 5.5: Summary of the stability test for TCT opt β 2 , using nominal LHC optics and making the tests for different transverse positions and current values, with nominal crossing angle.

5.3 BBC wire position Modified Optics

IP	IP dist	β_x	β_y	σ_x	σ_y
	[m]	[m]	[m]	$[10^{-3}$ m]	$[10^{-3}$ m]
IP1	105	1914.9	1142.1	0.98	0.75
IP5	105	1915.9	1142.4	0.98	0.75

Table 5.6: Summary of the optics parameter at the BBC location for modified Optics.

It could be interesting to check the effect of the wire compensator in the nominal location if we use the modified optics. As shown in the Table 5.6 in this case we have, as in the TCT location with nominal optics, the β_x greater than the β_y in both planea, but with a smaller difference and with a large value of β.

This configuration is not the best that we have studied, but gives results good enough for a possible use.
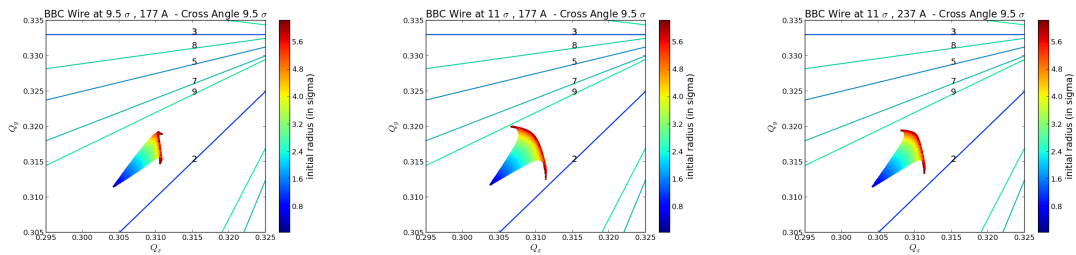
**Figure 5.5:** Tune footprint for BBC position with modified Optics.
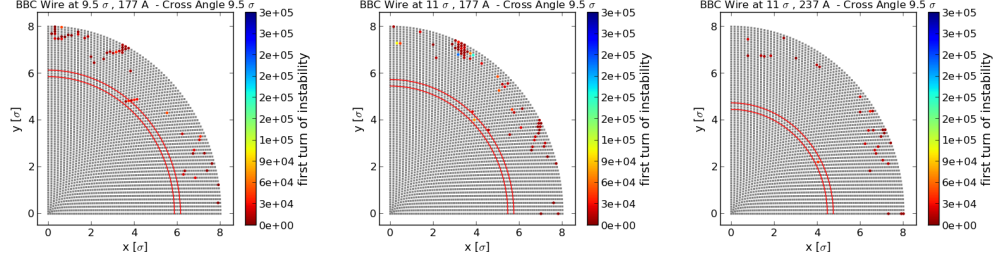
Figure 5.6: Test of stability for BBC position with modified Optics.

Transverse position [σ]	Current A	Unstables Particles [%]	Minimum Radius [σ]
HoLr		5.3	2.8
9.5	177	1.5	6.0
11	177	1.8	5.6
11	237	0.9	4.6

Table 5.7: Summary of the stability test for TCT, using modified LHC optics and making the tests for different transverse positions and current values, with nominal crossing angle.

5.4   Wire shape test

Until now we have always considered a pencil like wire, but this should not be the real situation, it has been requested to study the case of a square wire with 1 mm side.

The simulation program bbtrack does not allow us to set the wire shape, so we approximate the square wire with 4 pencil like wires positioned at the corner of square. For example in IP1 we replace the wire in [0.0 , -8.9] mm with the four wires [-0.05 , -8.9] mm, [0.05 , -8.9] mm, [-0.05 , -9.9] mm and [0.05 , -9.9] mm,

Percentage Unstables [%]			
Test	177 A 9.5 σ	177 A 11 σ 7	237 A 11 σ
Pencil like Wire	0.2	0.2	0.3
Square Wire	0.1	1.1	0.9

Table 5.8: Test of stabilityility comparison between pencil like wire and square wire for number of unstable particles.

The tests demonstrate that the wire shape does not much affect our results. In some cases from the stability point of view the results seems even better than the one obtained with a pencil like wire.
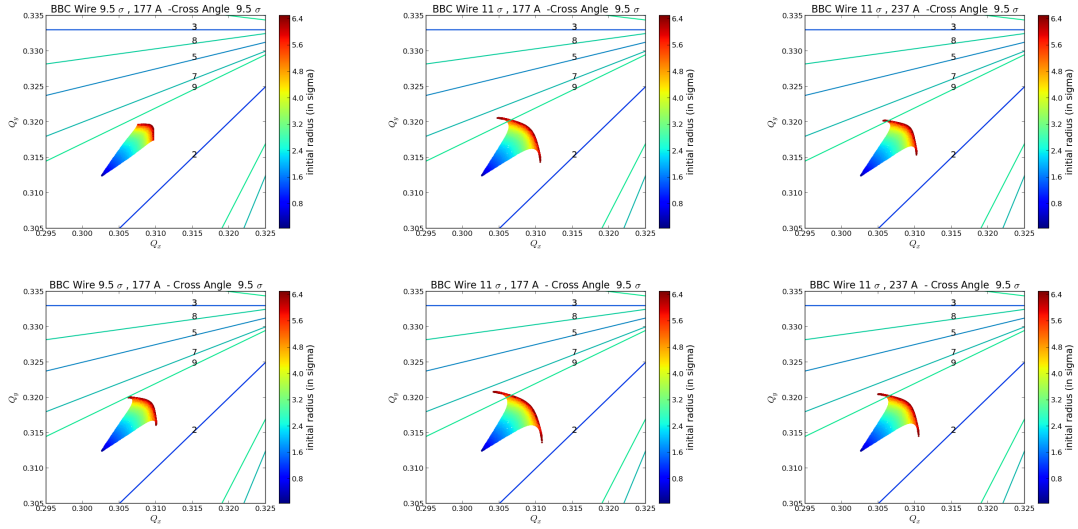
Figure 5.7: Tune footprint comparison between pencil like wire (first row) and square wire (second row).
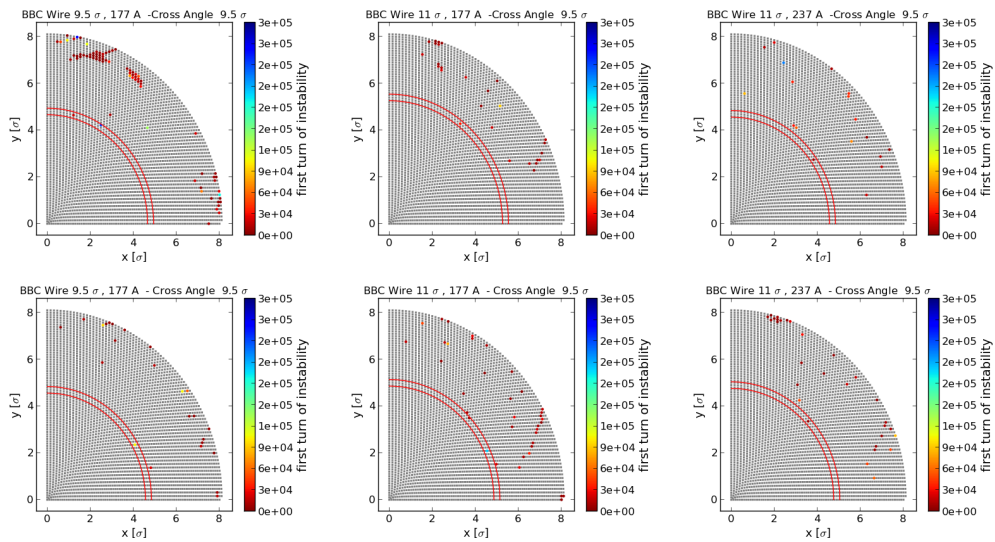

Figure 5.8: Test of stabilityility comparison between pencil like wire (first row) and square wire (second row).

6

Conclusions

The design of the Large Hadron Collider (LHC) at CERN involved many technical challenges.

To reach high energy and high luminosity it is important to compensate the negative effects due to the electromagnetic interactions between the two beam before and after the main collision points, the so-called long-range beam-beam effects.

This possible limitation to the collider performance can be partially mitigated with a DC wire compensator.

The best compensation is obtained when the β functions have the same value in the transverse planes, and when the betatron phase advance between the LR collision points and the wire is as small as possible.

For the nominal LHC optics we find that the original "BBC" location (105 m after the Ips 1 and 5) best satisfies these requirements, but this location would not be available for the 2014 shutdown.

In this thesis we have, therefore, examined several other possible configurations of LHC long-range wire compensation for an initial demonstration experiment with different wire locations, both for the nominal LHC optics and for a modified optics.

We have simulated the efficiency of the wire compensation for the various configurations using the weak-strong simulation program BBTrack, written in Fortran90 [6].

Several scripts were developed during this year for post-processing analysis, but also to simplify and speed up the input preparation and tracking.

In particular, for the post-processing a new method automatically detect a nonzero Lyapunov coefficient was implemented, and used in the stability analysis.

Comparison of the betatron tune footprints suggests that the best compensation is obtained when the wire has a distance from the beam equal to the average long range distance, which for nominal crossing angle means 9.5σ.

On the other hand if we consider the Lyapunov stability it seems better to move the wire at 11σ. This distance would also facilitate the technical realization of the compensator.

Our simulations show that the wire can give a good compensation also for reduced crossing angles.

Suitably placed LHC wire compensators should allow for a reduction of the crossing angle by the equivalent of at least 1-2 σ, while maintaining the same stable region in phase space, or, alternatively, for a substantial increase in beam current (e.g. by a factor of 2) at constant crossing angle.

Compensation effects are also important for the proposed location inside a tertiary collimator (TCT) and the modified optics, which could be studied experimentally in the LHC from about 2015 onward, as well as for a modified TCT location (obtained by moving the wire in Ip1 from before the IP to 150 m after the Ip, which implies adding a new TCT) with the nominal LHC optics.

The nominal TCT location, the Q5 location and another modified TCT locations (where we move the wire in Ip5 instead of the one in Ip1 to a location 150 m after the Ip) are not suitable solutions, since in the simulations they either do not yield any improvement or give results even worse than obtained without any compensator (the Q5 case for example).

Finally, our simulations have also demonstrated that the exact shape of the wire (round or square) has little effect on the compensation quality.

7

Acknowledgments

Bibliography

[1] M. Bassetti and G. A. Erskine. Closed expression for the electrical field of a two-dimensional gaussian charge. oai:cds.cern.ch:122227. Technical Report CERN-ISR-TH-80-06. ISR-TH-80-06, CERN, Geneva, 1980.

[2] P. J. Bryant. A brief history and review of accelerators. 1993.

[3] CERN. *Lhc Beam-Beam compensation using wires and electron lenses*, 2007.

[4] A. Chao and M. Wang. Lecture notes on accelerator physics. In *Accelerator Physics, USPAS 2007*, 2007.

[5] U. Dorda. Bbtrack - a weak-strong long-range beam beam interaction simulation code, 2008. http://ab-abp-bbtrack.web.cern.ch/ab-abp-bbtrack.

[6] U. Dorda. *Compensation of long-range beam-beam interaction at the CERN LHC*. PhD thesis, CERN, 2008.

[7] U. Dorda and Frank Zimmermann. Simulation of lhc long-range beam-beam compensation with dc and pulsed wires. Technical Report CARE-Conf-06-026-HHH. CARE-Conf-2006-026-HHH, CARE, 2006.

[8] U. Dorda and Frank Zimmermann. Simulations of long-range beam-beam interaction and wire compensation with bbtrack. oai:cds.cern.ch:971862. (CERN-AB-2006-043):4 p, Jul 2006. revised version submitted on 2006-08-21 16:53:18.

[9] U. Dorda and Frank Zimmermann. Long-range beam-beam compensation with wires. page 3 p, 2007.

[10] S Fartoukh. An achromatic telescopic squeezing (ats) scheme for the lhc upgrade. oai:cds.cern.ch:1382077. (CERN-ATS-2011-161):3 p, Sep 2011.

[11] C. Fischer and J.-P. Koutchouk. Reservations for beam-beam compensators in ir1 and ir5. (LHC Engineering Change Order), 2004.

[12] G. Guignard. A general treatment of resonances in accelerators. page 72 p, Geneva, 1978. CERN, CERN. CERN, Geneva, 1977 - 1978.

[13] W. Herr. Features and implications of different lhc crossing schemes. oai:cds.cern.ch:604005. Technical Report LHC-Project-Report-628. CERN-LHC-Project-Report-628, CERN, Geneva, Feb 2003.

[14] W. Herr. Beam-beam interactions. 2006.

[15] W. Herr. Lhc beam-beam. lhc beam-beam effects- review and outlook. 2010.

[16] W. Herr and B. Muratori. Concept of luminosity. 2006.

[17] W. Herr and F. Schmidt. A mad-x primer. *CERN-AB-2004-027-ABP*, 2004.

[18] B. J. Holzer. Lattice design in high-energy particle accelerators. 2006.

[19] E. Keil. Beam-beam interactions in p-p storage rings. 1977.

[20] S. Kheifetes. Three dimensional potential for gaussian bunch. *Desy Petra 119*, 1976.

[21] J.P. Koutchouk. Correction of the long-range beam-beam effect in lhc using electro-magnetic lenses. oai:cds.cern.ch:513685. (CERN-SL-2001-048-BI):4 p, Jul 2001.

[22] S.Y. Lee. *Accelerator Physics (Second Edition)*. World Scientific Publishing, 2004.

[23] H. Mais and C. Mari. Introduction to beam-beam effects. 1994.

[24] B. W. St. L. Montague. Basic hamiltonian mechanics. 1995.

[25] D. Neuffer and S. Peggs. Beam-beam tune shifts and spreads in the ssc - head on, long range, and pacman conditions. (SSC-63), 1966.

[26] Y. Papaphilippou and Frank Zimmermann. Weak-strong beam-beam simulations for the large hadron collider. *Phys. Rev. Spec. Top. Accel. Beams*, 2(10):104001, 1999.

[27] Y. Papaphilippou and Frank Zimmermann. Diffusive aperture due to long-range beam-beam interaction. oai:cds.cern.ch:462632. (LHC-Project-Report-402. CERN-LHC-Project-Report-402):4 p, Aug 2000.

[28] T. L. Rijoff, R. Steinhagen, and Frank Zimmermann. Simulation studies for lhc long-range beam-beam compensators. oai:cds.cern.ch:1450938. (CERN-ATS-2012-074):3 p, May 2012.

[29] T. L. Rijoff and Frank Zimmermann. Simulations on beam beam compensation with wire. Presented at CERN ICE Meeting, November 2011, 2011.

[30] J. Rossbach and P. Schmüser. Basic course on accelerator optics. (DESY-M-93-02):72 p, Feb 1993.

[31] F. Schmidt, F. Willeke, and Frank Zimmermann. Comparison of methods to determine long-term stability in proton storage rings. oai:cds.cern.ch:218662. comparison of methods to prove long term stability in proton storage rings. *Part. Accel.*, 35(CERN-SL-91-14-AP. DESY-HERA-91-07):249–256. 9 p, Apr 1991.

[32] R.J. Steinhagen. Lhc beam-beam compensator - a first proposal. 2011.

[33] G. Sterbini, J.P. Koutchouk, and L. Rivkin. *An Early Separation Scheme for the LHC Luminosity Upgrade. oai:cds.cern.ch:1229215.* PhD thesis, Ecole Polytechnique, Lausanne, Lausanne, 2009. Presented on 27 Nov 2009.

[34] H. Wiedemann. *Particle accelerator physics.* Springer Verlag, 1993.

[35] K. Wille. *The Physics of Particle Accelerators.* Oxford University Press, 2005.

[36] E. J. N. Wilson. Nonlinear resonances (particle accelerators). 1995.

[37] E. J. N. Wilson. Transverse beam dynamics; 2006 ed. 2006.

[38] Frank Zimmermann. *Emittance growth and proton beam lifetime in HERA.* PhD thesis, DESY, 1993.

[39] Frank Zimmermann. Weak-strong simulation studies for the lhc long-range beam-beam compensation, 2001.